Vibrational Spectroscopy of Corrosion Inhibitors Adsorbed on Cu(100)

A thesis submitted to the

University of Manchester

for the degree of

DOCTOR OF PHILOSOPHY

in the Faculty of Science

by

H. S. Dhariwal

Department of Chemistry,
University of Manchester,
Manchester,
M13 9PL.

September 1997

ProQuest LLC.
789 East Eisenhower Parkway
P.O. Box 1346
Ann Arbor, MI 48106 – 1346

To my close friends and family.

Acknowledgements

Firstly I would like to thank my supervisor, Geoff Thornton.

I would also like to thank ICI Chemicals & Polymers, who supplied some financial support for this project. I would especially like to thank Richard Oldman, whose advice and interest was much appreciated.

I would like to express my gratitude to my co-experimenters Steve crook and Sammy Haq. Others who contributed were F. Schedin, John Walsh, Andrew Thomas and C. Muryn.

Thanks to my Mum, Dad, Tom and Suki (for bailing me out a few times) and the rest of the family, for their support and financial help.

Special thanks to the mad lotsters on the 6th floorsters for a few decent piss ups, a damn good laugh, and some extrodinary conversations, these include Fred, Steve and Leon.

Special thanks to Michelle for some good times and for putting up with me, especially while I was writing this beast, and for the odd curry or two.

Weight training sessions and the dreaded pyramid wouldn't be the same without Harj, also the drinks afterwards, thanks for the support and friendship - Up the Wolves. Thanks to Onk, Jas and Ami for a few drinks and piss-takes along the way, some very close to the bone.

Thanks to thank Mark Murrie for helpful discussions. I would also like to thank others who took an interest and also had a few drinks along the way, these include Hibat, Sean, Matt, Ivan, Anthony, Rob, Ged, Steve Vinton, Chang, Aurora, Paul W and also Paul M for a few good drinks lately.

Contents

Abstract

This thesis describes the use of High Resolution Electron Energy Loss Spectroscopy (HREELS) and Reflection Absorption Infrared Spectroscopy (RAIRS) as tools for studying the orientation of molecules on single crystal surfaces. In particular, it describes studies of the orientation of ligands which are important in the field of corrosion inhibition

A vibrational study of Benzotriazole (BTAH) on Cu(100) at 298 K finds that the BTA^- anion is adsorbed on the surface. The anion is adsorbed with its molecular plane parallel to the plane of the surface at low exposures of BTAH but undergoes an orientational phase transition to a more upright geometry at saturation coverage. The RATIO method has been used to show that BTA^- adsorbs in a tilted geometry on the clean Cu(100) and oxygen pre-dosed Cu(100) surfaces. The smaller molecule 1, 2, 3 triazole was also studied and was shown to bond in a similar tilted configuration suggesting that both azoles have similar bonding modes.

The orientation of other successful and unsuccessful corrosion inhibitors have been studied on Cu(100) at 298 K. The successful corrosion inhibitor Indazole is found to a orient in a perpendicular geometry at all coverages. The unsuccessful corrosion inhibitor Benzimidazole is found to bond in a parallel geometry whilst 1 - Methyl benzotriazole does not bond to Cu(100) at 298 K. This suggests that alterations in the molecular framework of the azoles influences the orientation and bonding modes and therefore their ability to act as efficient corrosion inhibitors.

Most of the azoles have also been studied in the multilayer regime primarily to show the difference between the monolayer and multilayer bonding mechanisms and also to aid the assignment of vibrational spectra.

No portion of work referred to in this thesis has been submitted in support of an application for another degree or qualification of this or any other university or institute of learning.

The author graduated with a B.Sc. (Hons.) degree in Chemistry from Liverpool University in 1991. In 1992 he obtained an M.Sc. in Surface Science and Catalysis from the Leverhulme Centre for Innovative Catalysis at the University of Liverpool. From that time until 1996 he was engaged in full time research in the Department of Chemistry at the University of Manchester under the supervision of Dr. G. Thornton.

CHAPTER 1
Introduction

One of the most powerful tools available to study the chemical structure of molecules is vibrational spectroscopy. It is particularly popular amongst chemists as group frequencies serve as fingerprints for different functional groups. Hence, for organic and inorganic complexes the technique readily provides a direct means of accessing a wealth of information regarding bonding and structure. Naturally these ideas have been extended to surfaces and it is not surprising that surface vibrational spectroscopy has similarly developed into one of the most powerful techniques for studying both molecular and atomic adsorbates. Strict surface selection rules help to provide a wealth of information regarding the state of adsorbate, binding site and symmetry as well as interactions between molecules in the adlayer. When combined with other surface spectroscopies such as LEED and TDS, etc. a detailed structural analysis can be made.

This thesis describes the use of High Resolution Electron Energy Loss (HREELS) and Reflection Absorption Infrared Spectroscopy (RAIRS) as tools for studying the orientation of molecules on single crystal surfaces. In particular, it is aimed at studying the orientation of ligands which are important in the field of corrosion inhibition. Specifically, we have examined the orientation of benzotriazole and related molecules on copper.

A corrosion cost estimate has been carried out by most industrialised countries, revealing that the overall cost is several percent of the gross domestic product. The problem posed by such a costly process has therefore attracted quite an amount of investment, in an attempt at finding better and more cost effective solutions. One of the issues addressed by this thesis is the interaction of corrosion inhibitors with metal components.

A key point to be considered is the role played by the first bonding layer in

determining the success, or otherwise, of the chosen molecule, when its ability to protect a metal from corrosion is considered. The particular traits of a potent corrosion inhibitor, chosen from a related series of molecules have several factors which potentially contribute to its particular efficacy. These are the strength of bonding, the orientation of the first bonding layer and number of available anchoring points to the surface. In an attempt to clarify which are the more important factors for benzotriazole, a number of related molecules were selected for study. These include both good and bad corrosion inhibitors.

Surface vibrational spectroscopies, High Resolution Electron Energy Spectroscopy (HREELS) and Reflection Absorption Infrared Spectroscopy (RAIRS) were used in this work. The theoretical background and technical details asssociated with these techniques are described in Chapter 2.

Benzotriazole ($C_6H_5N_3$, BTAH) coating of copper and brass has been established as an efficient method of corrosion inhibition for the past 50 years. However, the origin of the particular efficacy of benzotriazole, in terms of its detailed bonding, is unknown. In chapter 3 we investigate the possibility that its properties arise from the specific nature of the first layer bonding to the substrate. The orientation of benzotriazole on Cu(100) has been studied using HREELS and RAIRS. At submonolayer coverage, benzotriazole is found to adsorb with the molecular plane close to parallel on the clean and O_2 pre-dosed Cu(100) surface, as indicated by the features seen in the vibrational spectra. It then undergoes an orientational phase transition to a more upright geometry at saturation coverage. Spectra were also taken in the multilayer regime (100 K) to show the difference in bonding mechanisms between the two regimes.

Primarily, the aim of the experiments was to examine the orientation and possible bonding modes, but a possible, although sometimes tentative, mode as-

signment has been suggested for all the azoles experimented on and a summary of the results obtained are displayed in the Appendix.

In chapter 4 we examine the vibrational spectra of indazole, another good corrosion inhibitor. Indazole is found to bond in a perpendicular geometry at all coverages in the monolayer regime but orients in a more flat geometry in the multilayer regime. Aspects of the bonding modes and orientation are compared with BTAH.

Finally, vibrational spectra of three related poor corrosion inhibitors are reported in chapter 5. Differences in the molecular framework of the molecules are shown to have a drastic effect on the orientation and possible bonding mechanisms. These are discussed with a view to explain their poor corrosion inhibition properties.

CHAPTER 2

Instrumentation and Theory

2.1 Introduction

The two most widely used techniques for measuring surface vibrational spectra are Reflection Absorption Infrared Spectroscopy (RAIRS) and High Resolution Electron Energy Loss Spectroscopy (HREELS), both have proven to be potentially powerful with each having its own particular merits. Whereas, RAIRS provides high resolution and only observes vibrational modes normal to a metal surface, HREELS can provide a higher sensitivity, larger spectral range and measure vibrational modes parallel to a surface. Although the majority of the work to date has been carried out using HREELS, RAIRS is becoming increasingly popular as commercial infrared spectrometers become cheaper and increasingly more sensitive. The two experimental systems used in this work will be described separately in this chapter. The electron energy loss spectrometer used was based at the University of Manchester, Chemistry Department whilst the Reflection Absorption Infrared Spectrometer was based at the Interdisciplinary Research Centre at Liverpool. The description of the chambers and associated equipment as well as the theory will be kept to a minimum as much literature is readily available concerning the instrumentation of HREELS [1-4] and RAIRS [1-7]

2.2 The EELS Experiment - The EELS Instrument

A schematic cross section through the EELS spectrometer is shown schematically in Fig 2.1. This instrument is the commercially available VSW EELS instrument and consists of a non-magnetic stainless steel bell jar with an electron analyser and monochromator situated at the lower level of the chamber. In normal operating conditions the chamber is pumped by a liquid nitrogen trapped diffusion pump and titanium sublimation pump. Oil free evacuation of the system is achieved using a carbon vane pump to obtain a pressure of ~ 2/3 bar

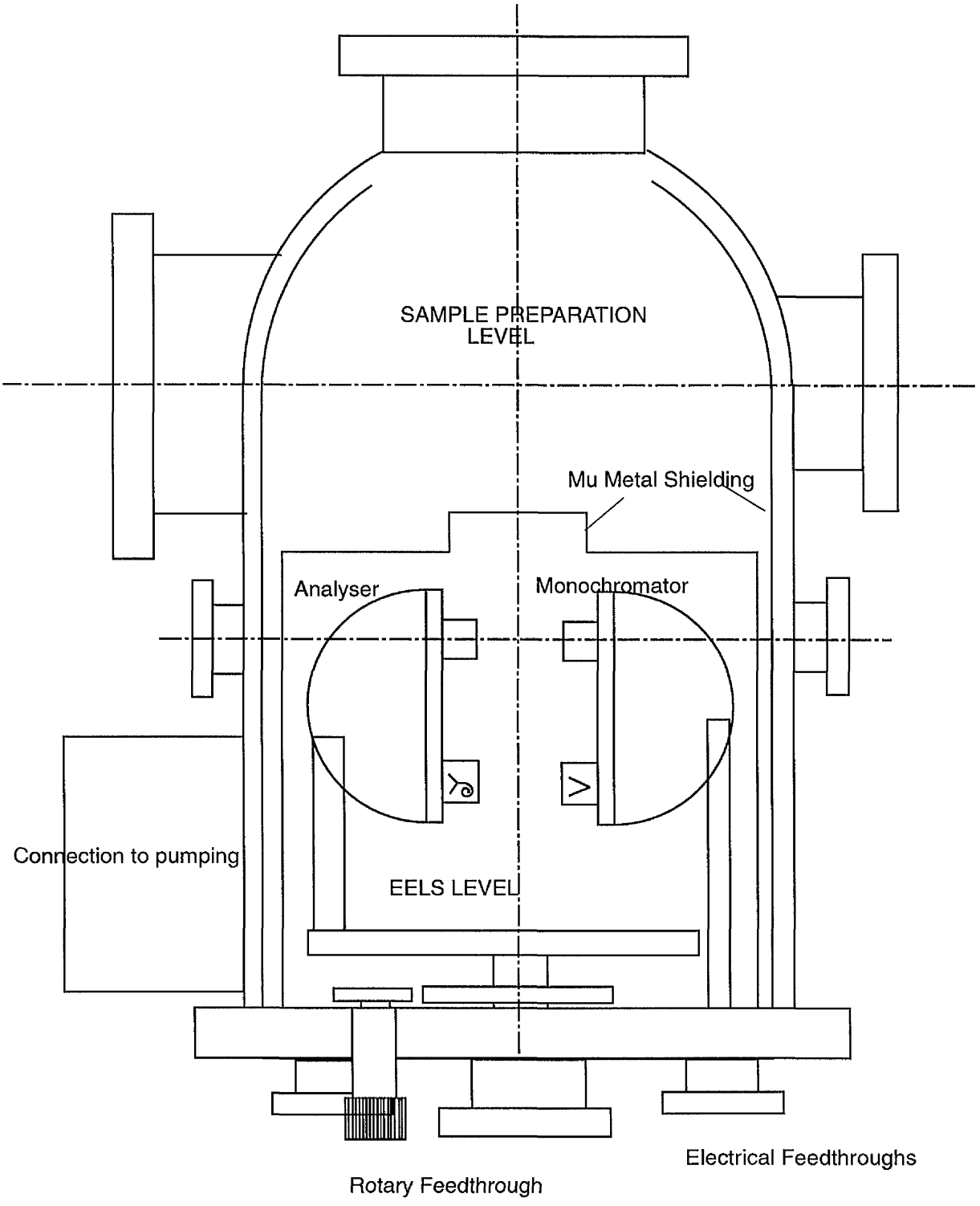

Figure 2.1 . Section through the EELS experimental chamber.

followed by the use of a liquid nitrogen cooled sorption pump to reach a pressure below $1x10^{-3}$ mbar at which point the chamber can be opened to the diffusion pump. A routine baking procedure achieves a base pressure in the region of 1×10^{-10} mbar. The pressure was monitored using ion gauges placed in the main chamber and near the diffusion pump. At all times UHV clean handling procedures were followed. The chamber is lined with a layer of mu metal (two layers in the lower half of the chamber) to prevent stray magnetic fields affecting measurements. Any magnetic fields will affect the trajectory of the low energy electrons used and this may have a detrimental effect on the resolution and the signal to noise ratio of the spectrometer.

2.2.1 The Upper Level

As can be seen in Fig 2.1, the experimental chamber consists of two distinct levels. The upper level is concerned with the preparation and characterisation of the single crystal samples. The equipment used for this is:-

i) VG Microtech LEED Optics for LEED and Retarding Field Auger (RFA) Spectrometer. This consists of three grid front view LEED optics with an inbuilt electron gun (VG LEG 22). The LEED mode is used to check the sample long range order from the LEED pattern. In this mode the two outer grids are grounded and the centre one at a variable potential to filter out any inelastically scattered electrons. The screen is at a high potential of ~5 kV. This produces fluorescence when the elastically scattered electrons accelerate and impinge upon the screen.

The RFA Auger mode is used to check for surface contamination and is described in detail in numerous references,e.g. [12]. The RFA collection procedure used in this system is described in detail in the work of Wincott [1].

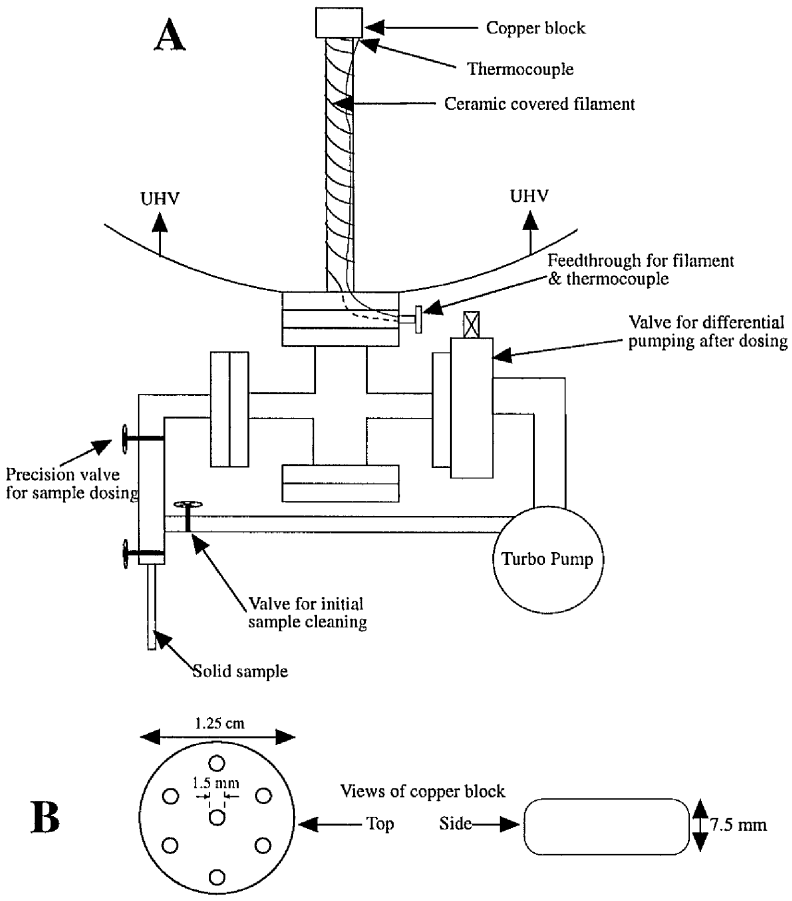

Figure 2.2 The setup used for dosing solids

ii) Phi Ion gun used for sample cleaning.

iii) Organic compound dosing source. The gas/solid dosing arrangement was constructed for dosing the solid samples such as benzotriazole, and the related molecules. These samples required a constant above-ambient temperature (100 - 150° C) throughout the doser to maintain a constant vapour pressure throughout the doser. Preparatory work showed that any cold spots were capable of condensing these solids. A schematic of the doser is shown in Fig. 2.2A. The addition of the copper block at the end of the dosing arm is to try to ensure a uniform dose.

over the surface area. However, considering the dose time and quantity dosed, this is not expected to be a limiting factor in achieving a uniform coverage. A schematic of the copper block with the central hole surrounded by a hexagon of holes is shown in Fig. 2.2B. The diameter of the holes are 1mm, and the thickness of the block is 1cm. The size of the holes in the doser, specified in Fig. 2.2B, is preferred over those in a microchannel plate normally used in these dosers, due to the fact that the solid compounds may become trapped in the small sized holes of the microchannel plates when dosing.

iv) VG Quadrupole Micromass 200 for residual gas analysis (RGA).

All of the equipment described above has been described in many references [2,13].

2.2.2 The lower level

The high resolution electron energy loss spectroscopy (HREELS) measurements were carried out in the lower part of the chamber. The instrumentation basically consists of a monochromator to produce a highly monochromated beam of electrons and an analyser to measure the energy lost from the electron beam after scattering from the sample surface. The analyser is mounted on a rotatable goniometer table to allow measurement away from the specular direction.

2.2.3 The EELS HA 50 Analyser

The EELS analyser is a HA50 hemispherical analyser (VSW Scientific Instruments Ltd.), which consists of two concentric hemispheres with a common centre, a lens system and an electron detector. The analyser takes electrons from

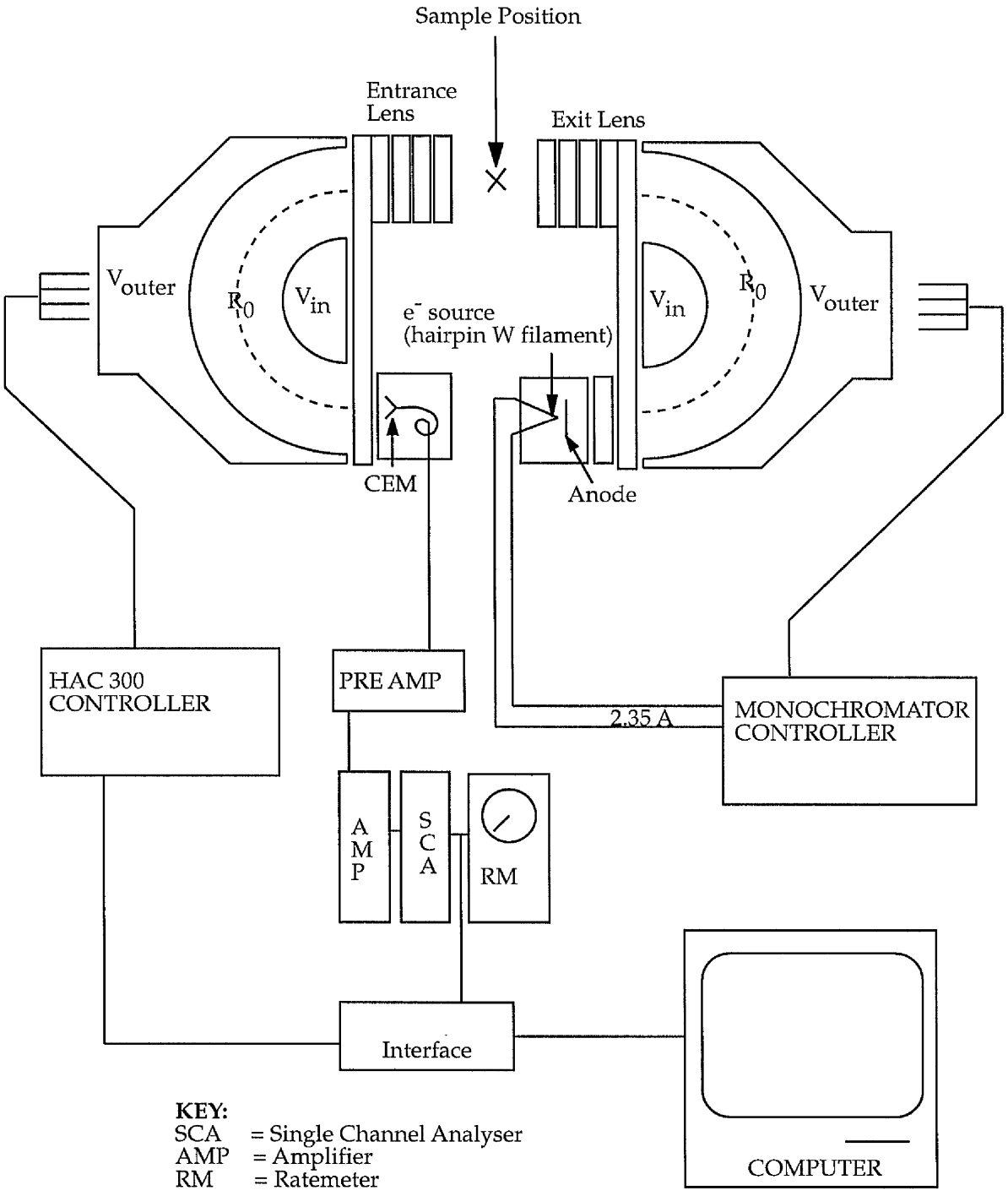

Figure 2.3 Schematic diagram of the analyser, monochromator and associated electronics

a narrow cone (typically 2°). The HA50 is mounted on a rotatable goniometer which allows rotation of 110° to -30° relative to the straight through position. This, in conjunction with the rotation of the sample, allows the angles of incidence and scattering to be varied. The four element input lens is designed to match the spot size on the sample and can zoom over a range of retardation ratios (retardation ratio = kinetic energy/pass energy). A three element lens configuration is also available. In this work, however, only the four element lens configuration was used. The lens focuses the incoming electron beam from the sample, which is positioned 20 mm away from the outer casing of the analyser, onto the 1 mm diameter entrance aperture of the hemispheres, at the same time accelerating/decelerating the electrons to a constant pass energy which determines the resolution. This mode of operation is known as Fixed Analyser Transmission (FAT) since a constant pass energy is used.

The outer hemisphere has a slot in it to allow electrons of energy higher than that chosen to pass through and thus eliminate this potential source of noise. This slot may also be used for alignment purposes, either with the sample or the monochromator, which has a similar slot. Shining a laser or other collimated light source through either the analyser or monochromator and looking through the other allows the straight through position to be attained easily. The electrons of the chosen energy of the analyser will then pass through the exit slit (1 mm) of the hemispheres which acts to reduce the effects of mechanical misalignment. Jost electrodes are used to reduce fringing field effects at both the entrance and exit planes of the hemispheres and thus keep the electron image distortion and the noise level low. The electrons then reach the channeltron, or channel electron multiplier (CEM, Mullard X919, BL/01). The front of the multiplier is kept at a potential approximately 10% of that at the rear, which was generally at 2.3 kV. The potential gradient across the CEM and its high secondary electron emissivity result in a cascade of electrons with a gain of approximately 10^8 [14].

Thus, for an electron striking the front of the multiplier a current pulse is produced at the rear which is converted to a voltage pulse by a charge sensitive preamplifier attached to the outside of the chamber. A schematic diagram of the analyser, monochromator and associated electronics is shown in figure 2.3.

There are seven different pass energies which may be chosen with the resolution being reduced as the pass energy is increased. In practice, for the high resolution electron energy loss spectroscopy in the experimental work presented here, a pass energy of 1 eV was used. With a pass energy of 1 eV in the monochromator a straight through resolution of 7 meV (measured as the FWHM of the elastic peak) was obtained and a resolution of approximately 7-8 meV was obtained for specular reflection from a clean Cu(100) sample.

2.2.4 The Electron Monochromator

Like the analyser, the monochromator consists of a hemispherical energy resolving section and a lens system. However, in place of the electron detector there is an electron source. The source consists of a hairpin tungsten filament, heated by passing a current through it (2.35 amps) which produces a Maxwellian thermal distribution of electrons. The monochromator control unit allows the potential of the filament and grid to be changed with respect to the rest of the spectrometer. This allows the user to tune in on the peak of the Maxwellian distribution and thus increase the intensity of the electron beam. A lens system transmits the electrons onto the entrance aperture of the hemispherical energy resolving part of the analyser. Radial and angular defining slits are used for good resolution; one in the anode and one in the selector entrance (0.5 mm). The hemispherical energy analyser is then used to select a narrow bandwidth in the centre of the Maxwellian distribution. The exit aperture of the energy selecting hemispheres is also 0.5 mm. The electrons are then accelerated / decelerated to

the required kinetic energy and will then strike the sample which, as for the analyser, is positioned 20 mm away. The exit lenses of the monochromator are designed to exactly match those of the analyser entrance lenses. As in the analyser there is a slot in the outer hemisphere of the monochromator. Shining a laser through this slot and observing the position of the spot on the sample gives a quick and simple check on whether the electron beam is striking the sample. The pass energy of the monochromator is continuously variable from 0 - 50 eV, although for the work on Cu(100) presented in this a pass energy of 1eV were used. This, in conjunction with a pass energy of 1 eV in the analyser, gave an acceptable resolution (approx. 8 meV) whilst maintaining a reasonably high intensity (generally 5000-50,000 s^{-1}) in the elastic peak.

2.2.5 Computer Control of Experiments

As can be seen in Fig 2.3 of the EELS instrumentation and associated electronics the data is acquired with a computer. The data acquisition used "in house" software [15] for Macintosh computers. Basically a 0-10 V ramp is produced by a 16 bit digital to analogue converter (DAC) in an interface. This is fed into the HAC 300 control unit (VSW Scientific Instruments) and can be used either to scan the whole energy range of the HAC 300 (0 - 300 eV) or between energies set by potentiometers on the HAC 300 control unit. The voltage pulses produced by the preamplifier are fed into a counter chip on the interface.

2.2.6 Sample Manipulator

The sample is mounted on an x,y,z manipulator (VG) allowing the sample to be moved between the two levels. The manipulator also allows 360° polar rotation of the sample and rotation in the azimuthal direction. In this work the sample is always kept in the same azimuthal direction. The sample is mounted on a 1.5

mm thick Mo plate via Ta clips. Sample heating to 1300 K is possible via an electron beam heater situated below the sample plate. A chromel-alumel thermocouple is attached directly to the sample plate for temperature measurement. During EELS measurements the sample is grounded via the manipulator to prevent problems associated with sample charging.

2.3 Theory of Electron Energy Loss Spectroscopy.

In the basic experiment, a monochromatic beam of electrons of energy, E_i, striking a surface will excite vibrational modes of energy, $h\omega$, on the surface. The energy of excitation is lost from the electron beam giving a characteristic energy loss E_s, for the vibrational mode which is stimulated.

This gives us the simple energy loss equation,

$$E_S = E_i - h\omega \qquad \text{- Equation 2.1}$$

Using low energy electrons (0-20 eV) means the penetration depth into the sample is small as these low energy electrons interact strongly with surface. In addition, using these low energies has an advantage in that beam damage to the sample is minimal. The initial application of HREELS was to study surface Fuchs -Kliewer phonons of the ZnO (0001), (000$\bar{1}$) and (1$\bar{1}$00) surfaces [3]. Since then the technique has been applied to numerous problems in surface science [3, 16, 17]. Developments in analyser and monochromator designs over the last few years have led to EELS spectrometers capable of resolutions better than 1 meV (measured as the full width at half maximum of the elastic peak). This compares to a typical resolution of 0.1 meV in ir spectroscopy. Although the resolution is considerably lower than that for infrared spectroscopy, HREELS has advantages such as an easily accessible large spectral range and the possibility of probing non-dipole excitations by measuring the loss spectrum away from the specular direction.

Dipole scattering is governed by the dipole selection rule, which states that only vibrational modes with a component perpendicular to the surface can be seen in HREELS, although this becomes relaxed for semiconducting and insulating materials.

This is illustrated schematically in Fig. 2.4 where CO is adsorbed on a metal surface. The perpendicular mode is "seen" by the incoming electron at a large distance from the surface r_e. As long as this distance is much larger than the distance of the dipole from the surface then only motion perpendicular to the surface is detected due to the induction of an image dipole as shown in figure 2.4a. Vibrational modes parallel to the surface, however, also produce an image dipole at the surface but here this almost cancels out the actual dipole (figure 2.4b) depending on the dielectric constant of the surface. It is found that dipole moments parallel to the surface will have a reduced scattering factor $\sim |\varepsilon|^{-2}$ [18].

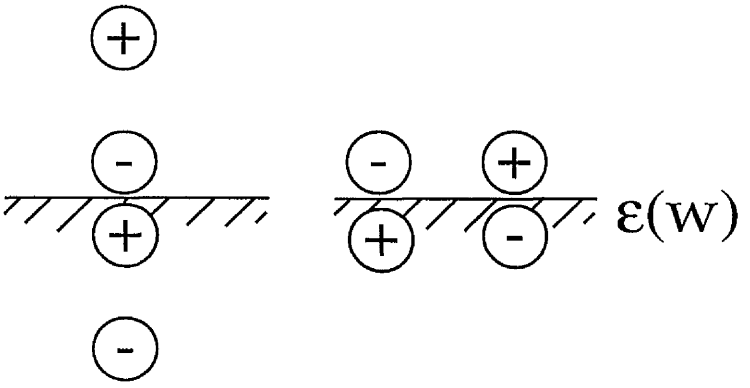

Figure 2.4 Effect of placing a dipole a) perpendicular and b) parallel to a surface.

2.3.1 Scattering in the Specular Direction

There are three limiting mechanisms by which the energy transfer between the electron and the surface can occur. These are,

1) Dipole scattering,

2) Inelastic scattering after formation of an intermediate negative ion resonance and

3) Impact scattering. Although it is implied there is a smooth transition from one mechanism to another it is simpler to treat them separately [3]. The specular direction is that where the angle of electron incidence is equal to the electron scattering angle. Dipole scattering arises when the vibrating species produces a time-dependent dipolar oscillation in the environment immediately above the surface. An electron approaching the surface will sense this long range oscillation and be deflected through a small angle by it. These dipolar scatterings are generally of a much higher intensity than scattering by any other mechanism, which makes EELS a useful tool for the study of vibrational modes.

The loss spectra obtained in the dipole region can be calculated from the dielectric response of the surface to the potential of the incoming electron beam [19,17]. As the momentum transfer parallel to the surface $k_{||}$ is very small in the dipole regime it can be assumed that the dielectric response function depends only on the frequency [20]. This then allows calculation of the probability $P(\omega)$ of an electron losing energy $h\omega$ from the electrostatic work done by the surface on the electron. A loss function is obtained and when integrated over all scattering angles, the intensity peaks strongly in the specular direction giving

rise to the so-called "dipole lobe" [21] This is due to the conservation of parallel momentum. For the purposes of this work it is not necessary to derive the loss function but further information on the theoretical aspects of dipole scattering, the reader is referred to Chapter 3 of "Electron Energy Loss and Surface Vibrations" [3].

2.3.2 Scattering in the Off Specular Direction

There are two mechanisms by which the electron may be scattered away from the specular direction, namely formation of a negative ion resonance and impact scattering.

Negative ion resonances occur when a surface molecule is able to capture an electron to form a negative ion. This is a well known process in the gas phase. However, when a molecule is chemisorbed, the coupling of the adsorbate/ substrate electron states leads to a very short lifetime. A recent review [22] describes the effects of negative ion resonances at surfaces in more detail.

Another type of excitation observable in the off specular scattering region involves the process of impact scattering. This leads to one of the advantages of HREELS over infrared spectroscopic methods in that dipole forbidden transitions and vibrations may be probed in this region. However for a full theoretical treatment of the impact scattering mechanism a complex quantum mechanical analysis is required. For further information on this the reader is referred to Chapter 3 of "Electron Energy Loss and Surface Vibrations" [3]. For the purposes of this work it is sufficient to mention some of the consequences of off specular

scattering. For instance it has been found found for H on W (100) that whilst the primary loss due to H vibrating perpendicularly to the surface decreases in intensity, its overtone and a parallel vibration actually increase with maxima at ~ 15° off specular [3]. Thus the intensity of the parallel vibrations is increased relative to the perpendicular vibrational modes in the off-specular direction.

2.4 The RAIRS Experiment

To measure the vibrational spectra of adsorbed species on metal surfaces using RAIRS, an existing dedicated uhv instrument was used, a schematic of which is shown in Fig 2.5.

The custom built instrument consists of a uhv chamber coupled to a Mattson Galaxy FT-IR spectrometer. The chamber has standard facilities for the preparation and characterization of single crystals, including, LEED optics (VG 3 grid system), with RFA/AES and VG mass spectrometer, an argon ion sputter gun (VSW, AS10) and various pressure measurement gauges and leak valves already described in section 2.2. The infrared cell has two KBr windows mounted in differentially pumped holders. The system is pumped with a Balzers turbo pump (330 ls^{-1}) in association with a water cooled titanium sublimation pump, routinely achieving a base pressure less than $2x10^{-10}$ mbar. Cooling is achieved by filling of a cold finger probe on the manipulator with liquid nitrogen, temperatures of ~90 K could be readily achieved in this way. The crystal is mounted with 0.2 mm tantalum wire.

2.4.1 Organic Compound Dosing Source

A different dosing source was constructed to enable compatibility with the RAIRS chamber. A schematic of the doser is shown in Fig. 2.6. It basically consists of a tungsten filament wrapped around a glass tube in which the organic compound is placed. The filament is connected directly to the feedthrough at point A in Fig 2.6 and is attached to a second feedthrough via a tungsten rod at point B. Temperatures of 150° C and above could readily be achieved. The glass tube was constructed such that there was a kink at its mid-point to ensure that none of the sample fell into the chamber.

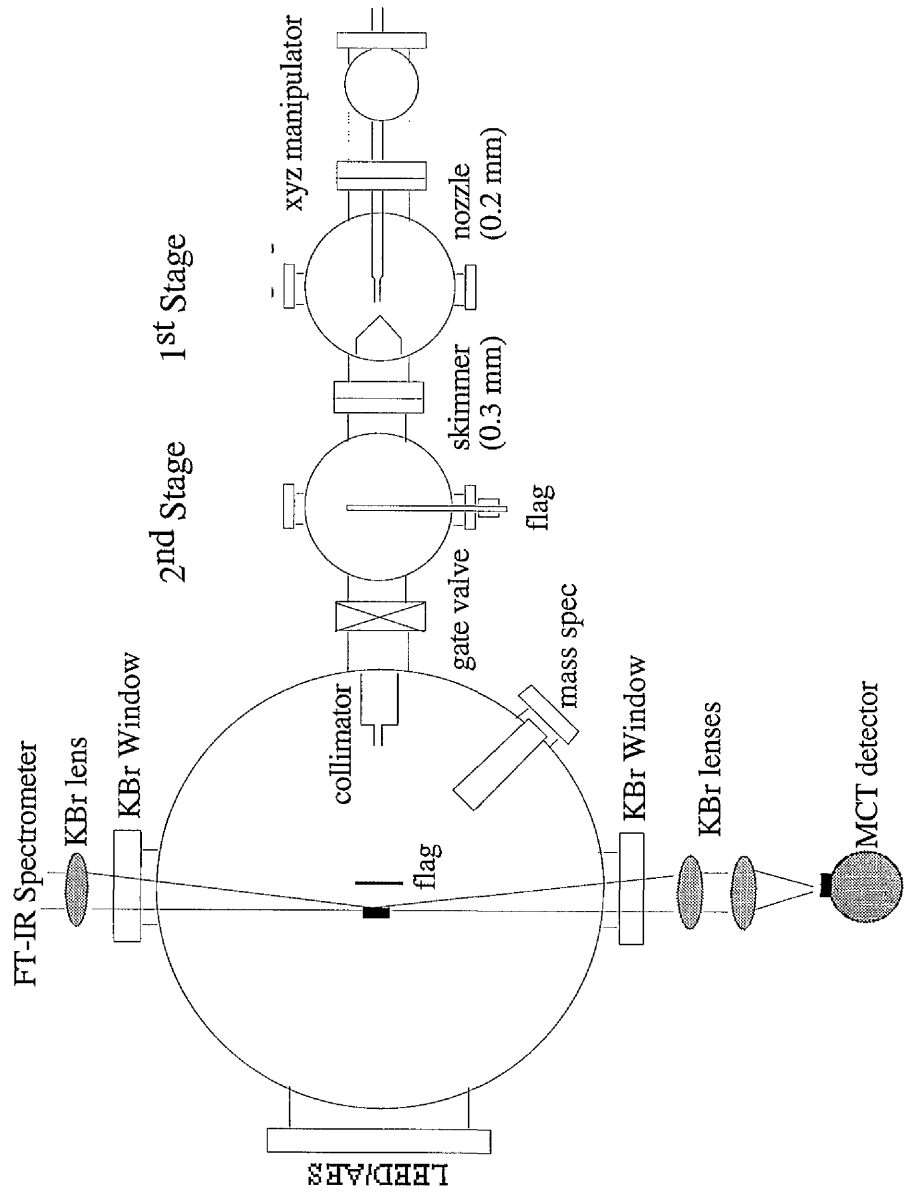

Figure 2.5 Section through the RAIRS experimental chamber.

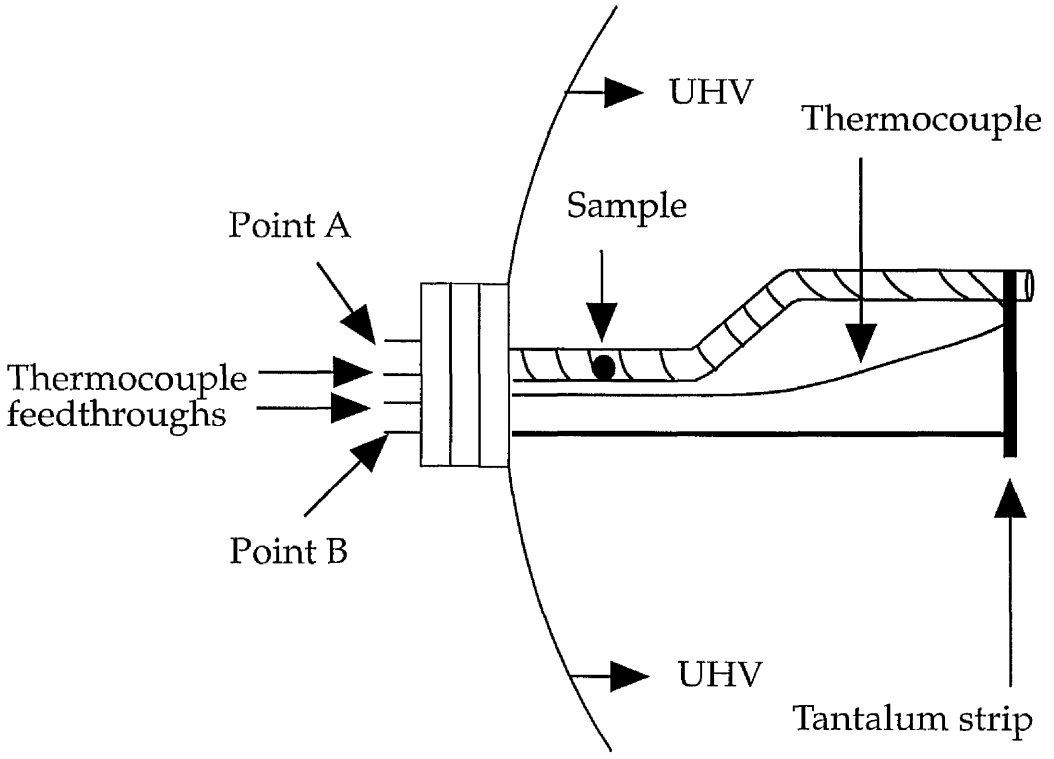

Figure 2.6 The setup used for dosing solids into the RAIRS chamber.

2.4.2 FT-IR spectrometer

A typical FT-IR spectrometer optical system is shown in Fig. 2.7 It generally consists of two mirrors, an infrared light source, an infrared detector and a beamsplitter. The general operation involves the beamsplitter dividing the incident light beam, allowing light to travel to both a stationary and moving mirror. The two mirrors reflect both beams back to the beamsplitter where the light rays recombine. Half the recombined light is transmitted to the detector and half is reflected back to the source. When the two light beams recombine at the beamsplitter, an interference pattern is generated. This interference pattern varies with the displacement of the moving mirror along its axis and is detected by the infrared detector as variations in the infrared energy level.

An example of how light is affected within the spectrometer can be given if we

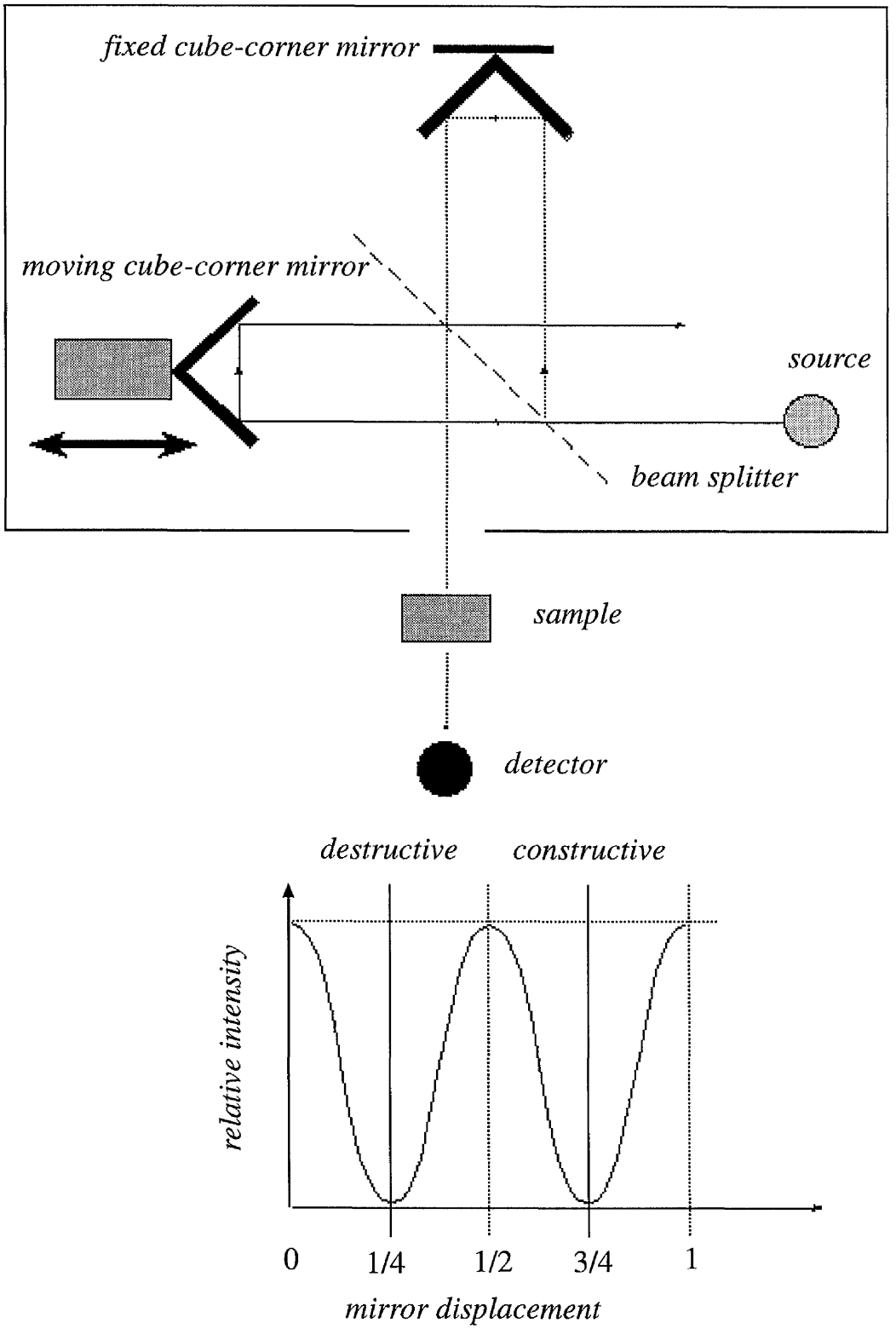

Figure 2.7 An FT-IR spectrometer's basic layout along with the optical paths followed by the light beam. Shown in the lower portion is an *interferogram* expected from a *monochromatic* source.

consider the interference pattern when a monochromatic light source is used. If at any given time the mirrors are equidistant from the beamsplitter, the two light beams travel equal distances, return to the beamsplitter in phase and recombine constructively. In contrast, if the moving mirror is displaced by one-quarter of the wavelength of the source, the returning light will be one-half wavelength out-of-phase with respect to the light returning from the fixed mirror. This results in complete destructive interference at the beamsplitter. The signal received by the detector produces an interferogram that is a cos function, illustrated in the lower portion of figure 2.7 Infrared sources emit light over a broad range of frequencies, each frequency producing a unique sine signal. The resulting interferogram represents the sum of each sine wave generated by each individual frequency component of the light source. The frequency and intensity of each sine wave can be resolved by a Fourier transformation procedure. A computer uses this algorithm to convert the measured intensity-displacement signal (the interferogram) into an intensity-frequency plot (a spectrum).

To ensure maximum spectrometer performance it is necessary to use a dry air purge. The primary criteria on the purge gas is that CO_2 and H_2O are not present

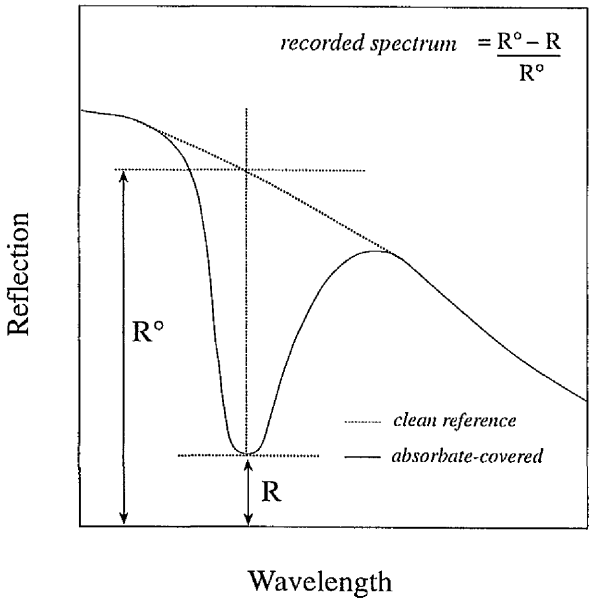

Figure 2.8 The definition of the measured absorbance spectrum

and that a continuous flow is directed through the optical cavity of the instrument. This prevents atmospheric absorption bands in the optical paths, which is particularly critical for the wavelength region below 2000 cm^{-1}, where water bands can be several orders of magnitude larger than the absorption signal from the sample.

All spectra presented have been processed from the absorption signal obtained from the adsorbate-covered surface (R) and that of a clean surface reference signal (R°), illustrated in Fig. 2.8. Each spectrum was collected at a beam resolution of 4 cm^{-1} with normally about 256 scans co-added. This was to allow a reasonable signal-to-noise to be achieved.

For a more technical description of the Mattson Galaxy series spectrometer the reader is referred to the comprehensive instruction manual and particularly, Chapter 2: Theory and Terminology [23].

.

2.5 Theory of Reflection Absorption Infrared Spectroscopy

A molecule in the gas phase may undergo a vibrational excitation by the resonant absorption of infrared radiation. The transition being induced by the interaction of the electric field vector of the incident radiation (E) with the electric dipole moment changes with the displacement of the normal coordinate, i.e. for a non zero dynamic dipole moment (μ). The intensity of the vibrational transition from an initial state $|i\rangle$ to final state $\langle f|$ is given by [5, 7],

$$I \approx \left|\langle f| \mathbf{E}.\mu |i\rangle\right|^2 \qquad \text{Equation 2.2.}$$

$\langle f|$

For maximum absorption to occur the electric field vector E has to be parallel to μ, the dynamic dipole moment. This dipole excitation rule is equally valid for a molecule adsorbed at a surface. Thus the absorption of infrared radiation by a molecule on a surface is dominated by the dielectric behaviour of the metal since the electric field of the incident radiation as well as that of the dynamic dipole moment of the molecule will interact with the metal conduction electrons.

The physical basis and the selection rules for the RAIRS experiment can be derived by considering the reflection of infrared radiation from a clean metal surface incident at an angle θ to the surface normal, as shown in Fig 2.9 [7].

The amplitude and phase changes experienced on reflection depend on the direction of the electric field vector of the incident wavefronts, hence it is convenient to resolve the electric field vectors into components parallel to the plane of incidence (p-polarisation) and perpendicular to the plane of incidence (s-polarisation). The phase shift calculations show that the s component (Es) undergoes a phase change of nearly 180° for all angles of incidence, thus giving a vanishing electric field at the surface for all angles of incidence. However, the phase shift of the p component (Ep) is strongly dependent on the angle of incidence. At high angles of incidence a resultant electric field normal to the surface is produced, being enhanced by nearly a factor of 2. Figure 2.10 shows the variation of the surface electric field with the angle of incidence, Ep has been resolved into components parrallel (Ep$||$) and perpendicular (Ep$\perp$) to the surface. The intensity of the absorption depends on the square of the surface electric field and the number of molecules the beam covers, ie $E^2\sec\theta$, this function plotted as a function of θ shows a sharp maximum at 87° and falls off rapidly to zero at 90°, this is shown for Ep$\perp$ in Fig. 2.10b [7]

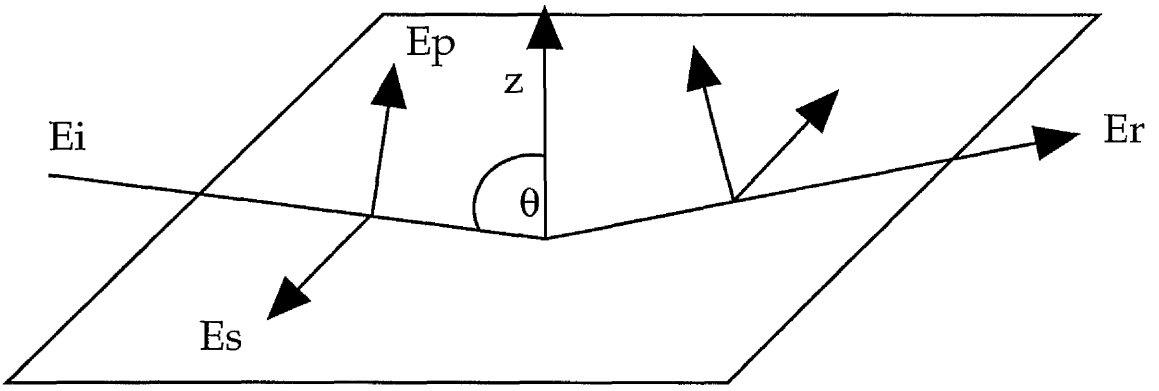

Figure 2.9 Reflection of infrared light from a clean metal surface

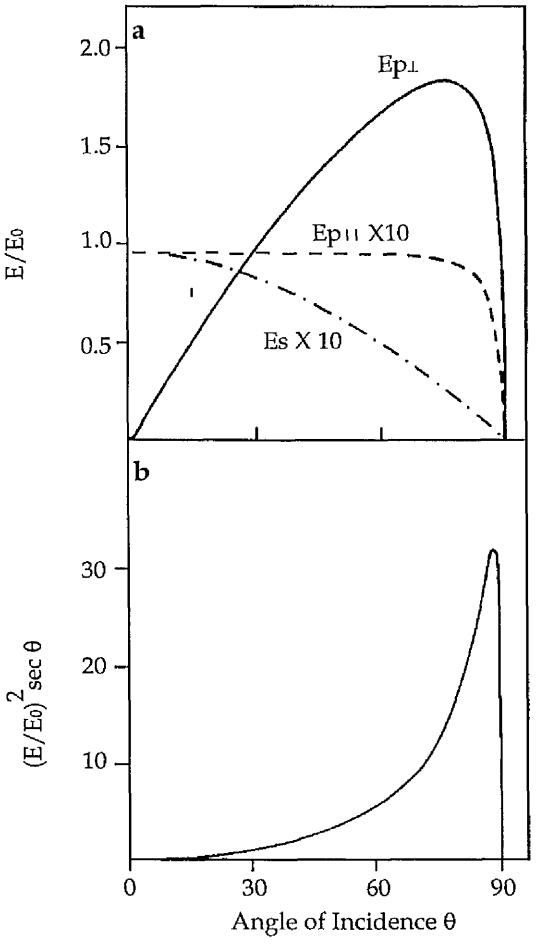

Figure 2.10 Variation of, a) surface electric field, b) surface absorption intensity, as a function of angle of incidence, θ.

However, when the surface is covered with an adsorbate the optical properties of the adsorbate have to be considered, and strictly a 3 phase model, vacuum-adsorbate-metal, should be solved. A more exact description has been formulated by Greenler [11], however the general principles already discussed remain.

Finally, as has already been mentioned the interaction of the dipole moment of a molecule with a metal surface has to be considered. The response of the metal surface that screens out the electric field parallel to the surface will also screen out any dynamic dipole moment appearing on the molecule in a direction parallel to the surface. This is visualised, similar to the HREELS experiment, as a virtual image dipole in the surface, as the metal conduction electrons in the vacinity of the adsorption site rearrange to screen out the dipole field. Figure 3 graphically shows two dipoles orientated parallel and perpendicular to the surface, whereas the latter is reinforced by its image in the metal, the parallel dipole is effectively cancelled out as it interacts with its image. The screening effect of the metal of both the incident radiation and the dynamic dipole moment leads to the metal surface selection rule that only those vibra-

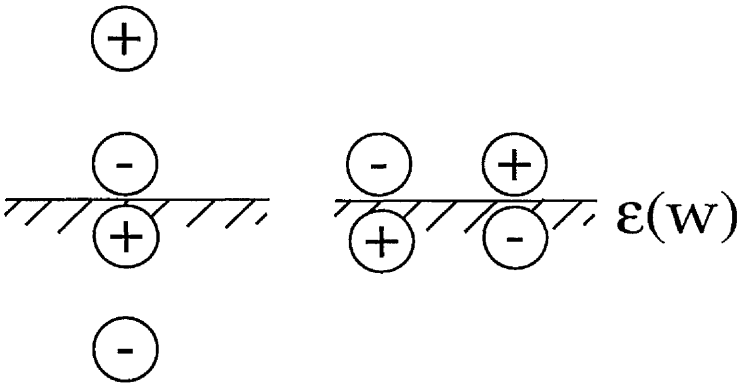

Figure 2.11. Screening of a dipole by the metal conduction electrons.

tions with a dipole moment perpendicular to the surface will be infrared active [7].

If the reader wishes further information on the experiment or theory he is referred to any of the references [5-11].

2.6 Wavenumbers and internal modes

If vibrational spectra for a molecule adsorbed on a metal surface are compared with those of the corresponding free gaseous species, two dramatic effects become immediately apparent, namely a change in vibrational frequency which often shifts with increasing coverage and an increase in the bandwidth. The factors contributing to the frequency shift include : a) an increase in frequency due to mechanical renormalisation, as the molecule is no longer free and is fixed to more or less rigid surface; b) lowering of frequency due to the electrodynamic interaction of the dipole with its own image, c) a chemical effect, with a change in electronic structure due to orbital overlap and mixing; and d) lateral interactions between neighbouring molecules in the form of dipole - dipole coupling. These effects have been exhaustively discussed for the adsorption of carbon monoxide on transition metal surfaces [7].

For adsorption of CO on metal surfaces there is generally a decrease in frequency from the gas phase value of 2143 cm^{-1}, by as much as 200-300 cm^{-1}, depending on the adsorption site or bonding character. In general, the coordination sites for CO are categorised to take values between 2100-2000 cm^{-1} for ontop bonding, 2000-1900 cm-1 for two fold bridge bonding and 1800-1900 cm^{-1} for bonding in three fold hollow sites. In the Blyholder model of CO bonding to metal surfaces, the bonding interaction is between the filled 5σ and empty $2\pi^*$ orbitals of the molecule with the metals states of the appropriate symmetry.

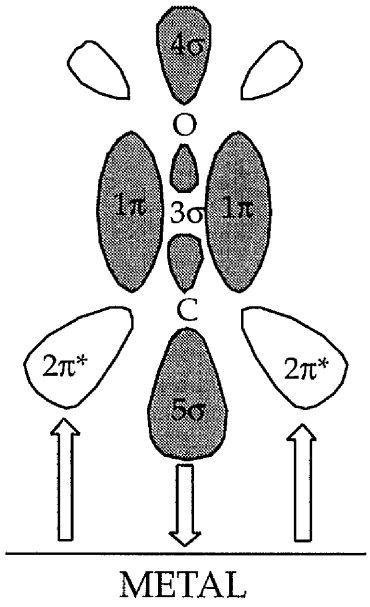

Figure 2.12. Schematic of the Blyholder bonding model for CO.

The depletion of electron density from the 5σ to the metal leads to a small increase in frequency, as this is weakly bonding in character with respect to the C-O bond. However, the $2\pi^*$ is strongly antibonding and donation of electron density from the metal into this orbital leads to a large decrease in the vibrational frequency. The latter largely determines the bonding shift which is dependent on the metal and the adsorption site.

Lateral interactions, whether through space or through substrate are important contributors to the observed frequencies. One of the strongest influences on vibrational frequencies of adsorbed molecules is long range dipole - dipole coupling. Dipole coupling is a coverage dependent phenomena largely arising from the depolarization of the dynamic dipole moment from the dipolar fields of neighbouring molecules. This generally leads to an increase in frequency with increasing coverage. Frequency shifts arising from dipolar coupling can be separated from chemical shifts by using a mixture of two different isotopes of the molecule. At constant coverage, the chemical shift is independent of

isotope, whereas the dipolar coupling is different as two molecules of different isotopes cannot couple.

Finally, the dramatic change in bandwidth from $1x10^{-3}$ cm^{-1} for gas phase molecules to values between 2-100 cm^{-1} for molecules adsorbed on a metal surface is directly attributed to the decrease in the lifetime from milliseconds to picoseconds for adsorbed molecules. In the gas phase a vibrationally excited molecule can only decay via the re-emission of an infrared photon or by an intramolecular relaxation process. For the adsorbed molecules two further channels become available, namely, the creation of electron-hole pairs and phonons in the substrate. Inhomogeneous broadening also becomes important as an ensemble of molecules may include some with different local environments. Electron-hole pairs can be created either through the oscillating electric dipole field or through charge transfer in the oscillation cycle as the $2\pi^*$ level crosses the fermi level as the molecule vibrates. For the internal modes of CO the probability of relaxation by creation of phonon is small as generally a number of phonons have to excited simultaneously.

A last point which needs mentioning is that of the phenomenon known as a Fermi resonance. If accidentally degenerate vibrations are of different symmetries, no intraction can occur between them, and the two are merely superimposed in the spectrum. If they are of the same symmetry interaction occurs between them , which is termed a Fermi resonance. The result of a Fermi resonance occurring between two vibrations of almost the same frequency is to decrease the frequency of the lower frequency mode and increase the higher frequency one, and if one of the bands would have been much weaker than the other, to equalise their intensities - the 'weaker' borrows intensity from the stronger. Fermi resonance can occur between two fundamentals or, quite commonly, between one fundamental and one combination or overtone.

References

[1] P. Wincott, PhD thesis, University of Manchester, 1986,

[2] N. Brookes, PhD thesis, University of Manchester1987,

[3] Ibach and Mills, Electron Energy Loss Spectroscopy and Surface Vibrations. Academic Press NY. (1982).

[4] P. Bailey and F. M. Quinn, Daresbury Technical Memorandum. 1993 DL/SCI/TM94E.

[5] F.M. Hoffmann, Surf. Sci. Rep. 3 (1983) 107.

[6]P. Hollins and J. Pritchard, Prog. Surf. Sci. 19 (1985) 275.

[7]Y. Chabal, Surf. Sci. Rep. 8 (1988) 211.

[8]B.E. Hayden, in Methods of Surface Characterisation Vol. 1, Ed. J.T. Yates and T.E. Madey (Plenum 1987) 267.

[9]R. Ryberg, in Advances in Chemical Physics, Ed. K.P. Lawley (John Wiley and Sons1989).

[10] A.M. Bradshaw and E. Schweizer, in Spectroscopy of Surfaces, Ed. R.J.H. Clark and R.E. Hester (John Wiley and Sons 1988).

[11]R.G. Greenler, J. Chem. Phys. 44 (1966) 310.

[12] G. E. Rhead, J. Vac. Sci. Technol., 13(1976) 603

[13] F. Schedin, PhD thesis, University of Manchester, 1993

[14] Mullard Technical Information, Publication No. 13 : Single Channel Electron, 1976.

[15] P. Hardman, PhD thesis, Manchester, 1992

[16] P. A. Cox, Transition Metal Oxides, Clarendon Press, 1992

[17] V. Henrich and P. A. Cox, The Surface of Metal Oxides. Cambridge University Press (1994).

[18] H. Froitzheim, Electron Spectroscopy for Surface Analysis. Topics in Current Physics 4, Springer-Verlag Berlin (1977).

[19] Ph. Lambin, J-P Vigneron, Computer Physics Commun. 60 (1990), 351.

[20] W. R. Flavell, J. H. Laverty, Daresbury Laborotory Preprint DL/SCI/P6956 (1990).

[21] B. N. J. Persson, Solid State Commun. 24 (1977) 573.

[22] R. E. Palmer and P. J. Rous, Rev. Mod. Phys. 49 (1982) 533.

[23] Mattson Galaxy series spectrometer instruction manual *Chapter 2: Theory and Terminology* [10].

CHAPTER 3

Vibrational Spectroscopy of Benzotriazole on Cu(100) in the monolayer and multilayer regimes

3.1 Background

Benzotriazole (BTAH) has the structure shown in Fig 3.1 and can be used to form a protective barrier on copper surfaces which consists of a complex between copper and BTAH. It can be formed by immersion of the Cu surface in a solution of BTAH, by vapour transport from impregnated paper or electrochemically [1-3]. This barrier is insoluble in water and many organic solvents, and grows with time to a certain thickness depending on BTAH concentration and pH of the solution into which the Cu surface is dipped [2]. BTAH

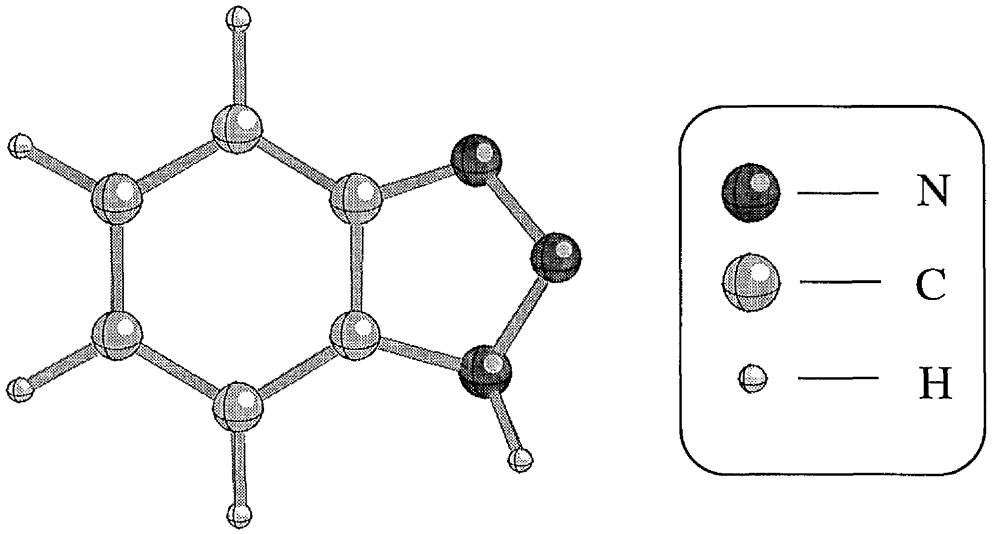

Figure 3.1 Benzotriazole (BTAH) in its molecular form.

and differently substituted derivatives of BTAH have been studied experimentally with respect to the inability to protect the surface from corrosion and to address the important adsorption sites of the molecule [1-14]. Some of the most important results from these studies will be briefly reviewed here.

Cotton and Scholes [1] showed that BTAH formed a protective layer on copper surfaces. The layer was found to consist of an insoluble Cu(I)BTA complex with a Cu : BTA ratio of 1:1. Poling and Ogle [2] investigated the adsorption of BTAH on copper surfaces with IR spectroscopy and electrochemical methods.

They proposed that the protective coating was a multilayer film consisting of Cu(I)BTA, the thickness of which increased at low pH. The formation of the multilayer involved transport of Cu to the solid/liquid interface where the physically adsorbed BTAH molecules reacted with Cu to precipitate in an in soluble Cu(1)BTA complex. Based on shifts in -N=N- bands and the absence of -N-H bands in the IR spectra, together with magnetic susceptibility measurements, Poling and Ogle proposed a structure containing chains of deprotonated BTAH molecules, every two BTAH molecules being linked via one Cu atom. This structure was also proposed by Cotton and Scholes.

Roberts [4] studied the adsorption of BTAH on Cu_2O and CuO surfaces with XPS. He found that the Cu(I)BTA complex formed during immersion of the Cu_2O surface in BTAH solution was gradually oxidised to the Cu(II)BTA complex after prolonged immersion. Chadwick and Haskemi [7] observed that the oxidation of the Cu(I)BTA to the Cu(II)BTA complex takes place during air exposure and not during immersion in the BTAH solution. Fox et al. [10] also reported some chemical aspects of the corrosion inhibition of copper by BTAH, and found that the rate of formation of cuprous and cupric complexes was almost identical. The effectiveness of the corrosion protection in an aggressive solution was strongly dependent on the presence of BTAH in the solution. Fox et al. [10] proposed from these results that the bulk precipitation of the complex on the surface provides the major corrosion protection.

Rubim et al [11] performed a CNDO/2 molecular orbital and an in situ surface enhanced Raman scattering (SERS) study of BTAH adsorbed on electrode surfaces. They made a model of the Cu(I)BTA polymer complex, thought to be produced, by introducing the benzotriazolate anion (BTA^- of C_2v symmetry), as a transition state. The C_2v symmetry of the molecule implies that the bond orders of the -N-N- bonds are equal and indicates that the π electrons are

delocalised over the 5- and 6- membered ring systems. Thierry and Leygraf [12] used SERS to address the concentration dependence on the orientation of the molecule on the Cu surface. Their results were taken to indicate a reorientation from a perpendicular to a more parallel configuration relative to the Cu substrate when the concentration was lowered. They also observed a strong frequency shift of the triazole ring breathing modes at higher surface coverages which was assigned to a charge transfer reaction between the triazole ring and the copper surface in the perpendicular configuration of the molecule.

Fang et al [6] reported UV photoemission measurements of BTAH chemisorbed on clean Cu and cuprous oxide in UHV. They proposed a bonding of the first chemisorbed BTAH layer via the lone pairs on the triazole ring and the Cu and $Cu(I)O_2$ surface. A structure for the first layer of chemisorbed BTAH was suggested. This structure was based on an almost perpendicular orientation of the molecule on the surface and a stabilizing force of aromatic hydrogen on the benzene ring and a nitrogen atom on an adjacent benzotriazole molecule. The assignments of the UPS peaks were taken from an earlier ab initio molecular orbital study combined with a UPS He(I) gas phase spectra of BTAH made by Palmer and Kennedy [13]. Zonnevyille and Hoffman [14] reported extended Hückel tight binding calculations of BTA^- on a one layer Cu(111) slab. These results support the experimental results and conclusions from Fang et al [6]. Hollander and May [15] proposed, on the other hand that the BTA structure, based on NMR spectra, was parallel to the copper surface. This was further reinforced by an STM and LEED study by K. Cho et al. [16] who studied the adsorption of BTA on the clean and oxygen adsorbed Cu(110) surface. They observed a c(4x2) commensurate phase film of BTA on the clean Cu(110)-1x1 surface with STM and LEED with adsorption taking place in the "flat" geometry. Conversely, STM images of BTA adsorbed on oxygen reconstructed sur-

faces showed a fully disordered structure.

Walsh et al. [17] deduced the orientation of the BTA^- to be tilted at $\pm 15°$ from the surface normal using NEXAFS of BTAH adsorbed on Cu(100) in the monolayer regime. Whereas, at multilayer coverage on the same surface they found BTAH to tilt at approximately 40° from the surface.

3.2 Benzotriazole at Monolayer coverage

3.2.1. Introduction

The aim of the work described in this chapter was to investigate and compare the orientation and coordination of the very first layer of BTAH on Cu(100) by combining the results of the surface sensitive techniques HREELS and RAIRS. Selection rules for active modes in HREELS and RAIRS together with RAIRS intensity ratios have been used to interpret the molecular orientation of the adsorbate on the Cu(100) surface.

The choice of the (100) surface of copper was made on the basis that the (100) surface is the least susceptible to attack after being treated with benzotriazole. The actual order is (100), (110) and (111) in decreasing order of protection [6].

The exact assignment of the vibrational modes of BTAH remains a matter of debate. To aid interpretation we compare the results from BTAH with those from the four related molecules shown in Fig. 3.2. The 1, 2, 3, triazole molecule was studied to try to identify vibrational modes associated with mainly the triazole part of the molecule. Indazole, benzimidazole and the more sterically demanding 1-methylbenzotriazole were also studied on Cu(100), principally

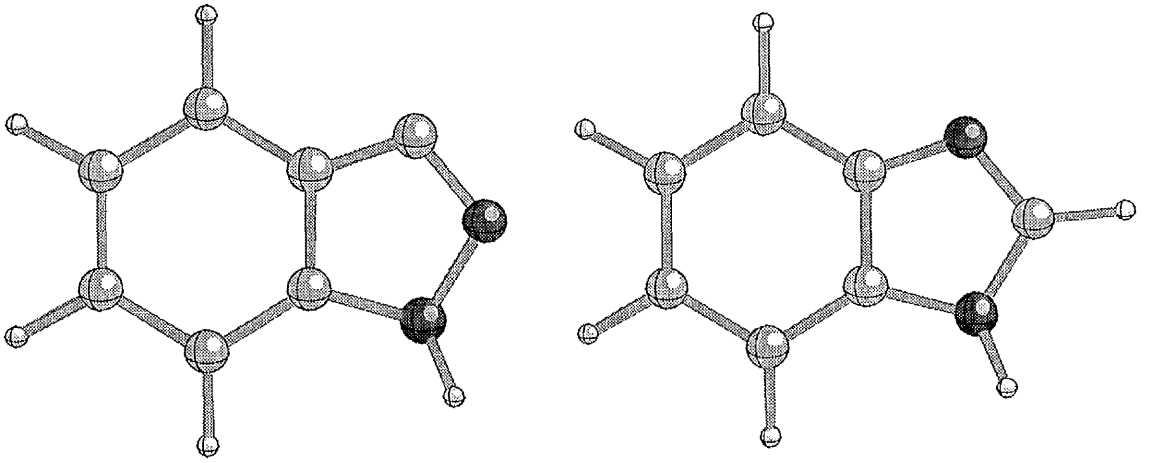

INDAZOLE BENZIMIDAZOLE

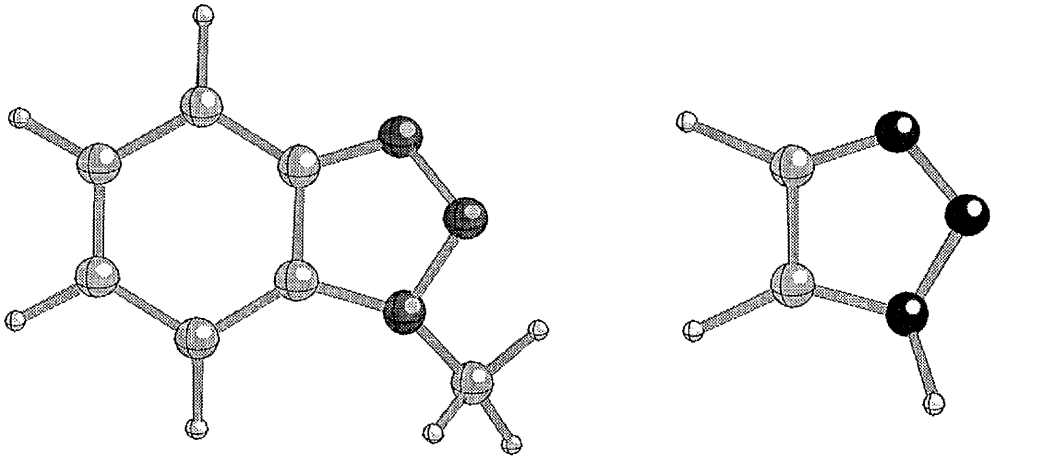

1-METHYL BENZOTRIAZOLE 1, 2, 3 TRIAZOLE

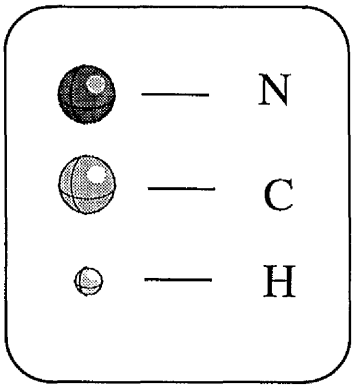

Figure 3.2 Four related azoles also studied on Cu(100) by HREELS and RAIRS.

to see if subtle changes in the molecular framework would influence the bonding, and thus explain their inability to act as efficient corrosion inhibitors. The vibrational data for these other molecules, which are presented in greater detail elsewhere in this thesis, are often referred to in this chapter.

3.2.2 Group Theoretical Considerations

It is well documented in the literature that benzotriazole adsorbs in the deprotonated form (BTA^-) [5, 11, 18, 19, 20], indeed considerable evidence for deprotonation can be seen later in the thesis. Therefore the adsorption of the BTA^- ion of C_2V symmetry (see Fig 3.3) is considered rather than the lower symmetry, C_s. Application of group theory then gives the BTA^- ion a total of 33 normal vibrational modes which can be represented:

$$C_2V$$

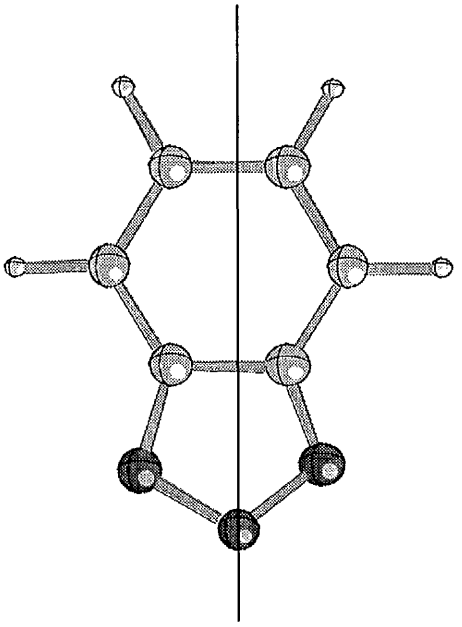

Figure 3.3 The deprotonated BTAH molecule (BTA^- anion, with the C_2 axis indicated).

$12A_1 + 5A_2 + 11B_1 + 5B_2$

all of which are IR active apart from the $5A_2$ mode [18].

3.2.3 Experimental

Experiments were performed in two separate UHV systems, both equipped with low electron energy diffraction (LEED), a retarding field analyser (RFA) for Auger, mass spectrometer and argon ion gun, allowing standard sample preparation and characterisation to be performed. The base pressure of the systems were $\sim 2\times10^{-10}$ mbar.

The HREELS experiment consisted of a 7 eV electron beam focused through a hemispherical deflector with a pass energy of 1 eV hitting the Cu(100) surface and being reflected through a similar hemispherical analyser with a similar pass energy acquiring spectra with a resolution of 9 meV (FWHM) (see section 2.2). In the specular collection mode the angle of incidence of the electron beam was 60° to the surface normal and the reflected electron beam was collected at the same angle. For the off-specular collection mode the angle of collection was changed to 67° to the surface normal, recording spectra at 7° off-specular.

The infrared facility (see section 2.4) consisted of an infrared beam from the FT-IR spectrometer (Mattson Galaxy) focused through a differentially pumped KBr window onto the sample mounted in the UHV chamber. The system was aligned to give a single reflection off the surface at an angle of incidence of ~82°. The reflected light was collimated and focused onto a narrow band MCT detector which accessed the spectral range between 4000 and 700 cm^{-1} and

spectra were acquired at a resolution of 4 cm^{-1}.

In both experiments the Cu(100) was cleaned via argon ion (1 keV) bombardment and annealing to a temperature of 900 K to produce a well ordered (1 x 1) LEED pattern. In the HREELS chamber, BTAH was dosed directionally at a pressure of 1×10^{-9} mbar for varying periods of time. In the RAIRS experiment the BTAH was dosed from the background at a pressure of 1×10^{-9} mbar onto a clean or O_2 predosed surface. The O_2 predosed surface was formed by exposing to Cu(100) 1500 L of O_2 whilst annealing the surface to 773 K, which formed a c(2x2) O overlayer. No LEED pattern was seen after dosing BTAH on to either surface.

3.2.4 Results

Here the results from the HREELS and RAIRS experiments are displayed together since both techniques complement each other well.

The HREELS spectra recorded at specular and in a 7° off-specular geometry can be seen in Fig. 3.4 and 3.5 together with a few assignments of the bands. The assignments are discussed fully in section 3.2.5. At low doses of BTAH onto the room temperature substrate, the specular spectra show the growth of two isolated features at 435 cm^{-1} and 740 cm^{-1}. Both the features grow until a maximum intensity is reached after an exposure of 0.2 L, at which point both features appear to decrease in intensity slightly, although this is not clear beyond doubt due to the sudden appearance of other close lying features. It is difficult to see this change in the 435 cm^{-1} feature, but it is seen clearly in the 740 cm^{-1} feature as the maximum of the broad peak in this region shifts to higher frequency. The emerging loss features are difficult to resolve but are assigned to frequencies tentatively at 250, 435, 580, 790, 935, 992, 1121, 1161,1210,1314,1387,1481, 1570, 1605, and 3079 cm^{-1}. The latter bands eventu-

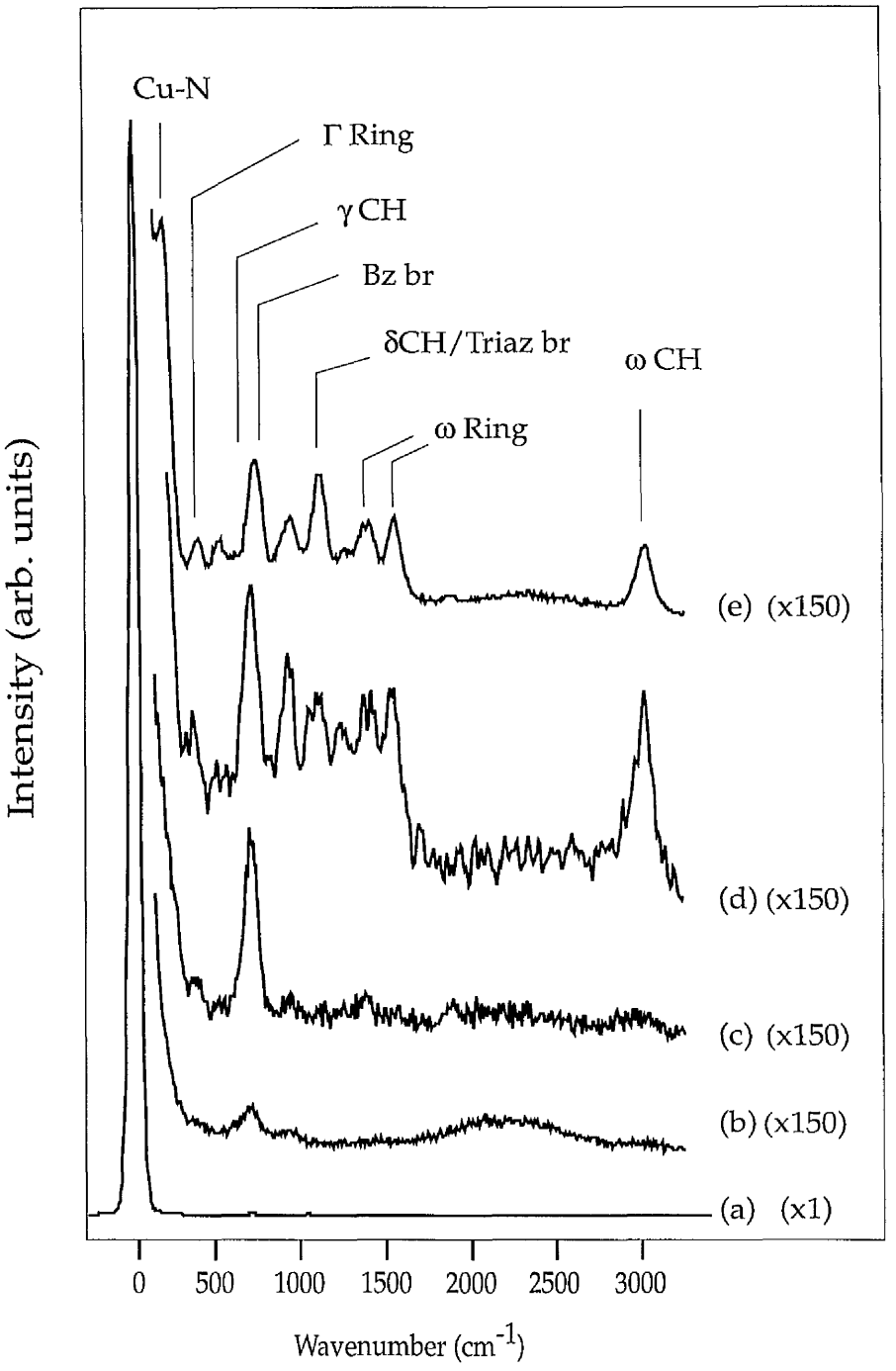

Figure 3.4 Specular HREELS spectra recorded following (a)0.05 L, (b) 0.1 L, (c) 0.2 L, (d) 0.4 L and (e) 2 L doses of BTAH onto Cu(100) taken at room temperature. ($\theta_i = \theta_r = 60°$, primary beam energy = 7 eV, FWHM (elastic peak) = 64 cm^{-1}. All spectra have been normalised to the elastic peak).

(γ = out of plane bend, Γ = torsion, δ = in-plane bend br = breathing, ω = stretching, Triaz = triazole)

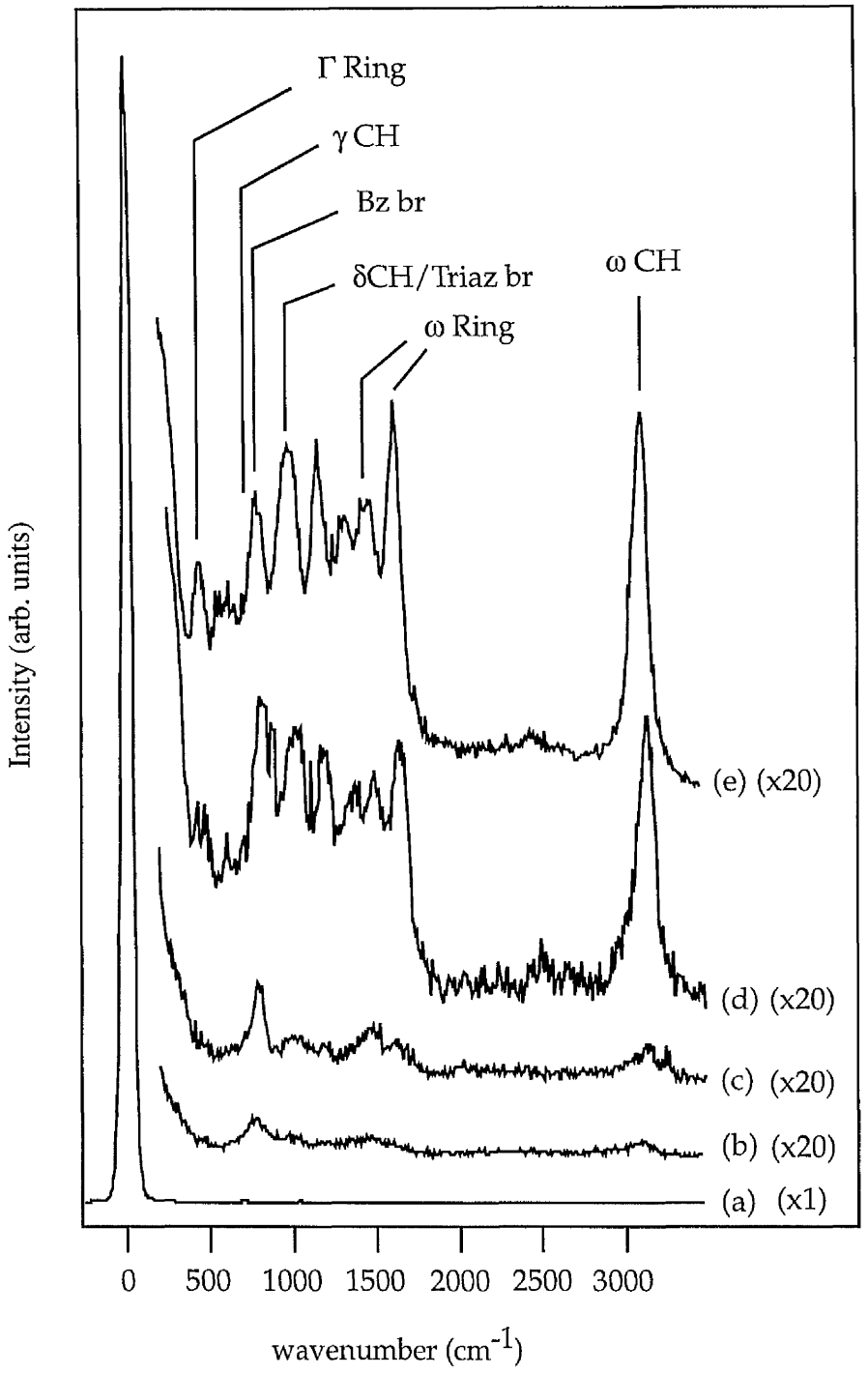

Figure 3.5 7° off specular HREELS spectra recorded following (a)0.05 L, (b) 0.1 L, (c) 0.2 L, (d) 0.4 L and (e) 2 L doses of BTAH onto Cu(100) taken at room temperature. (θ_i = 60°, θ_r = 67°, primary beam energy = 7 eV, FWHM (elastic peak) = 70 cm^{-1}. All spectra have been normalised to the elastic peak). (γ = out of plane bend, Γ = torsion, δ = in-plane bend, br = breathing, ω = stretching, Triaz = triazole, Δ = ring in-plane bend).

ally reach a maximum after a dose of 2 L. Further dosing fails to produce any change in intensity of the bands.

Fig. 3.5 shows the HREEL spectra recorded at 7° off-specular geometry at the same doses of BTAH at which the specular spectra were taken. At low coverage, the spectra show loss features in the 800 to 3089 cm^{-1} region which are not evident in the specular spectra at low coverage. These features become very intense at higher doses relative to the band at 740 cm^{-1} in the off-specular data.

The change in the spectra as the dose is increased can more fully be appreciated by observing the RAIRS spectra shown in Fig. 3.6 The RAIRS spectra have a resolution which is superior by a factor of 10 to the HREEL spectra. Hence the growth of the 787 cm^{-1} band (790 cm^{-1} in the HREEL spectra) and the simultaneous diminishing of the 738 cm^{-1} band (740 cm^{-1} in the HREEL spectra) can clearly be distinguished, which is not immediately obvious from the HREELS spectra. The growth of bands at 992, 1122, 1140, 1170, 1217, 1275, 1387, 1439, 1481, 1570, and 3059 cm^{-1} are also evident as the 740 cm^{-1} band drops in intensity.

The two vibrational techniques have been described in chapter 2 and it is well established that both excite the same vibrational modes and therefore any slight differences in frequency of the specific modes, which are very minor in this case, can be put down to the calibration of the two separate experiments. However, before proceeding further to discuss the results it must be noted that there are slight differences when comparing the intensities of the modes. The HREEL spectra show intense loss features particularly in the high frequency region in contrast to the generally weak RAIRS bands. These are attributed to the nature of the scattering mechanisms and the experimental technique. Aspects of the molecule involved and the orientation of the molecule on the surface will also

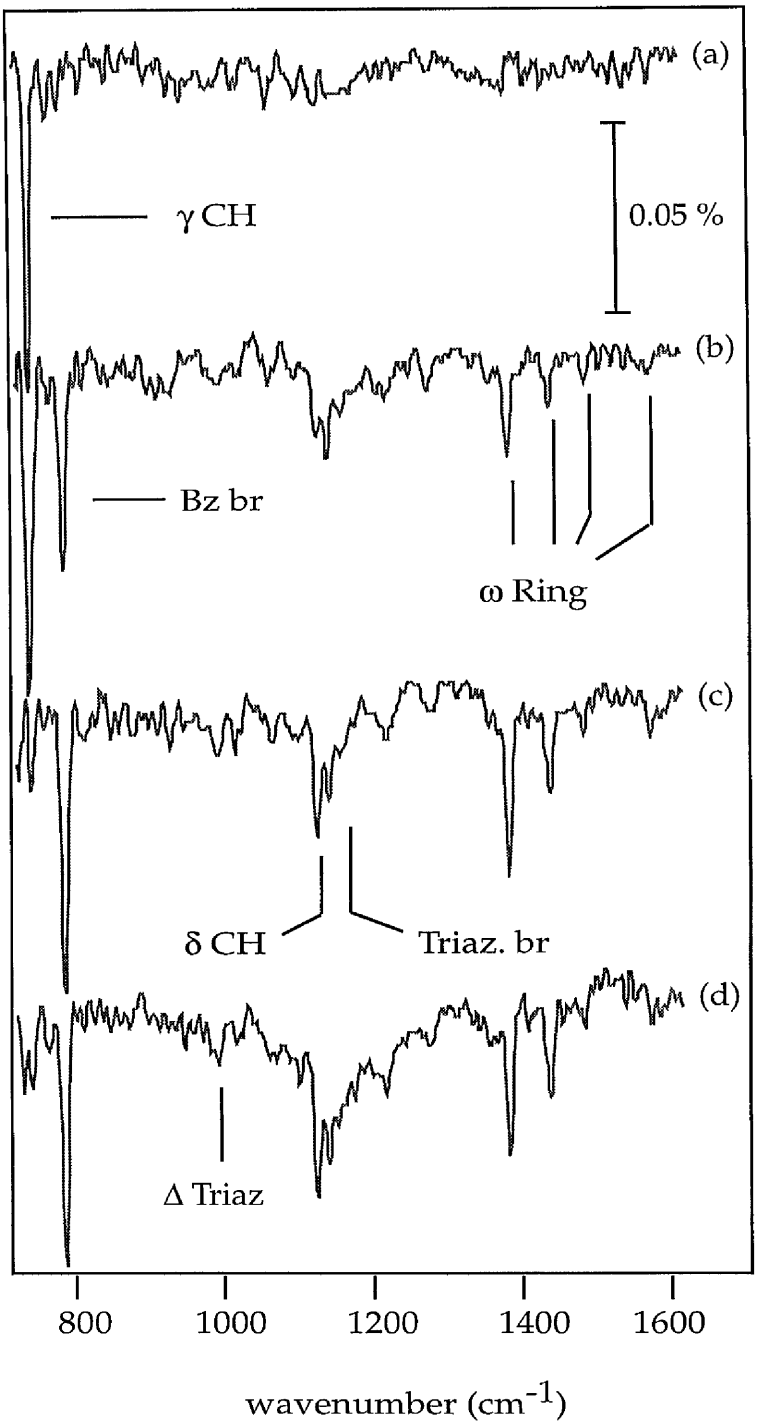

Figure 3.6 RAIRS spectra of BTAH adsorbed on Cu(100) after exposures of (a) 0.5 L, (b) 1.5 L, (c) 2 L and (d) 8 L. (Triaz = triazole, br = breathing, Δ= ring in-plane bend, δ = in-plane bend, br = breathing, ω = stretching).

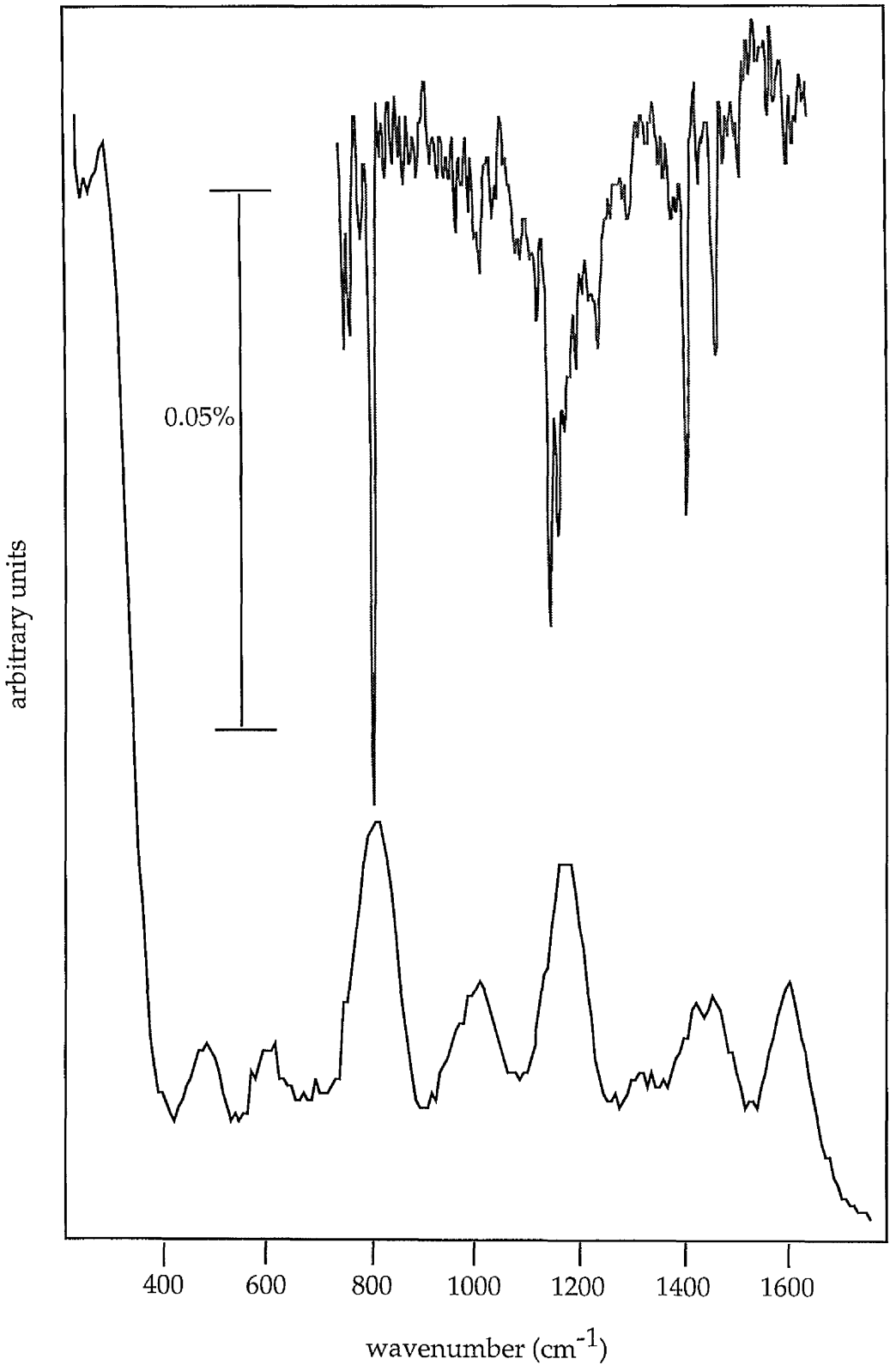

Figure 3.7 Comparison of specular HREEL (Fig. 4.4) and RAIR (Fig. 4.6) spectra of BTAH adsorbed on Cu(100) at saturation coverage taken at room temperature. (spectrometer settings are the same as the Fig 4.4 and 4.6)

have some effect on the intensities of features in the spectra when using either of the techniques.

The impact scattering mechanism [22] also contributes significantly to HREELS loss intensities even in the specular geometry particularly in our spectra at high frequencies where impact scattering contributions are high. However, generally the relative intensity ratios within both the HREEL and RAIR spectra are quite similar as can be seen from Fig. 3.7.

3.2.5 Mode assignment and discussion

The assignment of the individual vibrational modes of these types of corrosion inhibitor is not a trivial matter because of the complexity of the spectra. The task has been made easier by referral to previous IR and Raman spectroscopic work carried out on BTAH and similarly structured molecules [5, 8, 11]. In addition, our own selection of azoles and the vibrational techniques used allow us to invoke selection rules in conjunction with group theory to gain a fuller understanding of the mode assignment and orientation of the first bonding monolayer.

It is well documented in the literature that aromatic molecules containing benzene rings show out-of-plane vibrational modes in approximately the 690-800 cm^{-1} region [19]. Bands which occur above 800 cm^{-1} are generally assigned to in-plane modes associated with ring deformation or stretching of the bonds [23]. With reference to the vibrational spectra of BTAH on Cu(100), the features at 435 and 740 cm^{-1} are assigned to the out-of-plane ring torsion and the CH out-of-plane mode [11] both of B_2 symmetry. These are the only two features seen at low coverages in either the RAIR or specular HREEL spectra and therefore must be the only modes which have an appreciable component

of their transition dipole moments perpendicular to the surface according to the dipole selection rule for HREELS and RAIRS discussed in chapter 2. The in-plane A_1 and B_1 modes above 800 cm^{-1} are not visible. The latter observations would indicate that the molecule is lying flat with its C_2 axis parallel to the surface.

This interpretation is further reinforced by the HREELS off-specular data shown in Fig. 3.5 At low coverage, the off-specular spectra show bands in the 1000-1600 cm^{-1} region and also at 3089 cm^{-1} which are not evident in the specular data. These bands are seen more clearly in Fig. 3.8, which shows the low coverage specular and off-specular HREELS spectra taken following a 0.1L dose. The in-plane region is clearly identified. Following from the interpretation that the molecule lies with its C_2 axis parallel to the surface, the additional bands seen in the off-specular spectra must arise from modes parallel to the surface screened out by their image dipoles at specular collection but excited in the off-specular direction by the impact scattering mechanism.

As the exposure of BTAH to the surface increases, the in-plane A_1 and B_1 modes acquire a dipole component perpendicular to the surface, causing an increase in intensity of bands in the 1000-3100 cm^{-1} region of the vibrational spectra. The latter observation requires the molecule to undergo an orientational phase transition, such that the molecule adopts a more upright geometry. In keeping with this transition to a more upright geometry, the out-of-plane modes such as the 740 cm^{-1} feature lose intensity. This is expected due to the reduction in the size of the perpendicular transition dipole moments associated with these modes. The fact that neither the in-plane nor out-of-plane modes modes vanish when saturation coverage is reached makes it possible to exclude the two extreme orientations ie. flat or standing up. Hence the molecule seems to be tilted in relation to the surface normal in such a way that both the in-plane and

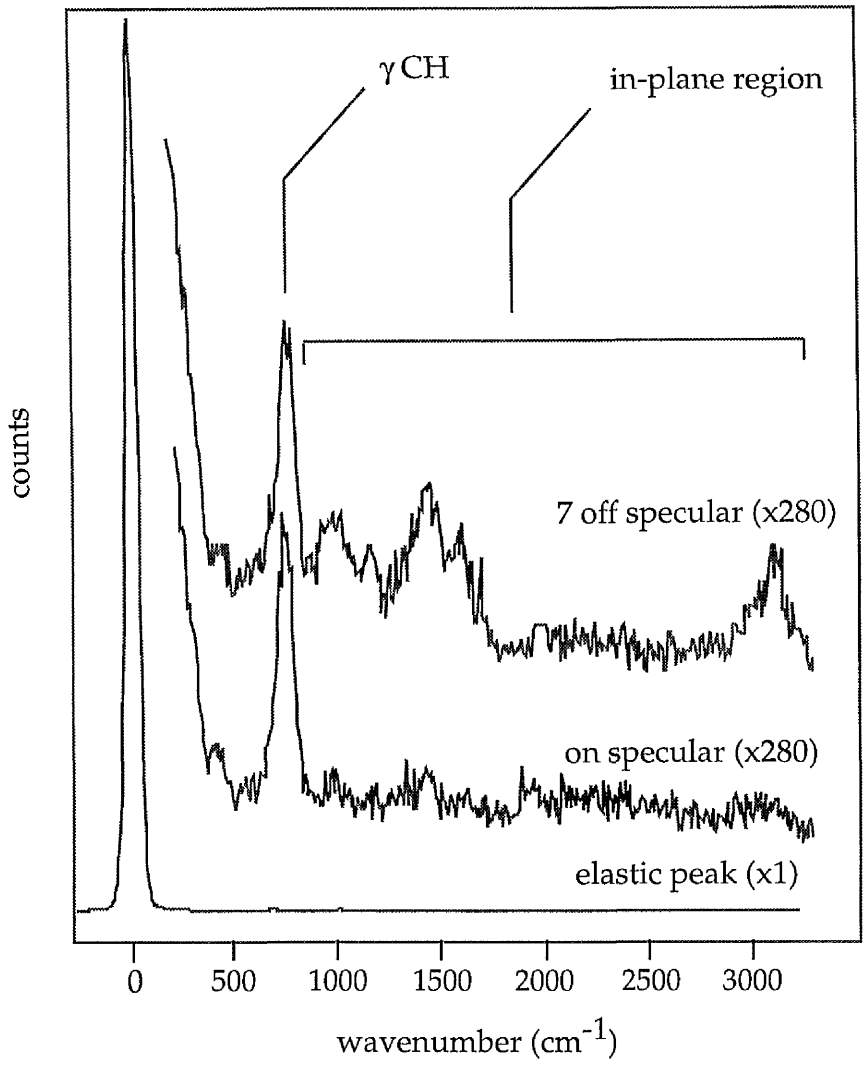

Figure 3.8 HREELS spectra following a 0.1 L BTAH exposure to Cu(100) at room temperature. Spectra were recorded on specular and 7° off-specular. (Specular, $\theta i = \theta r = 60°$; off specular $\theta i = 60°$, $\theta r = 67°$, primary beam energy = 7 eV, FWHM (elastic peak) = 64 cm^{-1}).

out-of-plane modes have components of their transition dipole moments along the surface normal. The orientation is discussed further in section 3.2.5. Alternatively a situation may exist where some of the molecules are lying flat and some standing upright. The vibrational spectra cannot distinguish between these two alternatives.

A point that must be mentioned regarding the HREELS technique is that it is

particularly susceptible to disorder on the surface. Indeed a count rate drop was encountered in the specular direction during the orientational transition. Spectra taken following a dose in the range of 0.1 - 0.4 L of BTAH registered a count rate drop in the elastic peak of approximately 50-75%. The reason for this is presumably that incoming electrons are scattered through larger angles due to the relative disorder on the surface during the change in orientation. Count rates were at a maximum when the molecules were lying flat (a 0.0 1L dose) or at saturation coverage. This type of occurrence has been recorded by several authors [24, 25] during their work recording HREELS of pyridine on metals and is documented in Chapter 1 of Vibrational Spectroscopy of Molecules on Surfaces by Yates and Madey [26].

The mode assignment becomes more straightforward after recognising the origins of the changes in the vibrational spectra. A summary of the experimental results and mode assignments is given in Table 3.1. IR and Raman assignments made by other authors in the literature is displayed for comparison [11, 18]. Table 3.2 shows an IR assignment of BTAH made by Rubim et al. [11]. Generally, there is a good agreement between our mode frequencies and those of the literature [11, 18] despite the different conditions, surfaces and vibrational techniques used. However, there are some important anomalies and mode assignments which need to be commented on further. The different regions of the vibrational spectra are discussed briefly; initially the 700-800 cm^{-1} region, followed by the high frequency region, then the 1100-1300 cm^{-1} region and finally the low frequency region of the spectra.

700-800 cm^{-1} region ; Figs. 3.4 and 3.6 show that the 789 cm^{-1} band increases in intensity as the 740 cm^{-1} band loses intensity. This is a clear indication that the two bands have their transition dipole moments directed along two orthogonal directions and both cannot be ascribed to CH out-of-plane bends, as assigned

HREELS and RAIRS frequencies of BTAH on Cu(100)				
HREELS (cm^{-1})	RAIRS (cm^{-1})	BTA^- [21] (cm^{-1})	Cu(I)BTA [21] (cm^{-1})	Assignment
3089	3059			ω CH
1605		1605		ω Bz
1570 (sh)	1570	1576	1578	ω Bz
1481	1481	1481	1489	ω Bz
1435 (sh)	1439	1447	1446	ω Bz
1387 (sh)	1387	1388	1391	ω Triaz
		1375		
1314		1283	1292	
	1275	1261		δ CH
1210	1217		1217	δ CH
1161	1170	1163	1190	Triaz br/ δCH
	1140	1134	1151	δ CH
1121	1122	1115	1123	δ CH
992	992	988	993	Δ Triaz Ring
935				
790	787		789	Bz br
740	738		744	γ C-H
580				Δ Bz
435				Γ Ring /Δ Ring
250				Cu-N

Table 3.1 HREELS and RAIRS frequencies and our assignments for BTAH adsorbed on Cu(100). Also shown are IRAS frequencies of BTAH in a solution of NaOH at pH 10 in a CaF_2 cell (BTA^-) and Cu(I)BTA in a KBr matrix taken from reference [21]. (Bz = Benzene, Triaz = Triazole, comp = complex, br = breathing, Δ = ring in-plane bend, δ= in-plane bend, γ = out-of-plane bend.)

IR and RAMAN frequencies of benzotriazole

Raman (cm^{-1})	Infrared (cm^{-1})	Assignment
	3340 (br)	Fermi resonance
	3250 (br)	
	3095 (vw)	υ(CH)
3077 (3.9)[a]	3080 (vw)	"
3067 (3.5)	3060 (vw)	"
	3040 (vw)	"
	2800 (vbr)	υNH (associated)
1625 (0.4)	1622 (m)	bz. ring stretching
1597 (4.2)	1596 (m)	bz ring stretching
	1533 (w)	combination
1517 (0.8)	1510 (vw)	bz. ring stretching
1500 (1.1)	1500 (w)	combination
	1468 (sh)	combination
1458 (0.6)	1458 (m)	bz. ring stretching
	1420 (m)	triazole ring sretching
1387 (9.3)	1383 (m)	triazole ring stretching
1373 (5.3)		bz. ring stretching
1312 (1.0)	1310 (w)	combination
1282 (3.2)	1280 (w)	δCH
1273 (sh)	1268 (m)	combination
	1260 (sh)	combination
1211 (2.7)	1210 (vs)	triazole ring breathing
	1210 (vs)	δCH
	1180 (sh)	combination
1149 (1.0)	1146 (m)	δch
	1140 (sh)	combination
1129 (2.4)	1122 (w)	
	1118 (sh)	combination
1098 (2.2)	1092 (m)	δNH
1081 (1.1)	1078 (m)	combination
1049 (1.0)	1048 (w)	ring stretching
1024 (6.0)	1020 (s)	
1008 (3.9)	1005 (s)	
992 (sh)		γCH
	982 (mw)	triazole ring bend
	950 (sh)	?
	940 (mw)	?
	910 (sh)	?
905 (0.6)	900 (sh)	γCH
	880 (ms)	γNH
	848 (sh)	?
783 (10.0)	780 (s)	bz. ring breathing
	772 (ms)	γCH
751 (0.2)	755 (vs)	ring bend
	743 (vvs)	γCH
	710 (ms)	combination
632 (3.7)	630 (sh)	triazole ring bend
	620 (sh)	combination
	605 (m)	triazole ring torsion
570 (0.3)		?
	562 (vvw)	?
540 (2.0)	533 (w)	triazole ring torsion
433 (0.4)	430 (sh)	bz. ring bend
	425 (s)	bz. ring torsion
410 (0.4)	408 (s)	bz. ring bend
272 (0.2)	278 (s)	bz. ring torsion
228 (1.1)	233 (ms)	?
213 (0.1)		?

υ = band stretching; δ = bending in-plane; γ = bending out-of-plane. [a]Intensity relative to the strongest band given arbitrary value of 10.0. [b]bz., benzene.

Table 3.2 IR and RAMAN frequencies of BTAH taken from reference [11].

by Thornkvist et al [5]. Indeed the 789 cm^{-1} feature must be an in-plane band. This is supported by the work of Nonnenmacher and Mecke [27] , who showed by investigating several ortho-di-substituted benzene derivatives (C_{2V} symmetry) that only one strong C-H out-of-plane mode appears in the 700-800 cm^{-1} region. The 789 cm^{-1} feature was assigned to a triazole in-plane bend by Nillson et al [18] but, we also disagree with this assignment since these are found to occur at higher frequencies according to our RAIRS work using 1, 2, 3, triazole adsorbed on Cu(100). This work is shown in chapter 5 and displays a band at 976 cm^{-1} assigned to a triazole in-plane bend [28]. The triazole in-plane bend is assigned here in the monolayer regime at a slightly higher frequency of 992 cm^{-1}.

Further light can be shed on the origin of the 789 cm^{-1} mode when we again refer to our RAIR spectra of 1, 2, 3, triazole, which show that only one band appears in the 700-900 cm^{-1} region, which can be assigned to the C-H out-of-plane bend of the 1, 2, 3 triazole molecule . This must indicate that the 789 cm^{-1} band appearing in the BTAH vibrational spectra is not derived from the triazole portion of the molecule. The band at 789 cm^{-1} is therefore assigned to a benzene breathing mode and this is further confirmed by the assignment in earlier work [11, 12].

High frequency region ; the species BTAH and BTA^- can be distinguished by some characteristic bands. Rubim et al [11] recognised that the BTAH bands at 1624, 1594,1515 and 1462 cm^{-1}, assigned to C-C ring stretching modes, are shifted to 1608, 1574, 1485 and 1448 cm^{-1} on deprotonation. The RAIRS spectra show large bands at 1387 and 1439 cm^{-1} and also two small bands at 1481 and 1570 cm^{-1}, the latter 3 bands correspond to the first three C-C stretches identified by Rubim et al [11].

The HREEL spectra in fig 3.4. fails to resolve these four features but clearly identifies two loss features at 1605 cm^{-1} and 1443 cm^{-1}. These peaks are very broad and almost certainly contain all the C-C stretches identified by Rubim et al [11]. Indeed the peak at 1605 cm^{-1} in the HREELS spectra ,being the highest energy C-C stretch, does not have any close lying bands at higher energy and can be assigned to a particular frequency rather more accurately than the other features and correlates well with the BTA^- peak of highest energy.

The deprotonation of the BTAH molecule would, of course, be recognised by the absence of a N-H feature in the HREELS or RAIRS monolayer spectra. This would be evidenced by the lack of the easily distinguishable N-H stretch in the high frequency region. This indeed is the case. However, importantly a N-H stretch ought to be able to be seen in the low temperature spectra of physisorbed molecules where deprotonation is not expected to occur, thus indicating the difference in the bonding mechanisms at the two temperatures. The low temperature RAIR spectra, which are discussed in section 3.3 do not contain a N-H stretch expected to occur in the 3100-3550 cm^{-1} region [29]. This is almost definitely due to the flat orientation of the molecule, judging by the very dominant C-H out-of-plane bend in the low temperature spectra (this point and the orientation of the molecule at multilayer coverage is discussed in more detail in section 3.3). In order to see the N-H stretch, relatively large doses of BTAH are required to be applied to the surface at low temperature. The difficulties in doing this are again outlined in section 3.3. However, the HREEL spectrum of BTAH on Cu(100) at 120 K did show a broad band centred at 2987 cm^{-1}. The peaks are not resolvable due to the relatively poor resolution of the low temperature spectrum, which is measured at 13 meV. The C-H stretch band on its own is expected to be seen at a higher frequency of 3078 cm^{-1}, so the feature is believed to be due to a combination of both the C-H and N-H stretch which is shifted to lower frequency due to hydrogen bonding, combination bands may

also be evident in this region. This is obviously a very tentative assignment but further evidence is derived from the RAIR spectra of the other azoles below.

The vibrational results of the other azoles studied are reviewed extensively in other chapters of this work. They are only briefly mentioned here in order to reinforce the conclusions regarding the deprotonation of the triazole ring. Basically, the data from the 1, 2, 3 triazole and indazole molecules suggest that both adsorb on Cu(100) at low temperatures in a more perpendicular geometry and therefore a more intense N-H stretch is expected to be seen. Indeed, the multilayer RAIRS spectra of the two molecules show several bands in the 2850-3200 cm^{-1} region which are not evident in the room temperature spectra of the same molecules. These are believed to contain the downshifted N-H stretch which may also split as a result of hydrogen bonding, depending on whether dimers or even trimers of molecules are formed. Further evidence for deprotonation comes from the presence of the N-H in-plane band, in the spectra of the other azoles but again these points are reviewed elsewhere. Overall there is strong evidence for deprotonation.

The 1100-1300 cm^{-1} region : this region contains bands associated with the triazole portion of the molecule and the CH in-plane bending modes [11, 18]. Important conclusions regarding the bonding to the surface can be made from analysis of this region. The band in the HREELS spectra peaking at 1161 cm^{-1} is clearly asymmetric and this is assigned to a mixture of the C-H in-plane bends and triazole breathing mode involving the N=N=N stretch, further information is gained from the RAIR spectra.

Although some of the bands in the 1100-1300 cm^{-1} region are very weak, the RAIR spectra in Fig. 3.6 resolves the bands at 1122, 1142,1170, 1217 and 1275 cm^{-1}. The BTAH spectra were recorded twice and bands were subject to growth moni-

toring as the dose was increased to ensure that bands of low intensity could be distinguished from the noise. Frederick et al [30] concluded that a more vertical orientation of the benzoic acid molecule is achieved when adsorbed on the O_2 predosed Cu(100) as opposed to clean Cu(100). If this were repeated on the present system then this would enable several peaks of low intensity to be distinguished clearly and aid the mode assignment. This was indeed the case and the corresponding set of spectra of BTAH adsorbed on the oxygen pre-dosed Cu(100) surface is shown in Fig. 3.9 All band frequencies only differ from the clean Cu(100) surface by a few wavenumbers and several bands in the 1100-1300 cm^{-1} region are more intense than on the clean surface. Spectra for the Cu(100) surface pre-dosed with O_2 shows bands at 1126, 1142, 1171, 1206, and 1271 cm^{-1}. All of the bands appear in the low temperature spectrum and are assigned to C-H in-plane bends [11, 18] with the exception of the band at 1170 cm-1 on the clean Cu(100) surface and 1171 cm^{-1} on the O_2 predosed surface, see Table 3.3. These bands correspond to the triazole breathing mode involving a symmetric N=N=N stretch . This assignment was proposed by Rubim at al [11] who suggested that the 2 nitrogen atoms adjacent to the carbon atoms in the triazole ring have equal bond orders after deprotonation. This gives rise to a symmetric and an anti-symmetric stretch. A very intense band at 1211 cm^{-1} is seen in the low temperature RAIR spectra of BTAH on Cu(100), discussed in section 3.3. There it is assigned to the triazole breathing mode involving the N=N stretch. This band does not appear in the room temperature spectra. Instead, the deprotonation of the triazole ring and subsequent bonding to the surface is said to cause downward shift in the 1211 cm^{-1} band [11], to the positions mentioned at 1170 or 1171 cm^{-1} [11] on the clean and pre-dosed Cu(100) surfaces, respectively.

Further evidence for this type of behaviour can be seen from the IR spectrum of BTAH taken on CaF_2 plates at atmosphere in various modelled conditions.

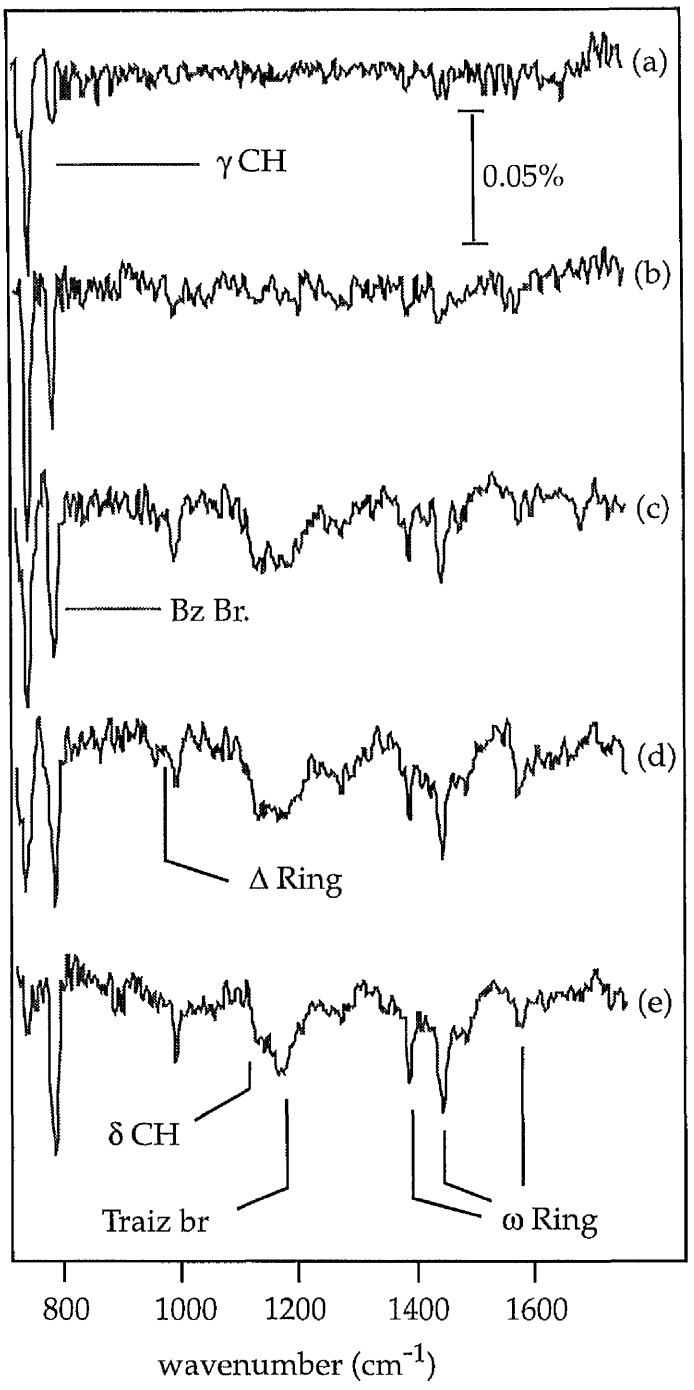

Figure 3.9 RAIRS spectra of BTAH adsorbed on Cu/O at exposures of (a) 1 L, (b) 1.6 L, (c) 2.25 L, (d) 3.4 L (e) 5 L. (Triaz = triazole, br = breathing, Δ= ring in-plane bend, δ = in-plane bend, br = breathing, ω = stretching). A c(2x2) LEED pattern was observed after adsorption of O_2.

RAIRS frequencies of BTAH on Cu(100) pre-dosed with O2			
RAIRS (cm^{-1})	Cu(I)BTA [5] (cm^{-1})	BTA/Cu(1)Ox [5] (cm^{-1})	Assignment
3056			ω CH
	1622		ω Bz
1573	1576	1580	ω Bz
	1489	1447	ω Bz
1443	1446	1391	ω Triaz
1387	1391		
	1292		
1271	1271		δ CH
1206	1210		δ CH
1171	1151	1149	Triaz br
1142			δ CH
1126			δ CH
989	993		Δ Triaz ipb
	927		Bz br
787	789	787*	γ CH
742	744	745	

Table 3.3 RAIRS frequencies of BTAH adsorbed on Cu(100) predosed with O_2. Also shown are IRAS frequencies of Cu(I)BTA in a KBr disc[5] and IRAS frequencies of BTAH etched on a Cu(I)/O surface taken from reference [5].

These are shown in Fig. 3.10. The BTAH spectrum shows a very intense band at 1211 cm^{-1} corresponding to the breathing mode involving the N=N stretch whilst the IR spectrum taken at pH 10, when BTAH is presumably deprotonated, does not contain this band but has a new band at 1161 cm^{-1} which probably corresponds to the breathing mode involving the symmetric N=N=N stretch,

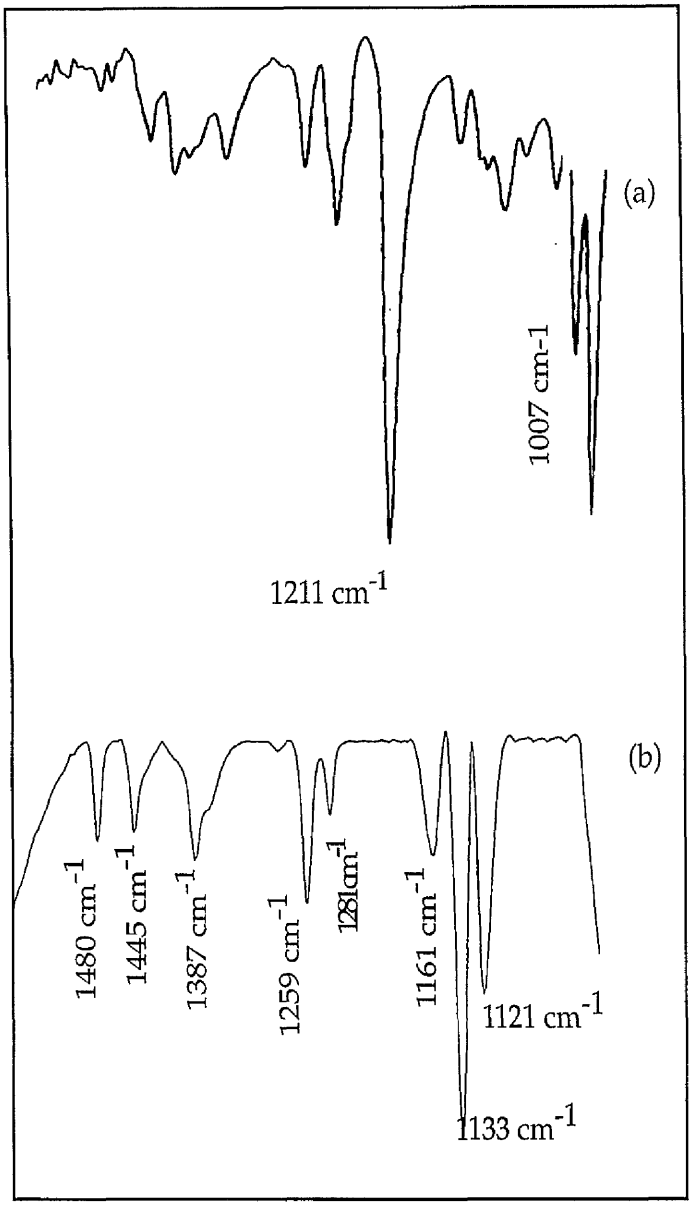

Figure 3.10. IR spectra of BTAH taken in CaF_2 plates (a) and BTAH in a solution of NaOH at pH 10 taken in CaF_2 plates (b).

although there are three intense bands in this region and their assignment is tentative. The latter observation can also be seen in the corresponding spectrum of the 1, 2, 3 triazole molecule (chapter 5) where the very intense band, assigned to the N=N stretch, at 1223 cm^{-1} appears in the IR spectrum of the molecule but fails to appear in the corresponding spectrum at pH 10. Instead a new band appears at 1142 cm^{-1} assigned to the symmetric triazole stretch. Im-

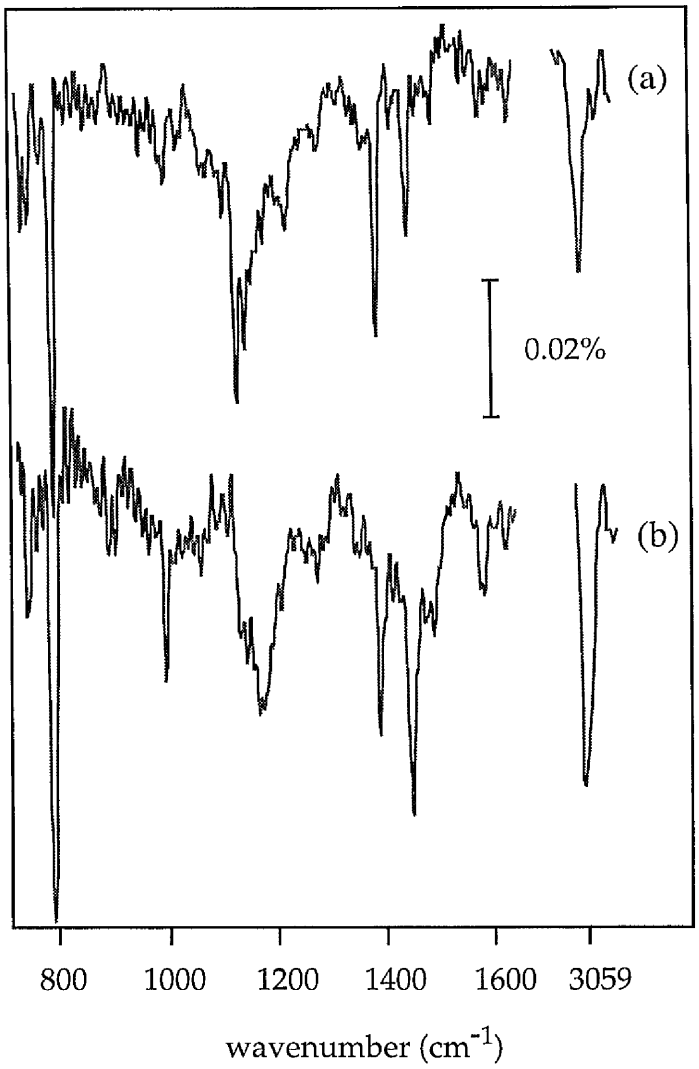

Figure 3.11 RAIR spectra of BTA- adsorbed on Cu(100) (a) and Cu/O (b) surfaces at saturation coverage at room temperature.

portantly, the triazole spectrum taken at pH 10 does not contain a N-H in-plane bend which is very intense in both the IR spectra of the triazole molecule taken at atmospheric conditions and also in the RAIR multilayer spectra shown in chapter 5, thus providing further comprehensive evidence that the azoles are in fact deprotonated at pH 10 as well as at room temperature on the Cu(100) surface.

An interesting point to note regarding the spectra of BTAH adsorbed on the

clean and O_2 predosed surfaces is the relative intensity of the modes within each RAIR spectrum. If both are compared, as shown by Fig 3.11, we see that the 992, 1165, 1439, and 1570 cm^{-1} modes are visibly more intense on the O_2 predosed surface than the corresponding bands on the clean surface. The 1443 cm^{-1} band on the O_2 predosed surface is more intense than the 1387 cm^{-1} band whereas this intensity relation is reversed on the clean surface. This indicates that the molecule is adsorbed in different orientations on each of the surfaces. This, and the possible orientations are discussed further in section 4.2.6.

Low frequency region ; The loss feature at 250 cm^{-1} in the HREELS spectrum at saturation coverage shown in Fig 3.4 is assigned to the Cu-N mode. This is slightly higher than that found by Rubim et al.[11] who found the absence of the δ(N-H) mode together with the appearance of a broad feature around 232 cm^{-1}, which was assigned to the Cu-N mode in SERS measurements of BTAH on a Cu electrode. The 250 cm^{-1} band also correlates well with other nitrogen containing molecules bonded to metals [24,25] which show the Cu-N mode in the 200-250 cm^{-1} region.

3.2.6 Orientation of Benzotriazole on Cu(100)

In the previous section strong evidence was presented which suggests that the BTA^- molecule undergoes an orientational phase transition from a relatively flat geometry to a more tilted geometry at saturation coverage.

The RATIO method is applied to evaluate the orientation at saturation coverage from the bands given in table 3.4, which shows the 11 strongest bands used in the analysis together with their intensities and their transition dipole mo-

ments. The method, described by Debe et al. [31] is shown schematically in Fig. 3.12 and in its simplest form can be used to determine 3 parameters. The first is an order parameter, f, which indicates the amount of order or disorder on the surface, and the other 2 parameters are the Euler angles θ and ψ which specify the orientation of the molecule on the surface.

The method requires three things:

(a) the measurement of as many individual band absorbances as possible from the system. Here the RAIRS measurements taken from BTAH adsorbed on the clean and oxygen pre-dosed Cu(100) surfaces are used.
(b) measurement of the same band absorbances from a totally randomised form of the same system. Here band absorbances taken from the IR spectrum of Cu(I)BTA in a KBr disc published by Nillson et al. [18] are used.
(c) a band assignment or knowledge of the direction of the bands' transition moments relative to the cartesian coordinates. Here knowledge of the likely assignments made clear in the previous section together with calculations shown by Nillson et al. [18] have been used for the analysis.

The intensities are summed for each transition dipole moment direction (x, y, z) so that three sums are obtained for the adsorbate and the reference sample: A(x), A(y) and A(z) for the adsorbate and $A_r(x)$, $A_r(y)$ and $A_r(z)$ for the disordered reference. These intensities form two ratios r(zx) and r(yx):

$r(zx) = A(z)\, A_r(x) \,/\, A_r(z)\, A(x)$; and
$r(yx) = A(y)\, A_r(x) \,/\, A_r(y), A(x)$.

The method provides us with equations 3.1 and 3.2 :

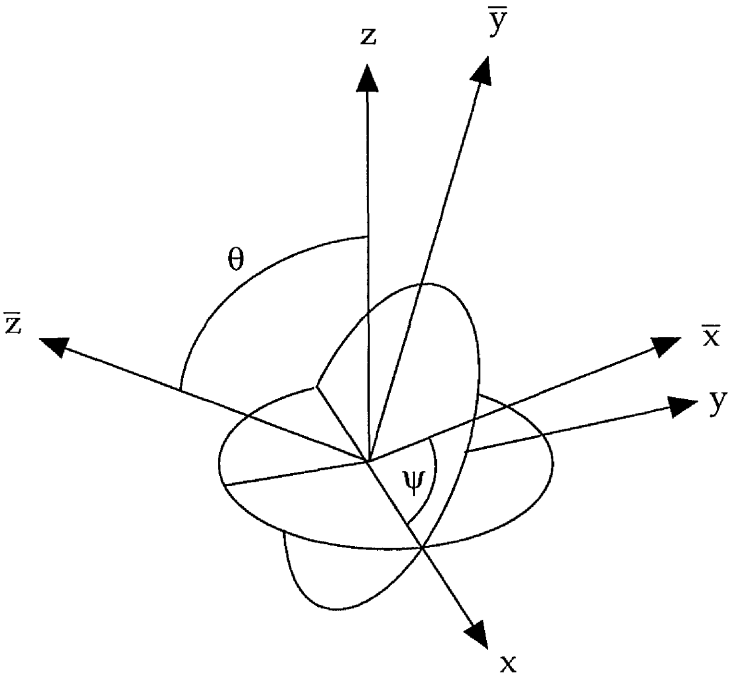

Figure 3.12. Illustration of the two plane rotations R_z (ψ)and R_x(θ) used to specify the orientation of the molecule on the surface. The surface is parallel to the xy plane [18].

υ (cm−1)	Symmetry and orthogonal direction	Cu(I)BTA [18]	Cu(100) ΔR/R%	Cu/O(100) ΔR/R%
1572	A_1 (x)	0.042	0.012	0.022
1489	A_1 (x)	0.026	0.013	0.028
1439	B_1 (y)	0.067	0.030	0.054
1387	A_1 (x)	0.040	0.045	0.043
1275	B_1 (y)	0.047	0.017	0.020
1170	A_1 (x)	0.134	0.029	0.040
1140	B_1 (y)	0.033	0.047	0.032
1122	B_1 (y)	0.015	0.055	0.028
992	A_1 (x)	0.015	0.022	0.035
790	B_1 (y)	0.119	0.072	0.071
740	B_2 (z)	0.296	0.028	0.025

Table 3.4 Vibrational modes and their transition dipole moments used in the RATIO analysis. Also shown are symmetry assignments and orthogonal directions taken from reference [18]. Transition dipole moments of Cu(I)BTA taken from reference [18].

$$\sin^2\theta = \frac{[1 + r(yx)] + \alpha[[1 - r(zx)][1 + r(yx)] - r(zx)\,[1 - r(yx)]]}{[1 + r(zx) + r(yx)]}$$; and -Equation 3.1

$$\sin^2\psi = \left(\frac{\alpha\,[1 - r(zx)]}{\sin^2\theta} + 1\right)[1 + r(zx)]^{-1},$$ -Equation 3.2

where α is :

$\alpha = (1 - f) / 3f$ (α=0 for a completely ordered surface, ie, f=1.)

The assignments and thereby the directions of the transition dipole moments for some of the modes in Table 3.2 are, as discussed above, slightly uncertain. However, a single misinterpretation is not expected to affect the result considerably, because we are using many modes in the analysis and the method uses the sum of the intensities in three orthogonal directions.

The results from the analysis shown in Table 3.4 are quite similar for the Cu(100) and Cu(100)/O surfaces. Fig. 3.13 shows the orientation of BTA^- in relation to the surface coordinate system, the angle θ is exaggerated for easier viewing.

The results correlate well with the tilt angle of 15° off-perpendicular obtained by Walsh et al [17] using NEXAFS of BTAH adsorbed on Cu(100) at saturation coverage. The evidence from the analysis also show that the BTA^- anion prefers to orient in a slightly more perpendicular and also a more 'canted' geometry on the Cu(100)/O surface, ie. the molecule is 'leaning' further to one side in the xy plane of the molecule.

3.2.7 Observations on possible bonding modes

The bonding modes differ depending on the surface coverage, as depicted in Fig. 3.14. At low coverages, due to its flat geometry, BTA^- is assumed to bond

surface	Euler Angles	
	θ	ψ
Cu(100)	75°	52°
Cu(100)/O	80°	58°

Table 4. Euler angles ψ and θ describing the orientation of BTA^- on Cu(100) and Cu(100)/O surfaces obtained from the RATIO analyis.

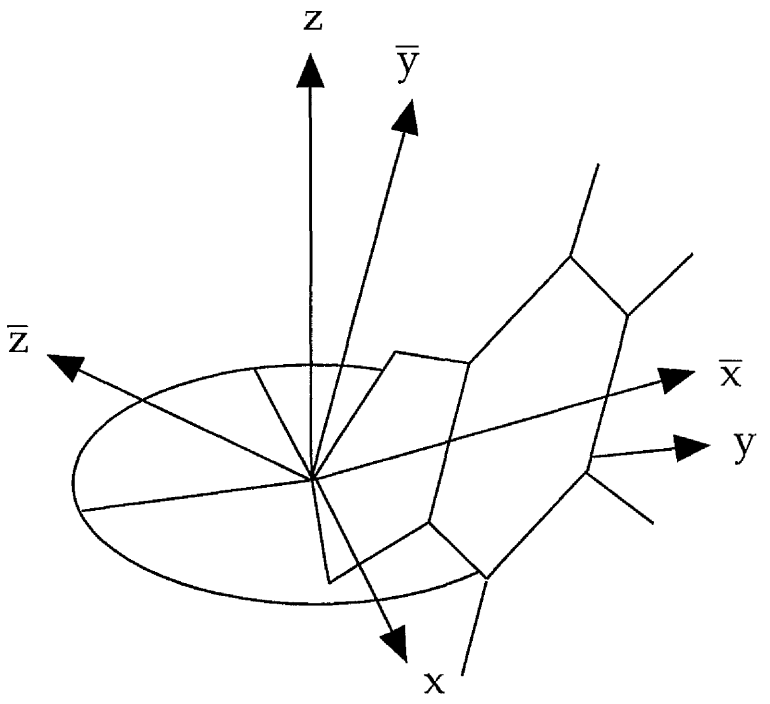

Figure 3.13 The orientation of BTA^- in relation to the surface coordinate system x, y, and z at saturation coverage. The Cu(100) surface is parallel to the x, y plane. (The tilt angle is slightly exaggerated.)

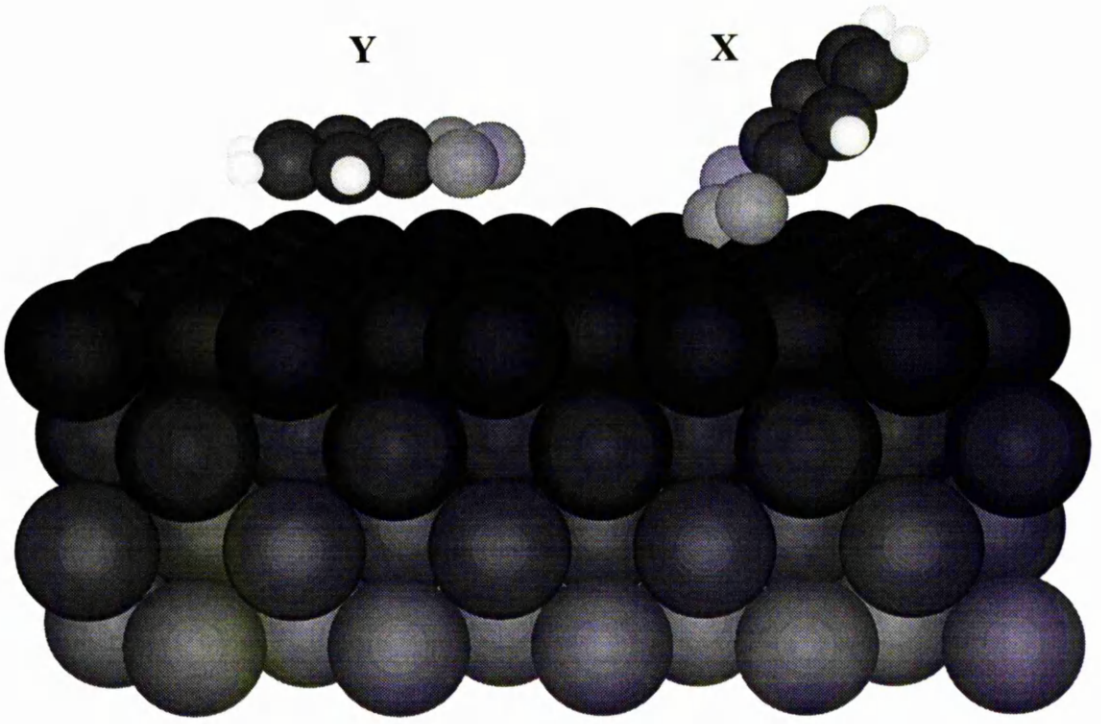

Figure 3.14 Orientational phase transition between the flat geometry at low coverage of BTA^- (Y) and saturation coverage (X) on Cu(100). The tilt angle is exaggerated for easier viewing.

to the surface via the π orbitals of the C and N atoms. However, at saturation coverage the bonding mode is assumed to change, accounting for the 'upright' geometry, and bonding probably takes place through the σ orbitals of the N atoms on the triazole ring.

The information for saturation coverage is compatible with the 3 possible bonding modes shown in Fig 3.15. Model A requires the terminal nitrogen atom to be the only one involved in the bonding to a surface copper atom. Here, there is an obvious ability for the molecule to rotate about this single bond which is inconsistent with NEXAFS data [17].

Model C is called the 'arrowhead' mode of bonding, an analogue of which occurs in the penta-nuclear copper cluster [32] depicted in Fig. 3.16. In this

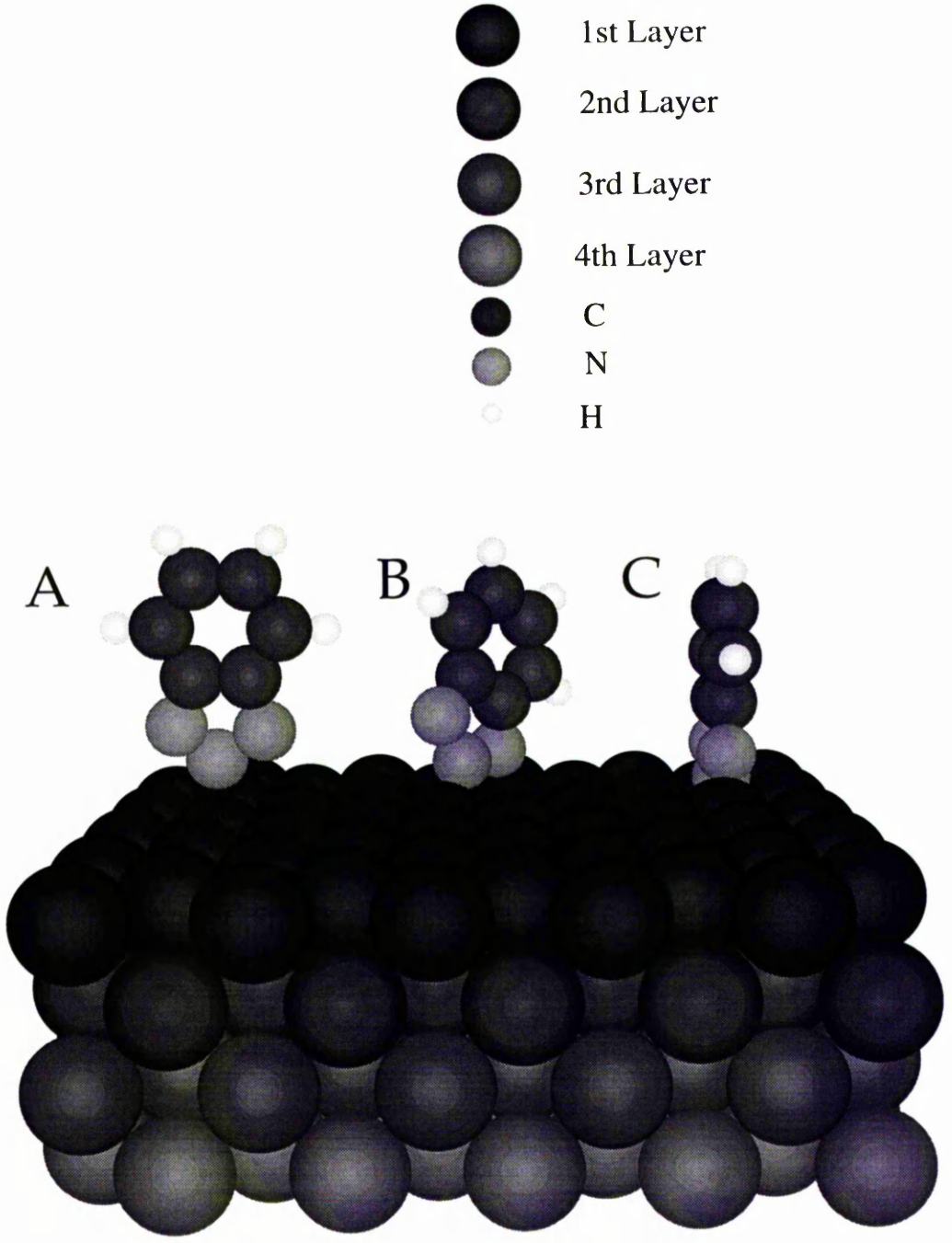

Figure 3.15 A side view of the proposed structural models for the adsorption sites of benzotriazole on Cu(100) : (A) bonded via the central nitrogen to one copper atom; (B) bonded via two adjacent nitrogens to two copper atoms; (C) bonded with each nitrogen atom bound to a copper atom, the central nitrogen being bound to a copper atom in the second layer, with adjacent nitrogen atoms each bound to a separate surface copper atom.

structure the three nitrogen atoms bond to copper atoms in a similar manner. On the surface we can imagine the peripheral nitrogen atoms bonding to copper atoms in the first layer, while the nitrogen at the 'head of the arrow' is bound to a copper atom in the second layer.

This 'arrowhead' mode of bonding [25, and others in preparation by the same authors] is seen to be characteristic of a number of complexes formed with the benzotriazole unit used as a base. In order for the bonding of benzotriazole on the Cu(100) surface to closely resemble that of the cluster shown in Fig. 3.16, then some slight movement of the copper atoms is required. In model C in Fig 3.15, the nitrogen copper bond lengths are 2.0 Å for the peripheral nitrogen atoms, and 2.8 Å for the terminal nitrogen atom bonding to the second layer copper atom. However, in the cluster, the nitrogen copper bond length varies between 2.0 and 2.3 Å for the peripheral nitrogens, and between 2.0 and 2.5 Å for the terminal nitrogen. Therefore, there is not much movement of the surface atoms required to match the bond lengths observed for the complex shown in Fig. 3.16. In model C we are assuming that the molecule is bonded in quite an upright geometry which is compatible with the results from the RATIO analysis where the tilt angle is calculated to be only 10° - 15° to the surface normal.

The distance across the copper atoms at the corners of the cube shown in Fig. 3.16 averages at 5.99 Å, while the corresponding distance in the model in Fig. 3.15 is 3.62 Å, the lattice constant of copper. To resolve this difference in distance, the benzotriazole is not assumed to penetrate the Cu(100) surface to as great a degree as it does the face of the cube in Fig. 3.16, if the surface bond lengths of 2.0 and 2.8 Å quoted for model C are to be considered correct. This would result in the bonds to the surface copper atoms being angled away from those in the ideal geometry shown in Fig. 4.16. However, the effect of a substrate relaxation would be expected to allow the surface copper-copper dis-

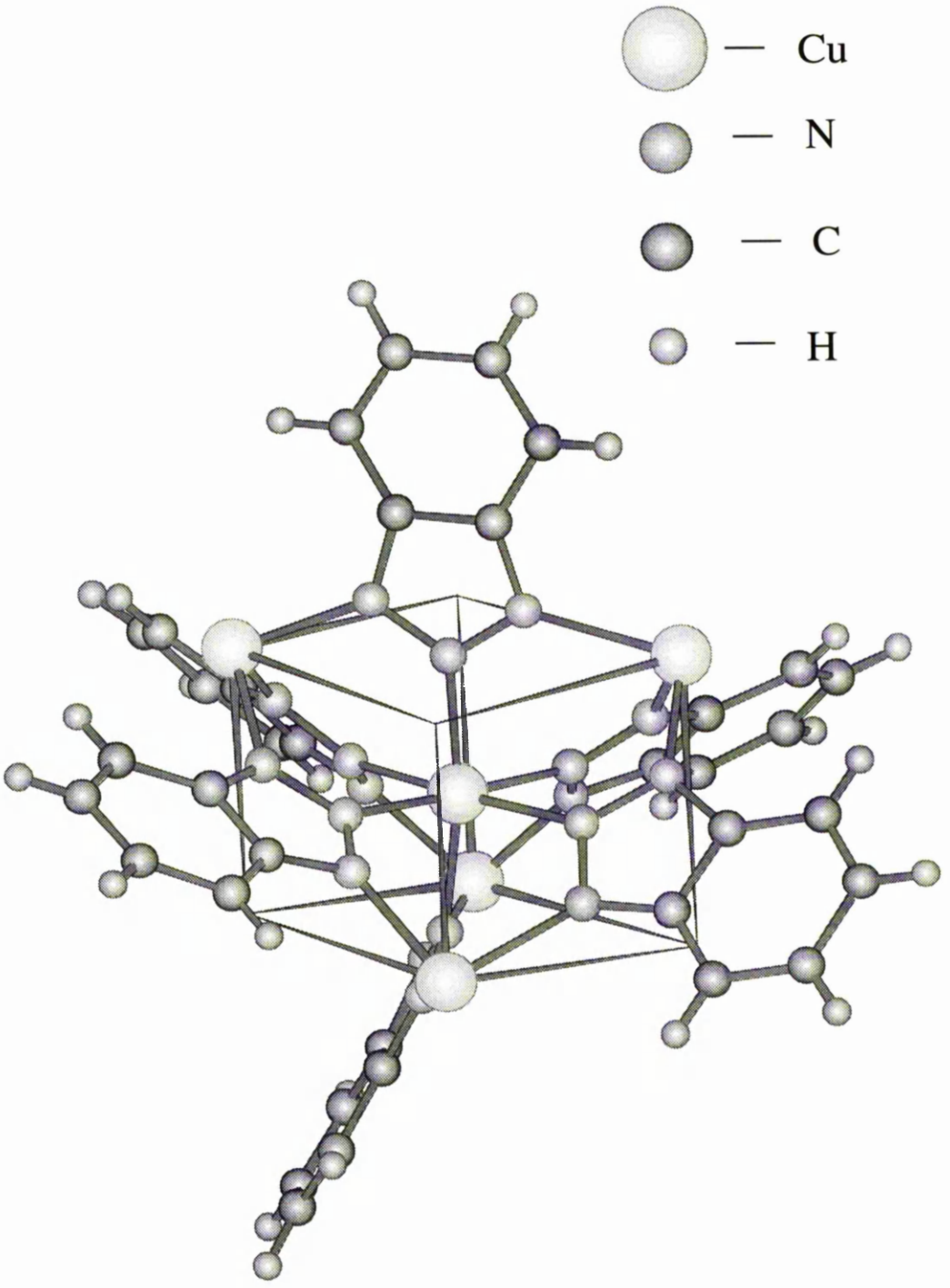

Figure 3.16 The $Cu_5(BTA)_6(acac)_4$ structure taken from reference [20], with the four acac groups are removed for clarity. (Space group $P2_1/n$, a=16.038 Å , b=22.836 Å , c=17.497 Å , α=90.0°, β=93.194°, γ=90.0°.)

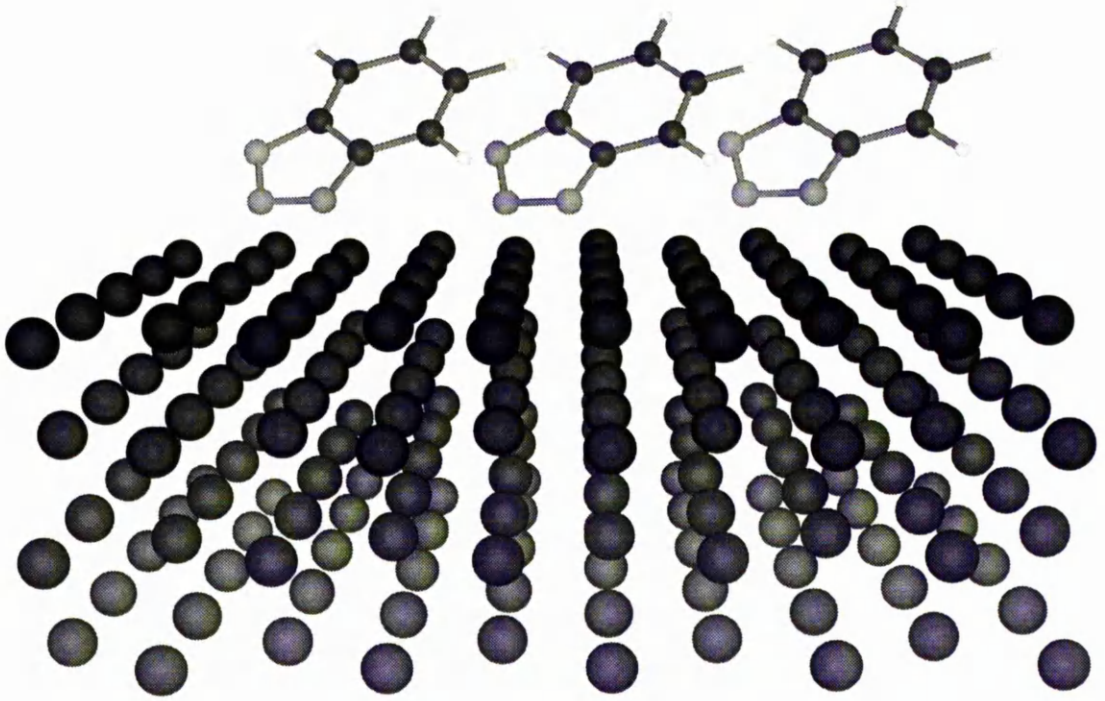

Figure 3.17 A depiction of how molecules of BTAH may order on the Cu(100) surface at saturation coverage according to Model B. The molecular tilt may aid interaction between one of the peripheral nitrogens in the triazole ring and the α-hydrogen on the benzene ring.

tance to vary, thus facilitating a geometry which would more closely resemble the inorganic analogue. Although if we take the molecular tilt or 'cant' in the xy plane, ψ, gained from the RATIO analysis, into account we must envisage that one of the peripheral Cu-N bond lengths is slightly larger than the other.

The unique corrosion inhibition properties of BTAH has often been ascribed to a canted orientation [6] on the surface similar to the orientation described in Model B in Fig 3.15. The tilted orientation gained from the analysis of the vibrational data is also compatible with this model. The tilt angle in the xy plane, , allows 2 N atoms to be anchored to the surface to two separate copper atoms, leaving the remaining N atom to interact with a H atom on an adjacent mol-

ecule, presumably the H atom closest to the triazole ring as shown by Fig 3.17. The N-N bond distance in complexes of BTAH is found to be approximately 2.21 A° [20] allowing the N-N atoms to bond across the copper atoms in the close packed direction which are separated by 2.56 A° (the nearest neighbour distance of Cu). For the bond distance to equal that of the average shown in Fig. 3.16 (2.0 - 2.5 Å), then the N-N pair would be approx. 2.0 Å above the surface plane.

When discussing the possible bonding and orientation of BTA^- on Cu(100), it is worth referring to the strikingly similar conclusions made in Chapter 5 in connection with 1, 2, 3 triazole to the same surface. The similarity in the molecular structure and orientation (tilted) of the two molecules on Cu(100) suggest that the bonding mechanisms are similar. The 1, 2, 3 triazole molecule does not have an attached benzene ring and therefore cannot strictly satisfy the requirements of Model B discussed above. Therefore it may be that both the BTA^- and triazolate anions bond via Model C, however further modelling of the system is required to resolve the latter point.

In summary, the relatively strong anchoring of the BTA^- anion to the surface via either 2 or 3 N atoms is possibly a major factor in its good corrosion inhibition properties and may also lead to the preferred tilting geometry. This may be an underlying factor in why BTA^- is a better corrosion inhibitor than the indazolate anion, which differs from BTA^- in that it has only 2 N atoms in the azole ring and also orients in a different geometry on the Cu(100) surface. This is discussed further in chapter 4. Further strong evidence suggesting the importance of the N atoms in the azole ring is referred to in Chapter 5, where the molecular framework of the azole ring is changed resulting in poor inhibition properties and very different orientations of the molecules on Cu(100).

3.3 Benzotriazole in the multilayer regime

3.3.1 Mode Assignment and Discussion

The multilayer RAIRS spectra of BTAH on Cu(100) are shown in Fig. 3.18. The spectra clearly show initially an increase in intensity of the band at 740 cm^{-1} after an exposure of 0.28 L which then decreases slightly in intensity as the 789 cm^{-1} band emerges. This point probably correlates to the transition between monolayer and multilayer coverage. In contrast to the RAIR spectra taken at room temperature, the intensity of the 740 cm^{-1} band then increases again and becomes by far the most intense peak in the spectra. New bands also appear which cannot be seen in the RAIR spectra taken at 298 K. These include bands at 905, 1013, and 1211 cm^{-1}. Also seen are bands correspond to equivalent bands in the spectra taken at 298 K, including the features at 1128, 1144, 1275 and 1387 cm^{-1}.

The 740 cm^{-1} band assigned to the CH out-of-plane bend is dominant in the multilayer regime spectra and this together with the relatively small in-plane bands indicates that the molecule prefers to lie 'flat' on the surface. However, the multilayer RAIR spectra should have enabled the detection of all of the BTAH vibrational modes assuming of course that the relevant modes contain a dipole moment perpendicular to the surface. However, the relatively 'flat' orientation of the molecule at 100 K means that many of the in-plane bands are not detectable. High doses are required in order to detect many of the bands. In general this is difficult because of the effects on noise and baseline but more importantly leads to water adsorption which can obscure many of the bands.

It is of course possible that a multilayer of BTAH molecules have not been adsorbed on the surface, resulting in the low intensity of the in-plane bands. This

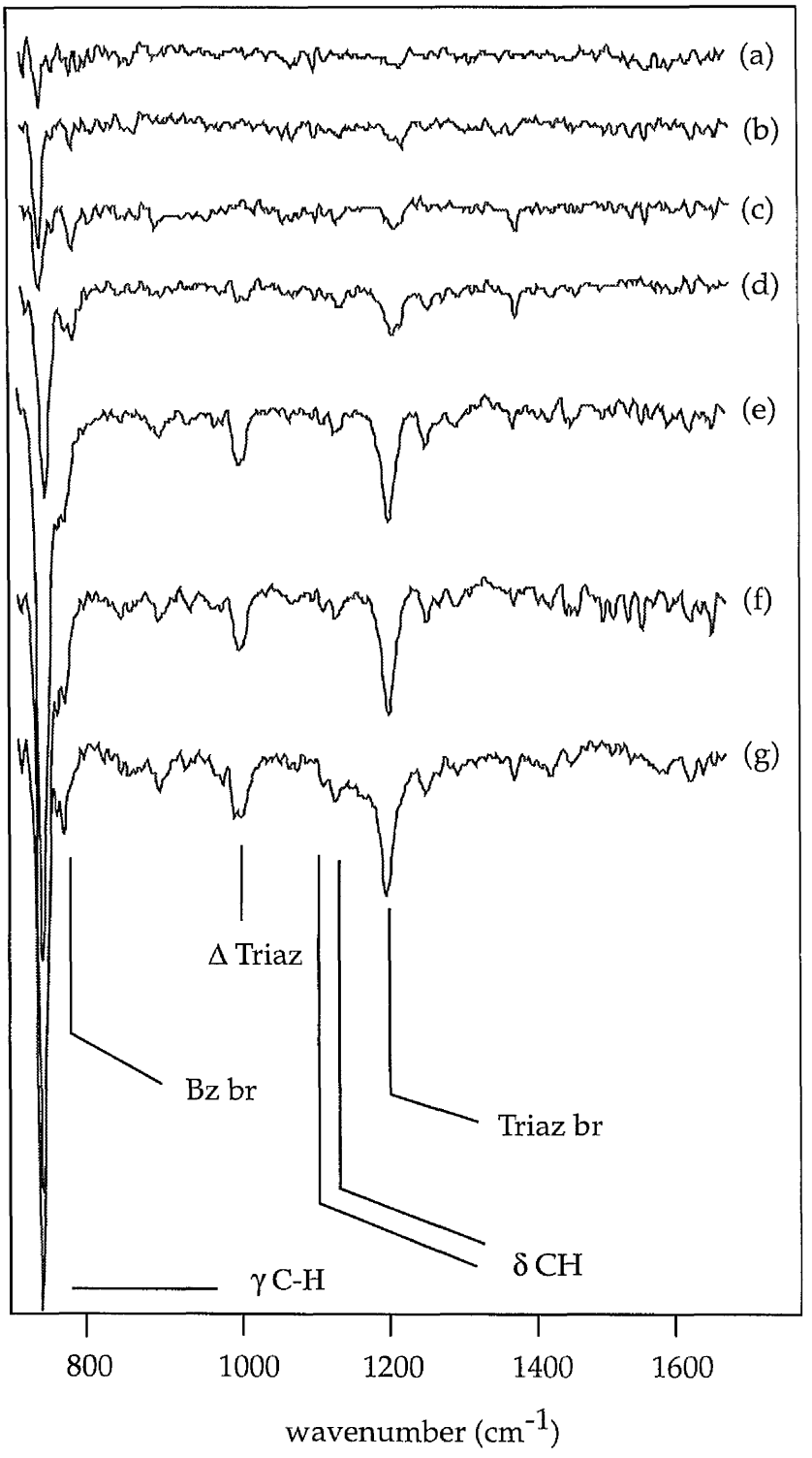

Figure 3.18 RAIR spectra of BTAH on Cu(100) taken at 100 K after exposures of (a) 0.01 L, (b) 0.28 L, (c) 0.8 L, (d) 1.2 L (e) 1.5 L, (f) 2 L, (g) 2.2 L. (γ = out-of-plane bend, br = breathing, δ = in-plane bend, Δ = ring in-plane bend).

is unlikely due to the doses used and the difference bands of the multilayer and monolayer spectra. Further support is derived from the size of the 740 cm^{-1} band which, at its most intense, has an intensity of 0.78% and is therefore by far the most intense band in the RAIR spectra of any of the azoles studied at 100 K. Indazole at multilayer coverage on Cu(100) produces the second most intense band of 0.37%.

The assignments of the bands are summarised in Table 3.5, together with a mode assignment made by Rubim et al. [11] for comparison.

The bands assigned to the CH out-of-plane bend at 740 cm^{-1}, CH in-plane bends at 1128, 1144, 1275 and the ring stretch at 1387cm^{-1} are not shifted to any great extent from the corresponding bands in the monolayer RAIR spectra and can be assigned similarly. The 905 cm^{-1} band is probably a CH out-of-plane bend which is just visible due to the parallel orientation.

The band at 1211 cm^{-1} is the most intense of the in-plane bands in the spectra and is important in that it distinguishes the difference between multilayer and monolayer adsorption through the triazole nitrogens. It is assigned to the triazole breathing mode involving the N=N stretch which shifts to 1170 cm^{-1} at monolayer coverage. Rubim et al [11] called this band a triazole breathing mode incorporating a N=N stretch for BTAH which is converted to a N=N=N stretch when the BTA^- ion is coordinated to the surface. The two smaller bands at 1140 and 1122 cm^{-1} are also seen in the room temperature spectra and are assigned to CH in-plane bends.

With reference to the crystal structure of benzotriazole [33], summarised in Fig. 3.19, the unusual 'flat' orientation of the multilayer can be understood in terms of a growth along the c-axis of the molecular solid. There are four molecules

RAIRS frequencies of BTAH on Cu(100) (cm^{-1})	IR frequencies taken from ref [11] (cm^{-1})	Assignment
740	743	γ CH
785	780	Bz br
905	900	γ CH
1013	1020	Δ Triaz
1126	1122	δ CH
1140	1146	δ CH
1211	1210	Triaz br / γ CH
1267	1280	δ CH
1387	1383	ω Triaz
1624	1622	ω Bz

Table 3.5 RAIRS frequencies of BTAH on Cu(100) at 100 K. ((γ = out of plane bend, Γ = torsion, δ = in-plane bend, br = breathing, ω = stretching, Triaz = triazole, Δ = ring in-plane bend). Also shown is a mode assignment taken from reference [11].

shown, with three being parallel to each other, and their molecular planes making an approximate angle of approx. 30° with the ab-plane of the unit cell. The remaining molecule makes an angle of approx. 115° with the other three, and 35° with the ab-plane. This gives an expected overall tilt of 31° if the growth mode is predominantly up the c-axis, in keeping with the predicted 'flat' orientation between the molecular plane and the plane of the surface expected from the RAIRS data. It is not possible to calculate an angle from the multilayer RAIRS data but the conclusions from the vibrational data compare well with the results of Walsh et al. [17], who showed a similar flat orientation of the multilayer, and derived an angle of 40° using NEXAFS of BTAH adsorbed on Cu(100) at 100 K.

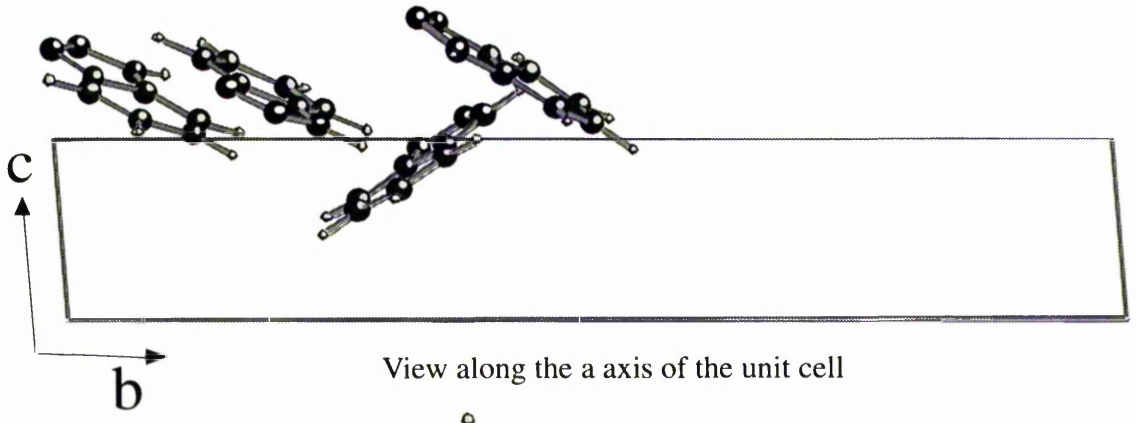

View along the a axis of the unit cell

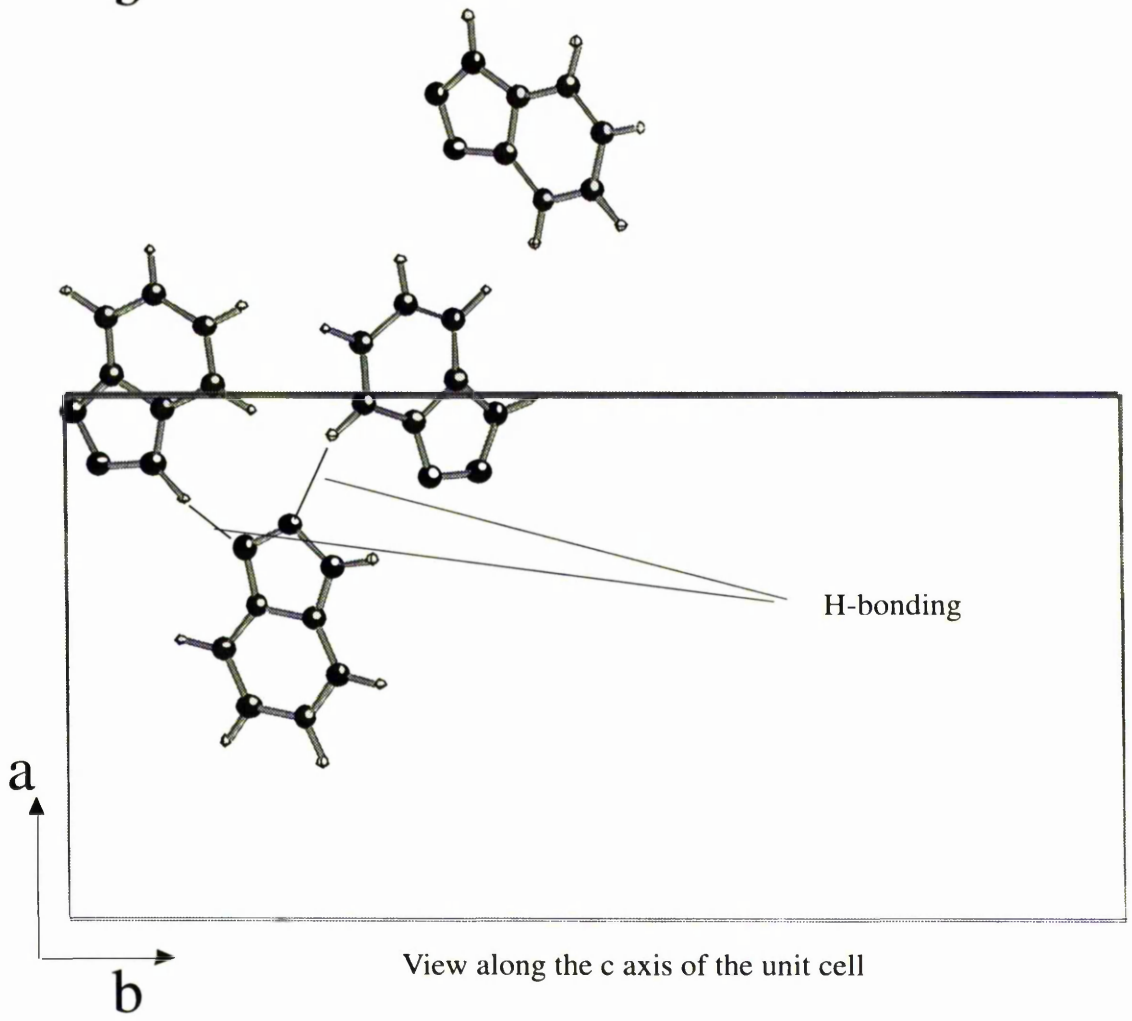

View along the c axis of the unit cell

Figure 3.13 Two views of the crystal structure of benzotriazole. (Space group $P2_1$, a=11.92 Å , b=23.55 Å , c=4.13 Å , α=90°, β=94.45°, γ=90°.) The view along the a-axis shows that 3 of the molecules in the unit cell are parallel to each other, with the remaining molecule making an angle of approx. 60° with them. The view along the c-axis shows the hydrogen bonding interaction. (Another 4 molecules in the unit cell are generated by symmetry, and are not shown.)

3.4 Summary

In summary, both HREELS and RAIRS spectra have shown benzotriazole to deprotonate on adsorption and orient in a flat geometry at low exposures (0.1 L) to the oxygen pre-dosed or clean Cu(100) surfaces. At higher coverages of benzotriazole the molecule undergoes an orientational phase transition such that it orients in a more 'tilted' configuration. Approximate Euler angles have been calculated from RAIRS intensity ratios on the oxygen predosed and clean Cu(100) surfaces which indicates that the molecule is probably 'canted' slightly as well as tilted on the surfaces. The results suggest the possibility that benzotriazole bonds via 2 or 3 of the nitrogens in the triazole ring . At multilayer coverage the molecule is not deprotonated and has been shown to orient in a relatively 'flat' geometry analogous to that seen in the crystal structure of BTAH [33]. The results suggest a specific first-bonding-layer origin for the corrosion inhibition properties of benzotriazole.

To resolve some of the questions raised by the work presented in this chapter, the following experiments are suggested for future work. An ultra high resolution EELS experiment is suggested to probe the bonding of benzotriazole to the surface and to possibly distinguish between whether 2 or 3 nitrogens atoms are bonded to the surface.

Frequency calculations are also suggested to assign those modes which are only tentatively assigned in this chapter. The Gaussian 92 method was used in an attempt to assign all the modes, but these broke down due to the complexity of the molecule.

Although models B or C in Figs. 3.14 are favoured, no information has been

obtained about the height of the molecule above the Cu(100) surface. There are techniques which could address this issue. Firstly, photoelectron diffraction of the N 1s core level using a synchrotron radiation beam line with a very high resolution would allow a more critical test of the chemical similarity of the nitrogen atoms. Chemical shift photoelectron diffraction, if the N 1s levels were resolved, could be used to extract bond distance and orientation information. Another technique which would allow us to determine the N-Cu distance(s), and thus the molecular displacement, is normal incidence standing x-ray waves (NISXW) which would give an accurate N-Cu distance, if model C were the correct model, or if there were two different N-Cu bond distances. Cross section would be the deciding factor using NISXW, since at the required photon energy of approx. 2 keV the cross section of the carbon and nitrogen core derived transitions would be extremely small.

An STM study has already been carried out on benzotriazole on Cu(110) [34 - get]. However, for a more comprehensive investigation using STM or AFM the resolution of the image should be improved, and the effect of the tip on molecular orientation should also be addressed.

References

[1] J. B. Cotton and I. R. Scholes, Brit. Corrosion J. 2 (1967) 1.

[2] G. P. Poling and I. C. G. Ogle, Annual Report INCRA Project No. 185, 1974. Inhibition of the Corrosion of Copper and its Alloys.

[3] I. Dugdale and J. B. Cotton, Corrosion Sci. 3 (1963) 69.

[4] R. F. Roberts, J. Electron Spectrosc. Related Phenomena 4 91974) 273.

[5] C. Thornkvist, D. Thierry, J. Bergman, B. Liedberg and C. Leygraf, J, Electrochem Soc. 136 (1989) 58.

[6] B. S. Fang, C. G. Olson and D. W. Lynch, Surface Science. 176 (1986) 476.

[7] D. Chadwick and T. Haskemi, Corrosion Sci. 18 (19780 39.

[8] G. W. Poling, Corrosion Sci. 17 (1970) 359.

[9] J. J. Kester, T. E. Furtak and A. J. Bevlo, Electrochem Soc, 100 (1982) 1716.

[10] P. G. Fox, G. Lewis and P. J. Boden, Corrosion Sci. 19 (1979) 457.

[11] J. Rubim, I. G. R. Gutz, O. Sala and W.J. Orville-Thomas, J. Mol. Struct. 100 (1985) 571.

[12] D. Thierry, C. Leygraf, in : Proc. 6th European Symp. on Corrosion Inhibitors. Ferrara, Italy, 1985.

[13] M. H. Palmer and S. M. F. Kennedy, J. Mol. Struct. 43 (1978) 203.

[14] M. C. Zonnevylle and R. Hoffman, J. Vacuum Sci. Technol. A 6 (1988) 885.

[15] J. E. Demuth, K. Christmann and P. N. Sanda, Chem. Phys. Lett., 76(1980)201

[16]K. Cho, Applied Surface Science, 87/88, 380, (1995).

[17] J. Walsh, PhD thesis, Manchester University, (1994).

[18] J. O. Nillson, C. Tornkvist, B. Liedberg, Applied Surf. Sci. 37 (1989) 306-326.

[19] D. Thierry, C. Leygraf, J. Electrochem. Soc., Vol. 132. No. 5, 1009, 1985.

[20] J. Handley, D. Collison, C.D. Garner, M. Helliwell, R. Docherty, J.R. Lawson and P.A. Tasker, Angew. Chem. Int. Ed. Engl. **32**, 1036, (1983).

[21] Y. J. Chabal, Surface Science Reports, vol 8, Nos. 5-7, (1988), 211-357.L. J. Bellamy, The Infrared Spectra of Complex Molecules, volume 2, second edition.

[22] H. Ibach and D. L. Mills, Electron Energy Loss Spectroscopy and Surface Vibrations, (1982), *publ. Acedemic Press Inc.*

[23] G. Socrates, Infrared Characteristic Group Frequencies, 2nd. Ed., (1994),*publ. Wiley.*

[24] V. H. Grassian, J. Phys Chem. (1986), 90, 5900 - 5907.

[25] J. E. Demuth, Chem Phys Lett 76, (1980), 201.

[26] Vibrational Spectroscopy of Molecules on Surfaces, by Yates and Madey, Plenum, 1987, Chapter 5, Chapter 7.

[27] G. Nonnenmacher and R. Mecke, Spectrochim. Acta, 17 (1961) 1049.

[28] E. Borello, J. Chem. Soc. B, (1969), 307.

[29] L. J. Bellamy, The Infrared Spectra of Complex Molecules, volume 2, second edition, Wiley, 1958

[30] S. Haq, B. Fredericks, to be published.

[31] M. K. Debe, J. Applied Phys. 55 (1984) 3354.

[32] P.A. Escande and J.L. Galigné, Acta. Cryst. B30, 1647, (1974).

[33] P.A. Escande, J.L. Galigné, and J. Lapasset, Acta. Cryst. B30, 1490, (1974).

[34] K. Cho, J. Kishimoto, T. Hashizume and T. Sakurai, Jpn. J. Appl. Phys. 33, L 125, (1994).

CHAPTER 4

Vibrational Spectroscopy of Indazole on Cu(100) in the Multilayer and Monolayer Regimes

4.1 Introduction

The aim of the work described in this chapter was to investigate and compare the orientation and coordination of the very first layer of indazole, a good corrosion inhibitor, on Cu(100) with that of BTAH on the same surface. Similar to the study of BTAH described in chapter 3, the surface sensitive techniques HREELS and RAIRS are used. Selection rules for active modes in HREELS and RAIRS are used to interpret the molecular orientation of the adsorbate on the Cu(100) surface.

The exact assignment of the vibrational modes of indazole is not clear. To aid interpretation we compare the assignment from BTAH and the other azoles studied.

4.2 Indazole in the Monolayer Regime

4.2.1 Group Theoretical Considerations

There is considerable evidence from the work presented in chapter 3 as well as the literature [1, 2, 3, 4] that the azoles adsorb following deprotonation of the molecule. Therefore the deprotonated indazolate anion is considered rather than the indazole molecule (see Fig 4.1).Group theory then gives the indazolate anion, of C_s symmetry a total of 39 vibrations which can be represented;

27 A' + 12A", all of which are IR active.

4.2.2 Experimental

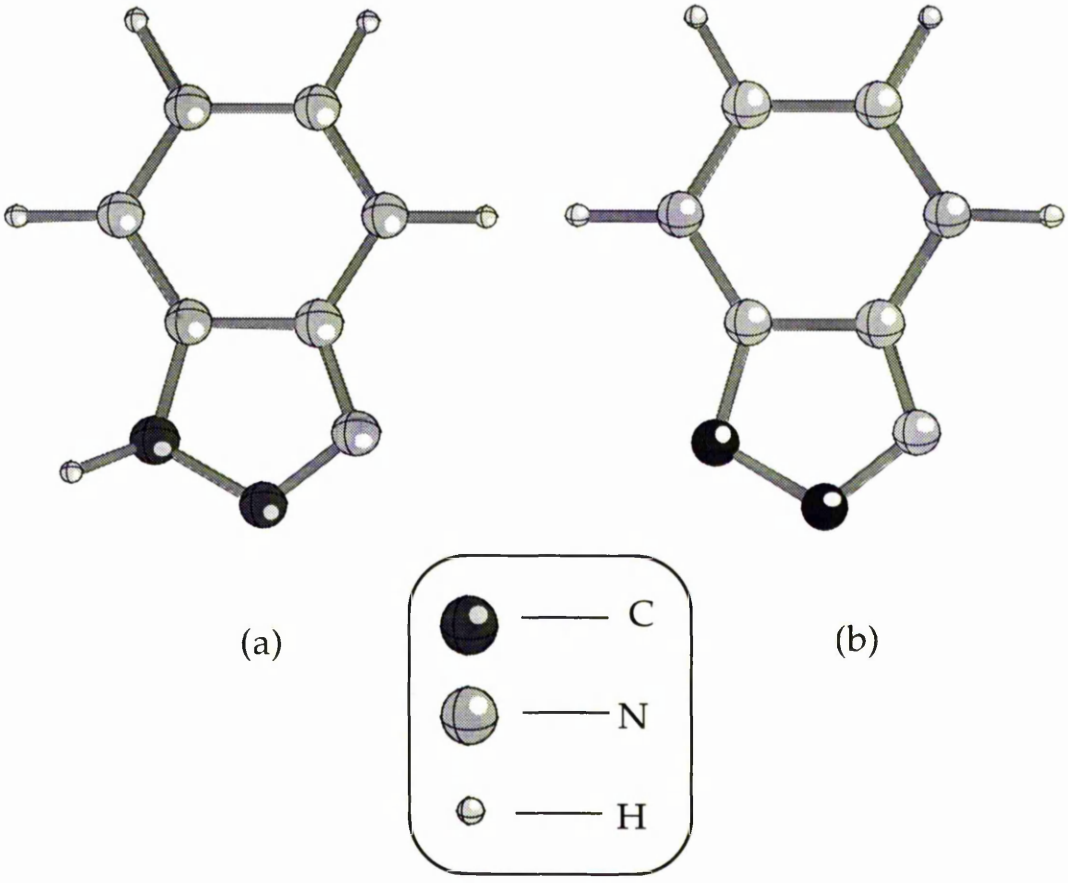

Figure 4.1 The indazole molecule (a) and the indazolate anion (b).

Experiments were performed in two separate UHV systems, both equipped with low electron energy diffraction (LEED), a retarding field analyser (RFA) for Auger, a mass spectrometer and argon ion gun, allowing standard sample preparation and characterisation to be performed. The base pressure of the systems were ~2×10^{-10} mbar.

The HREELS experiment (see section2.2) consisted of a 7 eV electron beam focused through a hemispherical deflector with a pass energy of 1 eV hitting the Cu(100) surface and being reflected through a similar hemispherical analyser with a similar pass energy acquiring spectra with a resolution of 9 meV (FWHM). In the specular collection mode the angle of incidence of the electron beam was 60° to the surface normal and the reflected electron beam

was collected at the same angle. For the off-specular collection mode the angle of collection was changed to 67° to the surface normal, recording spectra at 7° off-specular.

The infrared facility (see section 2.4) consisted of an infrared beam from the FT-IR spectrometer (Mattson Galaxy) focused through a differentially pumped KBr window onto the sample mounted in the UHV chamber. The system was aligned to give a single reflection off the surface at an angle of incidence of ~82°. The reflected light was collimated and focused onto a narrow band MCT detector which accessed the spectral range between 4000 and 700 cm^{-1} and spectra were acquired at a resolution of 4 cm^{-1}.

In both experiments the Cu(100) was cleaned via argon ion (1 keV) bombardment and annealed to a temperature of 900 K to produce a well ordered (1 x 1) LEED pattern. In the HREELS chamber, indazole was dosed directionally at a pressure of 1×10^{-9} mbar for varying periods of time. In the RAIRS experiment the indazole was dosed from ambient at a pressure of 1×10^{-9} mbar. No LEED pattern was seen after dosing.

4.2.3 Results and Discussion

Figures 4.2 and 4.3 show HREELS spectra of indazole in specular and 7° off specular geometries. Modes which can be assigned with some certainty are indicated (the mode assignment is discussed below). The specular data show that at low doses loss, features at 777 and 976 cm^{-1} are prominent. As the dose is increased, features at 435, 556, 637, 774, 911, 997, 1129, 1161, 1217, 1314, 1379, 1451, 1484 and 1621 cm^{-1} emerge, eventually reaching a maximum at a dose of 5 L. The off-specular spectra are similar to the on-specular data at all coverages except for features in the in-plane region (800-3089 cm^{-1}) being relatively more

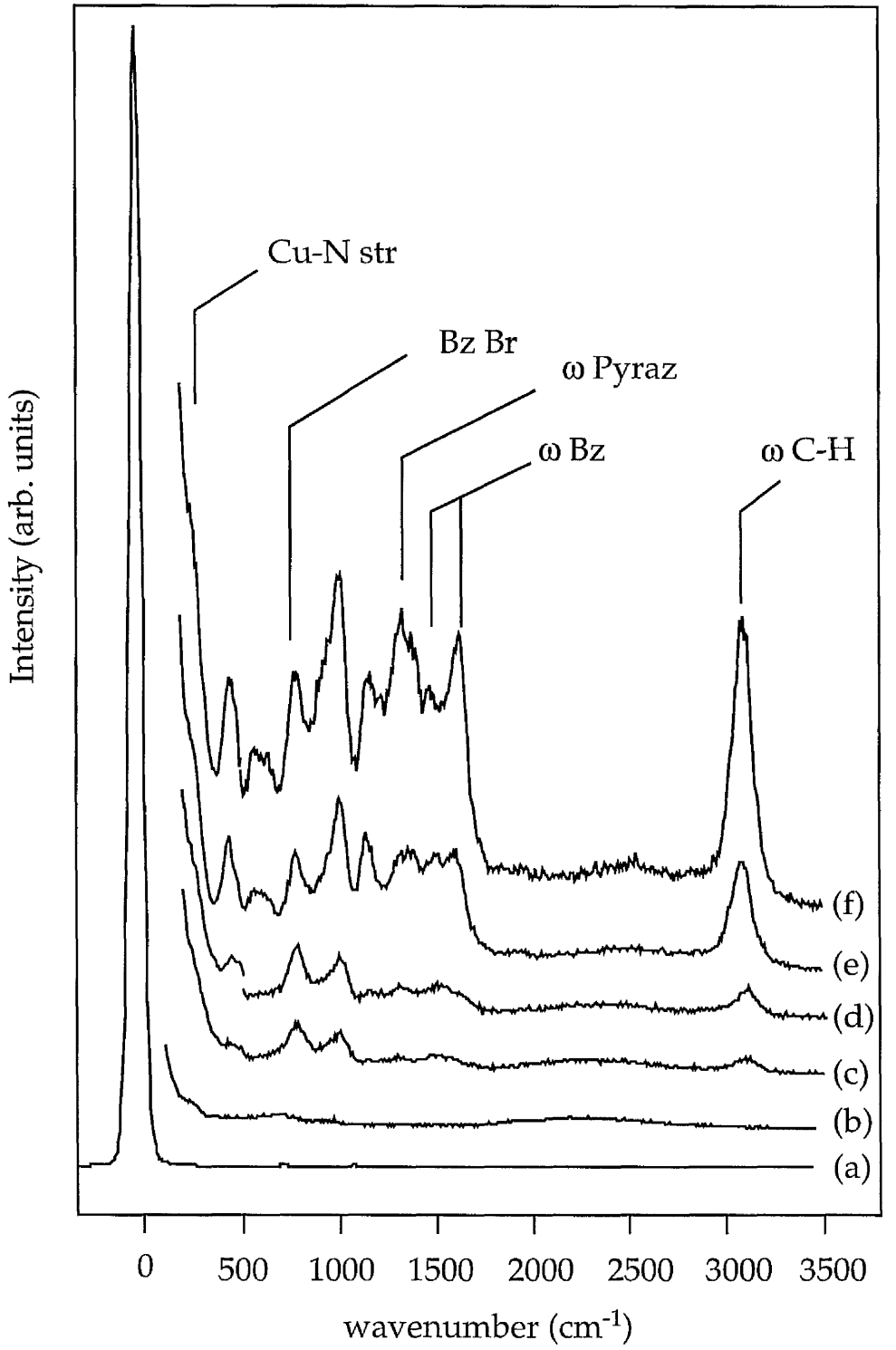

Figure 4.2 Specular HREELS spectra recorded following (b) 0.05 L, (c) 0.1 L, (d) 0.15 L, (e) 3 L and (f) 5 L doses of indazole onto Cu(100) taken at room temperature. ($\theta_i = \theta_r = 60°$, primary beam energy = 7 eV, FWHM (elastic peak) = 64 cm^{-1}. All spectra have been normalised to the elastic peak).

(γ = out of plane bend, Γ = torsion, δ = in-plane bend br = breathing, ω = stretching, Triaz = triazole)

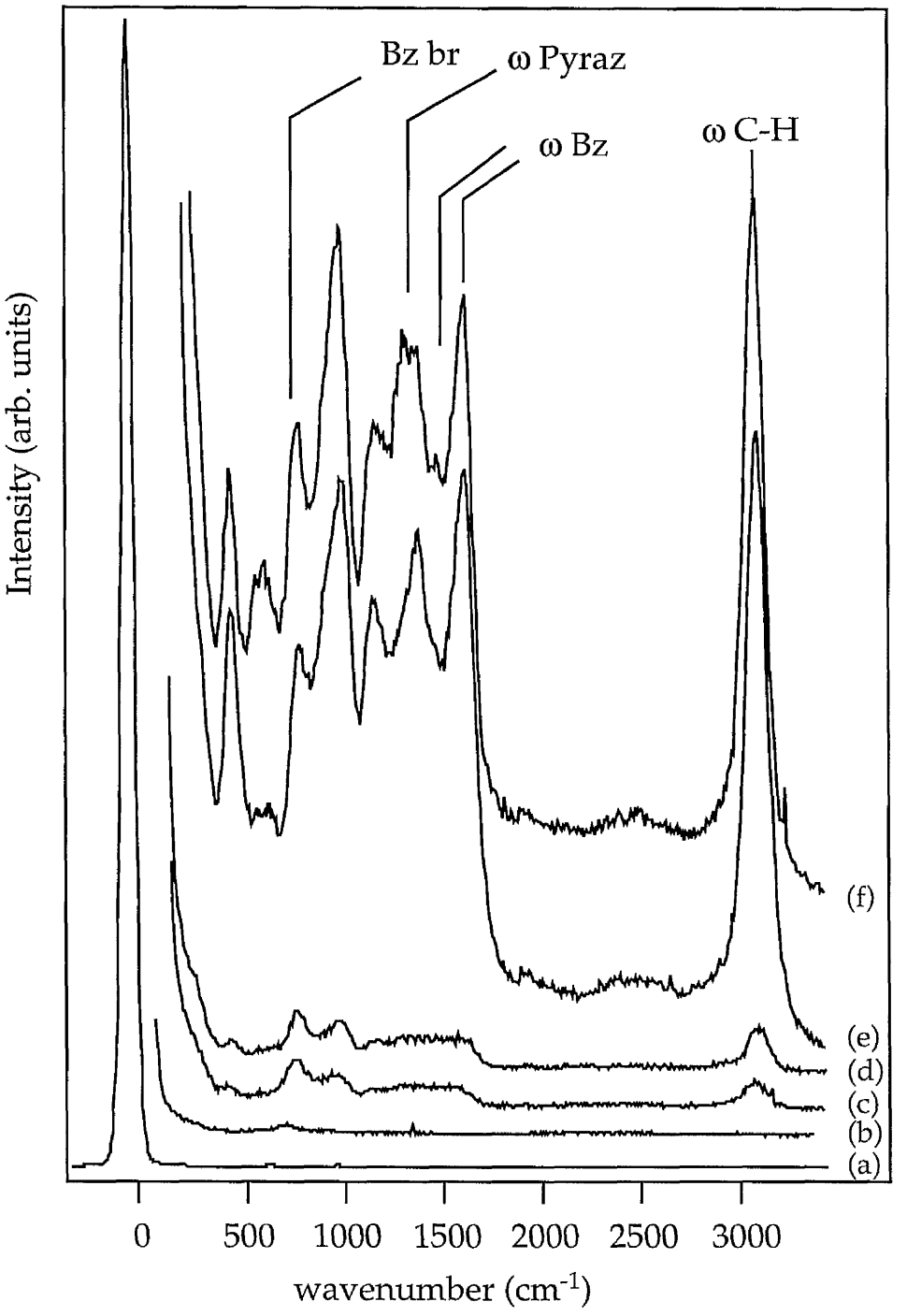

Figure 4.3 7° off specular HREELS spectra recorded following (a) 0.05 L, (b) 0.1 L, (c) 0.2 L, (d) 0.4 L and (e) 2 L doses of indazole onto Cu(100) taken at room temperature. (θ_i = 60°, θ_r = 67°, primary beam energy = 7 eV, FWHM (elastic peak) = 70 cm^{-1}. All spectra have been normalised to the elastic peak). (γ = out of plane bend, Γ = torsion, δ = in-plane bend, br = breathing, ω = stretching, Triaz = triazole, Δ = ring in-plane bend).

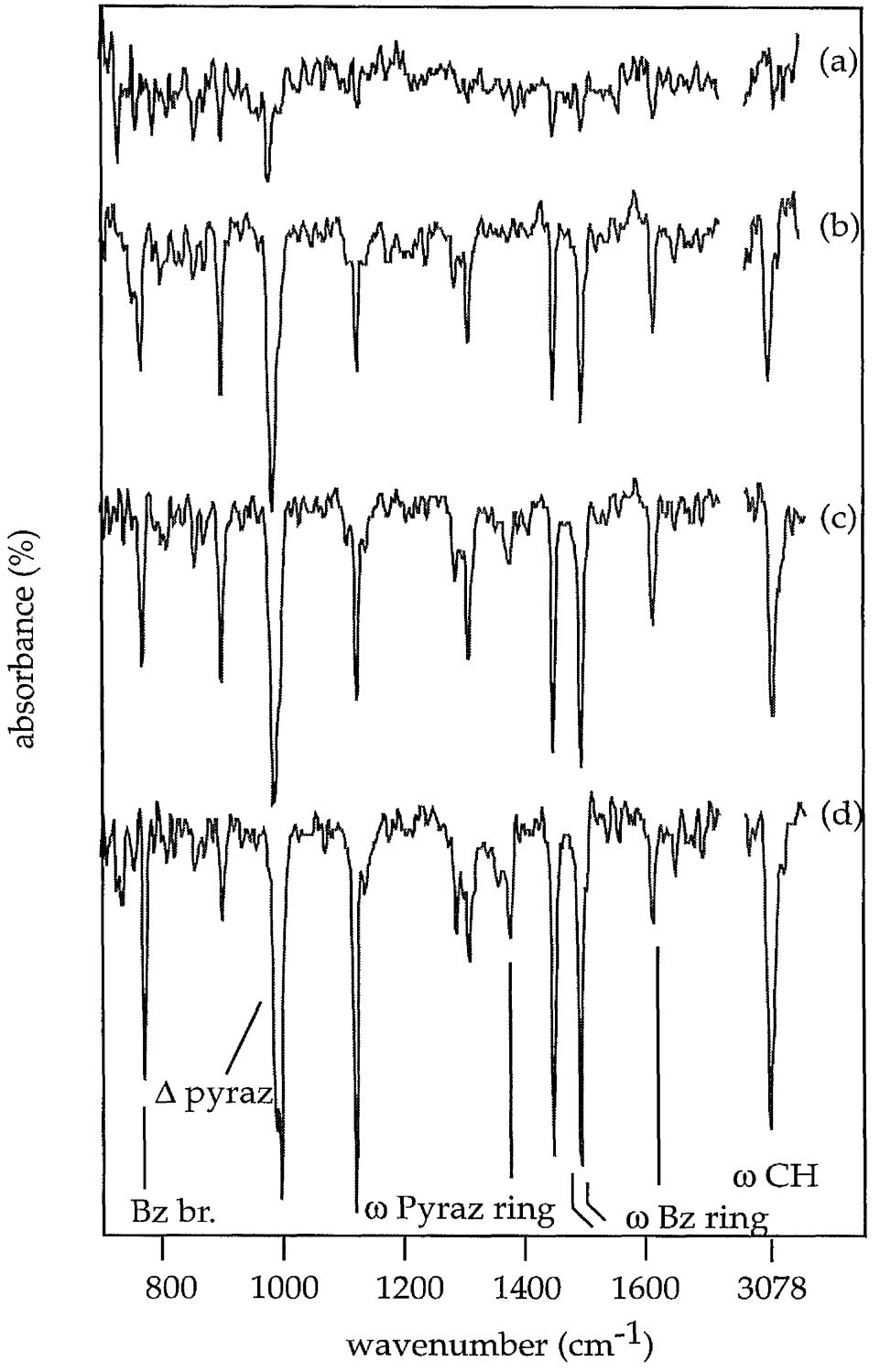

Figure 4.4 RAIRS spectra of indazole adsorbed on Cu(100) at exposures of (a) 0.59 L, (b) 1.89 L, (c) 2.38 L, (d) 2.7 L. (γ = out of plane bend, Γ = torsion, δ = in-plane bend, br = breathing, ω = stretching, Triaz = triazole, Δ = ring in-plane bend).

intense than those of the specular spectrum. This is due presumably to the increased impact scattering cross section of the modes in the in-plane region.

The corresponding RAIRS spectra which are displayed in Fig. 4.4 contain intense bands in the in-plane region of the spectra with bands at 774, 901, 997, 1123, 1285, 1308, 1377, 1449, 1497, 1615, and 1651 cm^{-1}.

An important initial observation is the lack of a feature at 740 cm^{-1} in spectra recorded in the monolayer regime. This mode, which would correspond to the CH out-of-plane bend [1, 2, 3, 4], is an intense characteristic feature in the vibrational spectra of benzotriazole, benzimidazole and is also seen in the RAIRS spectra of 1, 2, 3, triazole on Cu(100) (chapter 5) at a higher frequency of 790 cm^{-1}. An intense CH out-of-plane bend is indicative of a large molecular tilt angle relative to the surface normal. Hence, the absence of this feature in Figs. 4.2, 4.3 and 4.4 seems to indicate that the indazolate anion preferentially orients in a perpendicular geometry on Cu(100), both at low and at saturation coverage at 298 K. This point is discussed further in section 4.4. This interpretation is further supported by the size of the in-plane loss features in the 800-3100 cm^{-1} region relative to those seen in the analogous BTA^- HREEL spectra on Cu(100), although accurate conclusions cannot be made from this comparison since impact scattering contributions feature strongly in the HREEL spectra. Comparison of the relative intensities of the RAIRS bands is a better indicator of the degree of tilt, although relative surface coverage comparisons could account for some of the intensity differences. The relative intensities of the indazolate anion bands are compared with those of the BTA^- anion on the Cu(100) and Cu/O surfaces at saturation coverage in Fig. 4.5. The in-plane bands in the spectra of the indazolate anion on Cu(100) are generally more intense than the corresponding bands in the BTA^- spectra. This can clearly be seen from the intensity of the characteristic CH stretches in the 3052 - 3056 cm^{-1} region and

ring stretches. An example being the intensity of the ring stretch at 1449 cm^{-1} which is 0.08% in the indazolate spectra, with the analagous bands in the BTA^- spectra being 0.05% (1439 cm^{-1}), and 0.45% (1439 cm^{-1}) for the Cu/O and Cu(100) surfaces respectively.

The mode assignment of indazole is somewhat more complicated than the other azoles studied in this work due to the lower symmetry of the indazole molecule and the lack of previously published work. Whereas a certain amount of degeneracy is expected in the vibrational modes of BTAH, this is not the case with indazole. However, an assignment of the important modes can be made with reference to the vibrational spectra of the other azoles studied. The assignment of the important loss features and bands are shown in Table 4.1 together with some assignments from the literature shown in Table 4.2 [5]. Several regions of the spectra in which some of the more important modes are contained are discussed below.

The 700-1000 cm^{-1} region: the region shows peaks common to all the benzene ring containing azoles studied and can be assigned accordingly. These include the 773 cm^{-1} feature which is assigned to a benzene breathing mode [1, 4], and also the feature at 997 cm^{-1} can be assigned to the azole ring in-plane bend by comparison with the corresponding spectrum of benzotriazole on Cu(100), where it is seen at 992 cm^{-1}. This feature corresponds well with the assignments of azoles made in the literature [1, 8].

1400-1660 cm^{-1} region : The ring stretches seen at 1615, 1497 and 1449 cm^{-1} are characteristic of the azoles [1] and can be related to the 3 peaks in the BTA^- vibrational spectra at 1605, 1481 and 1439 cm^{-1} . Rubim et al. [1] showed these peaks to shift depending on whether the anion or molecule is adsorbed on the Cu(100) surface. Similarly, the peaks at 1615 and 1495 cm^{-1} are seen to shift

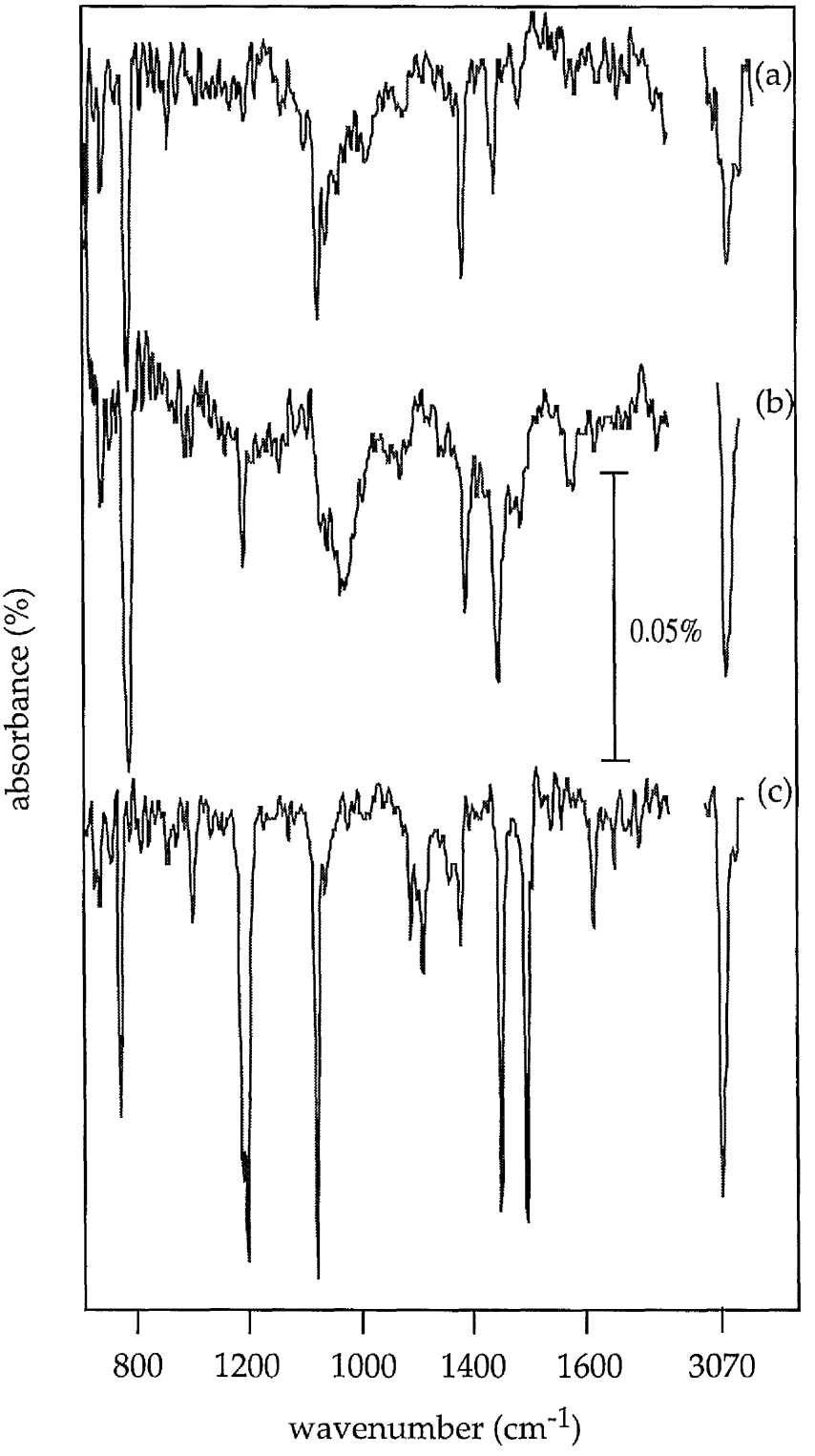

Figure 4.5 Comparison of RAIRS spectra of BTAH adsorbed on: (a) Cu(100); (b) Cu/O; and (c) indazole adsorbed on Cu(100) at saturation coverage at 298 K.

HREELS and RAIRS frequencies of Indazole on Cu(100)		
HREELS (cm^{-1})	RAIRS (cm^{-1})	Assignment
3089	3056	ω CH
	1651	ω CN
1621	1615	ω Bz
1484	1497	ω Bz
1451	1449	ω Bz
1379	1377	ω Pyraz
1314	1308	δ C-H
	1285	δ C-H
1217		δ C-H
1161		δ C-H
1129	1123	Pyraz br
992	997	Δ pyraz
911	901	Δ pyraz
774	774	Bz breathing
637		Δ Bz
556		Δ Bz
435		Δ Bz
233-250		Cu-N

Table 4.1 HREELS and RAIRS frequencies and assignments of indazole adsorbed on Cu(100) at 298 K. (Bz = Benzene, Triaz = Triazole, comp = complex, br = breathing, Δ = ring in-plane bend, δ= in-plane bend, γ= out-of-plane bend.)

IR frequencies and polarisation	Raman frequencies and polarisation	Assignment		
3181 s	3178 vw, br	A'	υ	NH
3158 s		A'		
3120 m		A'		
3106 m	3104 m (p)	A'	υ	CH
3087 m	3088 mw	A'	υ	CH
	3070 ms (p)			
3071 m		A'	υ	CH
	3067 ms			
3053 m		A'		
3040 m	3041 w	A'	υ	CH
	3031 w	A'	υ	CH
1622 m	1623 w (p)	A'	υ	skeletal
1585 w	1584 w (dp)	A'	υ	skeletal
1509 ms	1504 w	A'	υ	skeletal
1486 m	1488 m (p)	A'	υ	skeletal
1444 m	1443 m	A'	υ	skeletal
1409 w		A'		
1390 sh				
1382 m	1389 m (p)	A'	υ	skeletal
1357 s	1359 m (p)	A'	υ	skeletal
1315 w	1315 w (p)	A'	υ	skeletal
1305 w		A'		
1285 m	1284 w (p)	A'	υ	skeletal, δ CH
1249 m	1248 w (dp)	A'	δ	CH, υ skeletal
1205 m	1203 w (p)	A'	δ	CH
1171 w		A'		
1150 mw				
1144 mw	1144 vw	A'		
1123 m	1122 w (p)	A'	δ	CH
1076 ms	1077 ms (p)	A'	δ	CH
1020 w	1021 w	A'	δ	CH
1004 s	1002 m (p)	A'	δ	skeletal
971 *		(A")	γ	CH
951 s	949 w (p)	A'	δ	skeletal
941 ms	933 m	A"	γ	CH
894 mw	892 w (p)	A'	δ	skeletal
870 mw		A"	γ	CH
860 sh	859 w	A"		
848 s	846 w	A"	γ	CH
805 w				
785 m, br **		A"	γ	NH
768 ms	769 vs (p)	A'	δ	skeletal
746 vs	751 vw	A"	γ	CH
656 w				
616 m	616 m (dp?)	A'	δ	skeletal
563 w	559 w	A"	γ	skeletal
540 vw	541 m (p)	A'	δ	skeletal
510 vw				
470 vw		A"	γ	skeletal
436 m				
430 m	427 vw	A"	γ	skeletal
405 w				
400 w	402 w (dp)	A"	γ	skeletal
275 w		A"	γ	skeletal
240 vw	238 w			
225 vw	223 vw (dp?)	A"	γ	skeletal

Table 4.2 IR and RAMAN frequencies of indazole taken from reference [5].

(bz = Benzene, υ = stretch, δ= in-plane bend, γ = out-of-plane bend.)

from the higher frequencies values observed in the low temperature spectra of 1624 and 1501 cm^{-1} (section 4.3).

O Sullivan et al [6] assigned bands in the 1660-1620 cm^{-1} region to the C=N stretches in a number of molecules containing benzene rings fused to five membered rings. The band at 1654 cm^{-1} clearly distinguishable in the RAIRS spectra in Fig 4.4 is assigned to the C=N stretch. This is interesting in that BTAH, at either room or low temperature, shows no such band in this region indicating the lack of any C=N linkages.

The 1100-1400 cm^{-1} region : this region contains several features, at 1123, 1285, 1308 and 1377 cm^{-1}, the assignment of which can be seen in Table 4.1. Similar to BTAH, the features are thought to be CH in-plane bends [5] apart from the 1377 cm^{-1} band which is assigned to an azole ring stretch, which characteristically occur at lower frequencies than the benzene stretches [1, 6, 7]. The other exception is possibly the 1121 cm^{-1} feature which is commented on further below.

If the RAIRS spectra are compared with the low temperature spectra discussed in section 4.3, we see that the 1100-1300 cm^{-1} region in the low temperature spectra contain bands of low intensity relative to other bands in the spectra. This is in contrast to the 1100-1300 cm^{-1} region in the room temperature RAIRS spectra which shows a very intense feature at 1121 cm^{-1}, indeed one of the most intense bands in the spectra. The latter observation may occur due to the breathing motion of the azole ring becoming very intense on adsorption. This was also the case in the vibrational spectra of the BTA^- ion on Cu(100). The breathing motion of the ring is seen at 1124 cm^{-1} in the IR spectrum of pyrazole [8]. Alternatively, it may be assigned to a CH in-plane bend.

High frequency region : Similar to the other azoles, the high frequency region of the spectra shows just the CH stretch at a frequency of 3056 cm^{-1} . The spectra do not contain a N-H stretch. This reinforces the view that the proton is lost on adsorption. This is in direct contrast to the low temperature spectra which show several stretches, of which 2 are thought to be N-H stretches due to the formation of polymers on hydrogen bonding of the molecules. Hydrogen bonding also causes the N-H stretch/stretches to shift to lower frequency [9, 10]. This is discussed further in section 4.3.

Low frequency region ; The loss feature at 233-250 cm^{-1} in the HREELS spectrum at saturation coverage shown in Fig. 4.2 is seen as a shoulder on the elastic peak and occurs at a similar frequency to a band seen at 250 cm^{-1} in the HREEL spectrum of BTAH adsorbed on Cu(100). The band is similarly assigned to the Cu-N mode. The frequency of the Cu-N mode correlates well with that of a broad feature seen at 232 cm^{-1} assigned by Rubim et al.[1] to the Cu-N mode in SERS of BTAH on Cu electrodes. Various authors [11, 12] have observed features in the 200-250 cm^{-1} region when assigning the Cu-N mode in vibrational work of pyridine on metals.

4.2.3 Observations on Orientation and Possible Bonding Modes

The absence of out-of-plane modes and presence of in-plane modes at all exposures of indazole to Cu(100) suggests that indazolate anion is oriented in a perpendicular geometry at all coverages. As with BTA^- and the triazolate anions on Cu(100), the evidence of the previous section suggests that the 5 membered ring is deprotonated and probably bonds to the surface through the azole ring.

Indazole is envisaged to bond to the surface via either of two bonding mecha-

nisms, these are shown as Model A and Model B in Fig 4.6. Model A requires the terminal nitrogen atom to be the only one involved in the bonding to a surface copper atom. Here, there is an obvious ability for the molecule to rotate about this single bond and is deemed unlikely since it does not suggest a highly stable surface. Model B requires the 2 N atoms in the pyrazole ring to be bound to the surface. The N-N bond distance, which is expected to be similar to that of BTAH, is approximately 2.21 A° [13], and is compatible with bonding to two neighbouring Cu atoms, the nearest neighbour distance being 2.56 A°. Bonding is expected to occur through the σ orbitals of the N atoms.

With reference to the possible bonding models of all the good corrosion inhibitors, the evidence suggests that the azoles require at least 2 adjacent N atoms in the 5 membered ring to anchor to the surface and thus bond in a more upright geometry. This is the case with BTAH and indazole which satisfy the requirements of a good corrosion inhibitor. On the other hand, benzimidazole, which is a poor corrosion inhibitor, has two N atoms separated by a C atom in the azole ring, hence the molecule would prefer to bond to the surface using its π orbitals in a flat orientation. This and other differences in the molecular framework of the poor corrosion inhibitors are discussed further in chapter 6.

Now let us address the reasons for BTAH being a better corrosion inhibitor than indazole. The reason probably lies in the role of the N atoms in the azole ring. BTAH has advantages in that the third N atom may either take part in bonding to the surface in an 'arrowhaed' mechanism thus securing a stronger bond to the surface. Alternatively, one of the peripheral N atoms may be able to interact with the a hydrogen on the benzene ring of an adjacent molecule. Both these mechanisms are mentioned in section 4.2.7. Indazole, on the other hand, has a C atom adjacent to the two N atoms in the azole ring which is unlikely to take part in bonding to the surface due to bonding being inhibited by the H

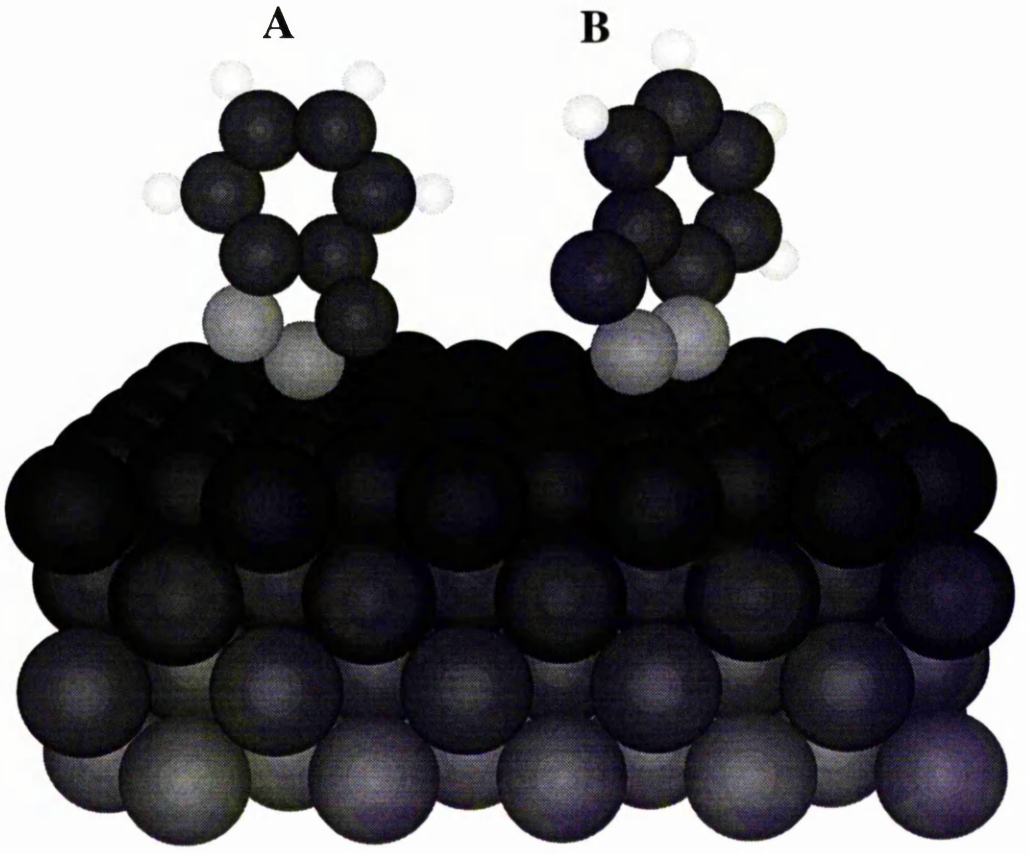

Figure 4.6 A side view of the proposed structural models for the adsorption sites of indazolate anion on Cu(100) : (A) bonded via the central nitrogen to one copper atom; (B) bonded via two adjacent nitrogens to two copper atoms.

atom attached to it. This is further supported by the fact that resonance stabilised ringed molecules rarely stand upright if the molecule relies on using a C atom to σ bond to the surface to enable it to do so. This is observed when comparing the bonding of pyridine and benzene. The latter bonds in a parallel geometry to metal surfaces whereas the former can bond in a parallel geometry at submonolayer coverage but can revert to an upright geometry at saturation coverage, where it is thought to bond through the N atom [13, 14].

Intermolecular interaction was encorporated into Model B of the 3 bonding

mechanisms suggested for the bonding of the BTA^- anion on Cu(100). It was suggested that the N atom, could interact with the α hydrogen (adjacent to the azole ring) on the benzene ring through a H-bonding interaction. The analogous bonding mechanism for the indazolate anion (Model B in Fig. 4.6) could not provide these advantages due to the obvious presence of the C-H atoms rather than an N atom, the latter having a lone pair of electrons.

The origins of the molecular tilt of the BTA^- anion as apposed to the perpendicular geometry of indazole may also have its origins in the factors mentioned above. Further modelling of the system is required to resolve the latter point However, the above reasons do possibly go some way to explaining the better corrosion inhibition properties of BTAH compared to indazole.

4.3 Indazole in the Multilayer regime

4.3.1 Results and discussion

The RAIRS spectra of indazole adsorbed on Cu(100) at 100 K can be seen in Fig. 4.7. The modes which can be assigned with some degree of certainty are indicated. A tentative mode assignment is also made in Table 4.3 with some of the modes being discussed below.

700-1000 cm^{-1} region : The initial point to note from the low temperature RAIRS spectra is the very intense band at 740 cm^{-1} which is absent in the spectra taken at 298 K. This mode is typical to all the azoles studied and is assigned to the CH out-of-plane bend. The high intensity of this band relative to the other bands shows the preference for a more parallel molecular orientation compared to the perpendicular geometry of the indazolate anion at room temperature on the Cu(100) surface. The band also seems to show some evidence of a Fermi

resonance in that it seems to grow as a single band at exposures of 0.6 L and below but then decreases in intensity at 0.9 L, where it splits into a doublet at giving a band at 752 cm^{-1} at higher exposures. Hence, it is likely that the 740 cm^{-1} band would be of even greater intensity but for the intensity sharing with the band at 752 cm^{-1}, which is either another CH out-of-plane bend or possibly the NH out-of-plane bend. The 833 cm^{-1} and 852 cm^{-1} bands show similar characteristics. The benzene breathing mode is of low intensity as expected from the parallel geometry and is shifted from the room temperature value of 773 cm^{-1} to 769 cm^{-1}.

A feature which is expected to be prominent, considering the parallel geometry of the indazole molecule, is the the N-H out-of-plane bend. The problem with assigning a band to this mode is the effect that hydrogen bonding between adjacent molecules has upon the N-H features. The effect on the frequency of the N-H stretch is quite drastic and is discussed later in this section, however it does suggest that the N-H out-of-plane bend may also be affected to a large degree. Cane et al [15] assigned a band as low as 404 cm^{-1} to the N-H wagging mode in the gas phase spectra of indazole whereas in pyrazole the analogous bend was assigned to a band at 943 cm^{-1} when in the single crystal form. Bigotto et al. [5] assigned the mode to a band at 750 cm^{-1} in the IR spectra of indazole. Various other authors have also assigned the NH out-of-plane bend of the azoles in this higher region of the spectra [16, 17]. Therefore it is quite difficult to assign a band to this mode, but it is suspected that there is a large shift to higher frequencies at liquid nitrogen temperatures. Any of the three bands at 752, 833, or 854 cm^{-1} could possibly be assigned to the N-H wagging motion.

The pyrazole in-plane bends again occur characteristically in the 900 -1020 cm^{-1} region. Two characteristic bands are seen in the 900 - 1020 cm^{-1} region assigned

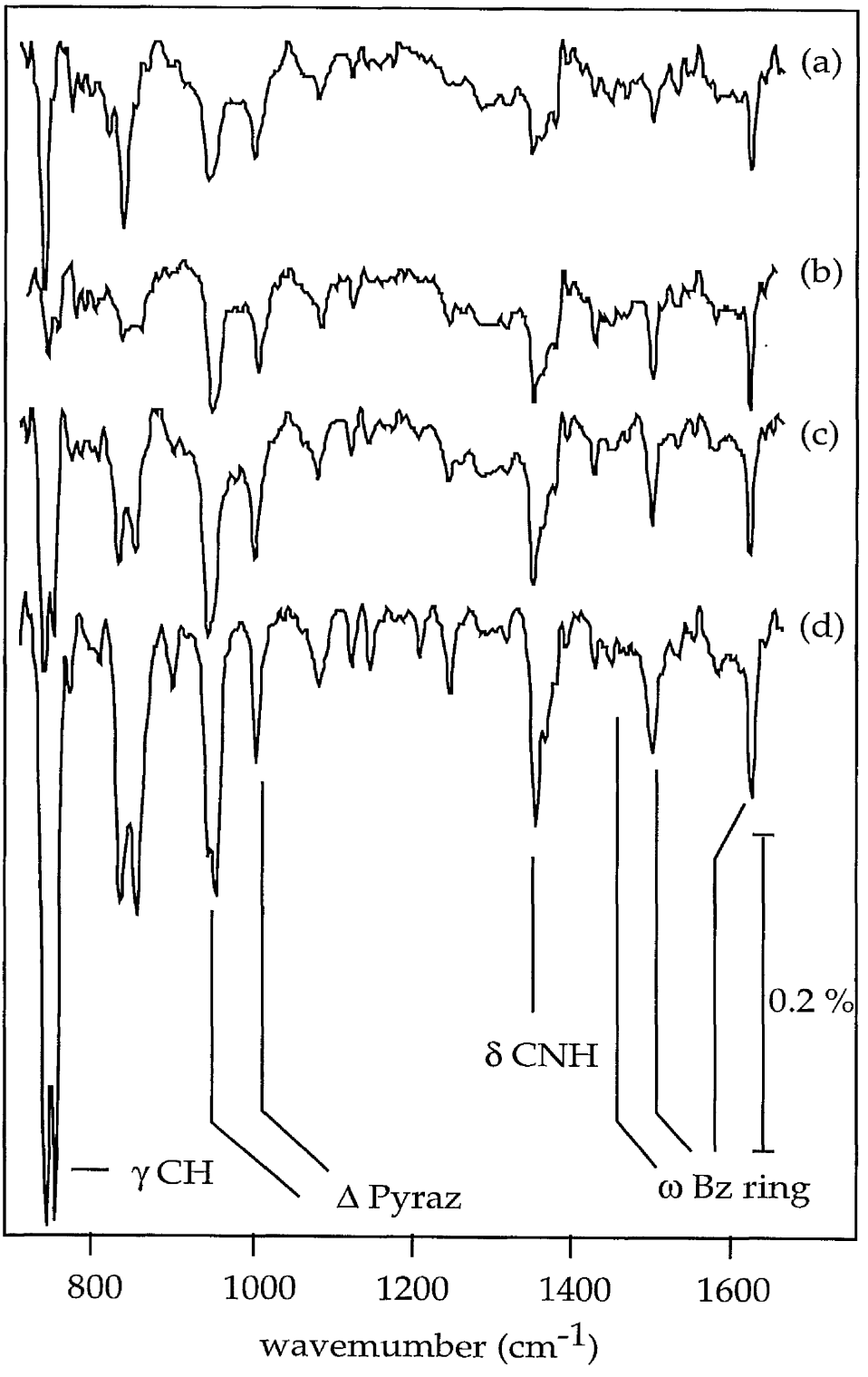

Figure 4.7 RAIR spectra of indazole adsorbed on Cu(100) at 100 K at exposures of (a) 0.6 L, (b) 0.9 L, (c) 1.2 L and (d) 1.8 L. (γ = out of plane bend, Γ = torsion, δ = in-plane bend, br = breathing, ω = stretching, Triaz = triazole, Δ = ring in-plane bend).

RAIRS frequencies of Indazole on Cu(100) at 100 K	
RAIRS (cm^{-1})	Assignment
3217	N-H str (dimer)
3120	N-H str (trimer)
3150-2900	combinations (see table X)
3056	ω CH
1624	ω Bz
1584	ω Bz
1501	ω Bz
1368	ω Pyrazole
1354	δ CNH
1244-1080	δ CH /skeletal
1001	Δ Pyraz
953	Δ Pyrazole
854	γ NH or γ CH
833	γ NH or γ C-H
769	Bz breathing
752	γ CH or γ NH
742	γ C-H

Table 4.3 RAIRS frequencies of the indazole molecule adsorbed on Cu(100) at 100 K. (Bz = Benzene, Triaz = Triazole, comp = complex, br = breathing, Δ = ring in-plane bend, δ= in-plane bend, γ = out-of-plane bend.)

to the azole in-plane bends [8, 16, 17]. These are seen in the corresponding BTA^- spectra. Also a large band at 976 cm^{-1} appears in the RAIR spectra of 1, 2, 3 triazole on Cu(100) taken at 100 K in chapter 5 assigned to the triazole in-plane bend. Here the corresponding bands are seen at 953 and 1001 cm^{-1}.

1400-1650 cm^{-1} region : Bands common to all the azoles as well as the indazolate anion at room temperature are evident in the 1400-1650 cm^{-1} region. The C=C stretches are seen at 1624, 1584, and 1501 cm^{-1} and tend to be shifted to slightly lower frequency on deprotonation in the monolayer data [1]. This also occurs in the BTAH vibrational spectra in chapter 4. A small band at 1449 cm^{-1} can be seen to be growing with increasing coverage which may correspond to another characteristic ring stretch which is also seen in the spectra taken at 298 K. This band is very small and therefore cannot be assigned with certainty.

1100 to 1300 cm^{-1} region : The region contains many bands of relatively low intensity which probably correspond to the mainly CH in-plane bends as assigned by Bigotto et al. [5] (see Table 4.2). Other skeletal modes cannot be assigned with any degree of certainty.

1300-1400 cm^{-1} region : A large feature is seen at 1352 cm^{-1} together with a small shoulder on it at 1368 cm^{-1}. There is some evidence from the literature that a NH rocking mode or a vibration dominated by this vibration occurs at a similar frequency. Wolff and Muller et al [9] assigned a band at 1359 cm^{-1} to a N-H deformation mode of associated pyrazole (hydrogen bonded), and found that a band at 1343 cm^{-1}, originally assigned to a N-H deformation mode of non-associated (not hydrogen bonded) pyrazole by Tabacik et al [18], disappeared on association. Therefore the 1354 cm^{-1} feature, which is the most intense feature in this region of the RAIRS spectra of Indazole may be related to the N-H deformational mode, when also considering that this band does not appear in

the spectra taken at room temperature , where the proton is lost. The other peak in this region is the 1368 cm^{-1} feature which is almost definitely the pyrazole stretch seen also in the spectra taken at room temperature (1377 cm^{-1}). This band can be seen to shift gradually to lower frequency with exposure in figure 4.7. Thus reinforcing the view that the 1354 cm^{-1} band is unique to the multi-layer data. The pyrazole/azole stretches are commonly observed at lower frequency than the benzene stretches [1, 6, 7]. They also seem to behave similarly to the benzene stretches and diminish in relative intensity in a similar proportion to the benzene stretches when comparing the room and low temperature spectra.

High frequency region : Figure 4.8 shows the 2900 - 3500 cm^{-1} region which should only contain the N-H and C-H stretches. In fact there seems to be a number of peaks at 2950, 2983, 2995, 3076, 3093, 3130, 3162, and 3182 cm^{-1} respectively. This effect is also seen in the low temperature RAIR spectra of 1, 2, 3 triazole on Cu(100) shown in chapter 5. The bands are very close to the large water band but appear as a large 'hump' on the side of the water band. This 'hump' is not usually present and therefore seem to be distinct from the water band. However, the higher frequency bands are assigned tentatively. The multiple peaks are thought to occur as a result of hydrogen bonding and Fermi resonance effects. The self association of pyrazole has been examined by Anderson et al [19], who find that, even at low concentrations in CCl_4 solution, monomers, dimers, and trimers coexist. These give rise to a very broad peak between 3400 and 2000 cm^{-1} with six major maxima. Of these, a band at 3175 cm^{-1} is attributed to the dimer absorption. Wolff and Muller [5] showed two main band areas, one at 3260 cm^{-1} and another at 3170 cm-1 which is accompanied by as many as eleven sharp peaks on the low frequency side. As with imidazole [6] data, they were able to show that, apart from the CH bands, all of these originate in Fermi resonance effects, four of them with combinations in-

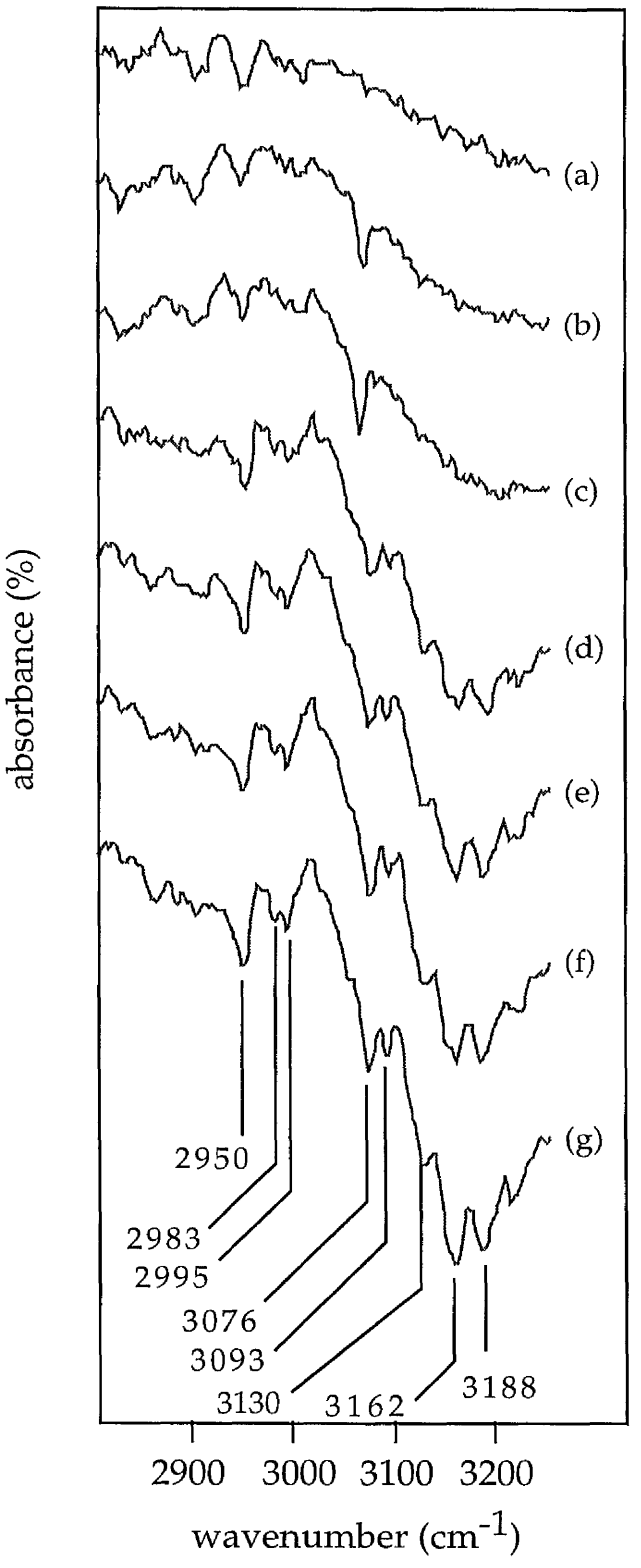

Figure 4.8 High frequency region of the RAIRS spectra of indazole adsorbed on Cu(100) at 100 K at exposures of (a) 0.6 L, (b) 0.9 L, (c) 1.4 L, (d) 3 L, (e) 5L, (d) 8 L, (e) 12 L, (f) 15 L and (g) 20 L (γ = out of plane bend, Γ = torsion, δ = in-plane bend, br = breathing, ω = stretching, Triaz = triazole, Δ = ring in-plane bend).

RAIRS combination bands of Indazole on Cu(100) at 100 K	
RAIRS (cm^{-1})	Assignment/Possible combination
3217	N-H str (dimer)
3188	N-H str (trimer)
3162	(2 X 1582 = 3164)
3130	(1624 + 1501 = 3125)
3093	(1582 + 1501 = 3083)
3076	CH str
2995	(2 X 1501)
2983	(1624 + 1368 = 2992, 1624 + 1352 = 2976)
2950	(1501 + 1449 = 2950, 1582 + 1368 = 2950)

Table 4.4. RAIRS frequencies and possible combinations in the 2900-3250 cm^{-1} region of Indazole adsorbed on Cu(100) at 100 K.

volving a ring mode at 1543 cm^{-1} and the remainder with interactions with the N-H deformation at 1359 cm^{-1}. Changing the nature of the acceptor molecule did not alter the position of these sub-peaks although there were intensity changes related to the shift of the main 3170 cm^{-1} band with which they interact. The Fermi resonance interpretation is therefore well substantiated for compounds of this type.

Similarly, with indazole the strength of the hydrogen bonds are increased as a result of the N-H bond gaining considerable polarity due to the resonance in the Indazole molecule. Hence the N-H stretch is decreased in frequency possibly to 3217 cm^{-1} associated with the dimer and 3188 cm^{-1} associated with the trimer by analogy with the pyrazole association result by Wolff and Muller [5]. However, the results of Wolff and Muller [5] were transmission spectra taken in a series of solvents and when also considering the large water band in this

region of the RAIR spectra, the assignments of the N-H stretches are made very tentatively as mentioned earlier. The other peaks are assigned to combination bands involving the peaks shown in Table 4.4 and increase in intensity due to fermi resonance interaction with the N-H stretch. The exception is the band at 3076 cm^{-1} which is seen at all exposures in Fig 4.7 and is assigned to the C-H stretch by analogy with the room temperature spectra.

4.4 Summary

In summary, both HREELS and RAIRS spectra have shown indazole to deprotonate on adsorption and orient in a perpendicular geometry at both low and high exposures on Cu(100) at 298 K. Results and assignments from the vibrational spectra of BTAH and the other azoles adsorbed on Cu(100) have been used to assign the modes. The probability that the indazolate anion bonds via the 2 N atoms in the pyrazole ring has been discussed and compared with the bonding of the analogous BTA^- anion. At multilayer coverage the molecule is not deprotonated and has been shown to orient in a more 'flat' geometry than that seen at room temperature. The results suggest a specific first-bonding-layer origin for the corrosion inhibition properties of indazole.

To resolve some of the questions raised by the work presented in this chapter, the following experiments are suggested for future work. An ultra high resolution EELS experiment is suggested to probe the bonding of indazole to the surface and possibly compare it with the BTA^- anion to distinguish between whether 2 or 3 nitrogens atoms are bonded to the surface.

Frequency calculations are also suggested to assign those modes which are only tentatively assigned in this chapter.

References

[1] J. Rubim, I. G. R. Gutz, O. Sala and W.J. Orville-Thomas, J. Mol. Struct. 100.

[2] J. O. Nillson, C. Tornkvist, B. Liedberg, Applied Surf. Sci. 37 (1989) 306-326

[3] J. Walsh, PhD thesis, Manchester University, (1994).

[4] D. Thierry, C. Leygraf, J. Electrochem. Soc., Vol. 132. No. 5, 1009, 1985.

[5] A. Bigotto and C. Zerbo, Spectroscopy Letters, 23 (1), 65-75 (1990).

[6] O Sullivan, J. Chem Soc., (1960) 3278, 3653

[7] G. Socrates, Infrared Characteristic Group Frequencies, 2nd. Ed., (1994),*publ. Wiley.*

[8] A. Zecchina and E. Borello, J. Chem. Soc. (B) 1363 (1967).

[9] H. Wolff and H. Muller, Spetrochim. Acta, 1976, 32A, 561.

[10] H. Wolff and H. Muller, J. Chem. Phys., 1974, 60, 2938.

[11] J. E. Demuth, Chem Phys Lett 76, (1980), 201.

[12] V. H. Grassian, J. Phys Chem. (1986), 90, 5900 - 5907.

[13] J. Handley, D. Collison, C.D. Garner, M. Helliwell, R. Docherty, J.R. Lawson and P.A. Tasker, Angew. Chem. Int. Ed. Engl. **32**, 1036, (1983).

[13] M. R. Cohen and R.P. Merrill, Surface Science 245 (1991) 1 - 11.

{14} P. Jakob, D.R. Llotd and D. Menzel, J. Elect. Spec. and Relat. Phenom. 44 (1987) (131 - 139).

[15] E. Cane, P. Palmieri, R. Torroni and A. Trombetti, J. Chem. Soc., Faraday Trans., 1993, 89, 4005

[16] D. Bougard, J. Chem Phys, Vol 64, 5152, 1976.

[17] E. Borello, J. Chem. Soc. B, (1969), 307.

[18] V. Tabacik, J. Mol. Spectroscopy. 45, 319 (1973)

[19] D. M. W. Anderson, J. L. Duncan and F. J. C. Rossotti, J. Chem. Soc., 1961, Part I, 140.

CHAPTER 5

Vibrational Spectroscopy of Poor Corrosion Inhibitors on Cu(100) in the Monolayer and Multilayer regimes

5.1 Introduction

The aim of the work described in this chapter was to investigate the relatively poor corrosion inhibitors of the azole series. A combination of the surface sensitive techniques HREELS and RAIRS are used to investigate the orientation and coordination of 1, 2, 3 triazole, benzimidazole and 1-methyl benzotriazole (depicted in Figure 5.1) on Cu(100). The results are compared with those of the relatively good corrosion inhibitors, BTAH and indazole described in chapters 3 and 4.

1, 2, 3 triazole was studied to try to identify vibrational modes associated with the triazole part of the larger molecule. This has aided the vibrational assignment of the other azoles, BTAH in particular. The orientation and possible bonding modes were also of some interest due to the similar structure of BTAH and 1, 2, 3 triazole. Benzimidazole and the more sterically demanding 1-methylbenzotriazole were also studied on Cu(100), principally to see if subtle changes in the molecular framework would influence the bonding, and thus explain their inability to act as efficient corrosion inhibitors.

5.2 Experimental

Experiments were performed in two separate UHV systems, both equipped with low electron energy diffraction (LEED), a retarding field analyser (RFA) for Auger, mass spectrometer and argon ion gun, allowing standard sample preparation and characterisation to be performed. The base pressure of the systems was ~2×10^{-10} mbar.

The HREELS experiment (see section 2.2) consisted of a 7 eV electron beam focused through a hemispherical deflector with a pass energy of 1 eV hitting

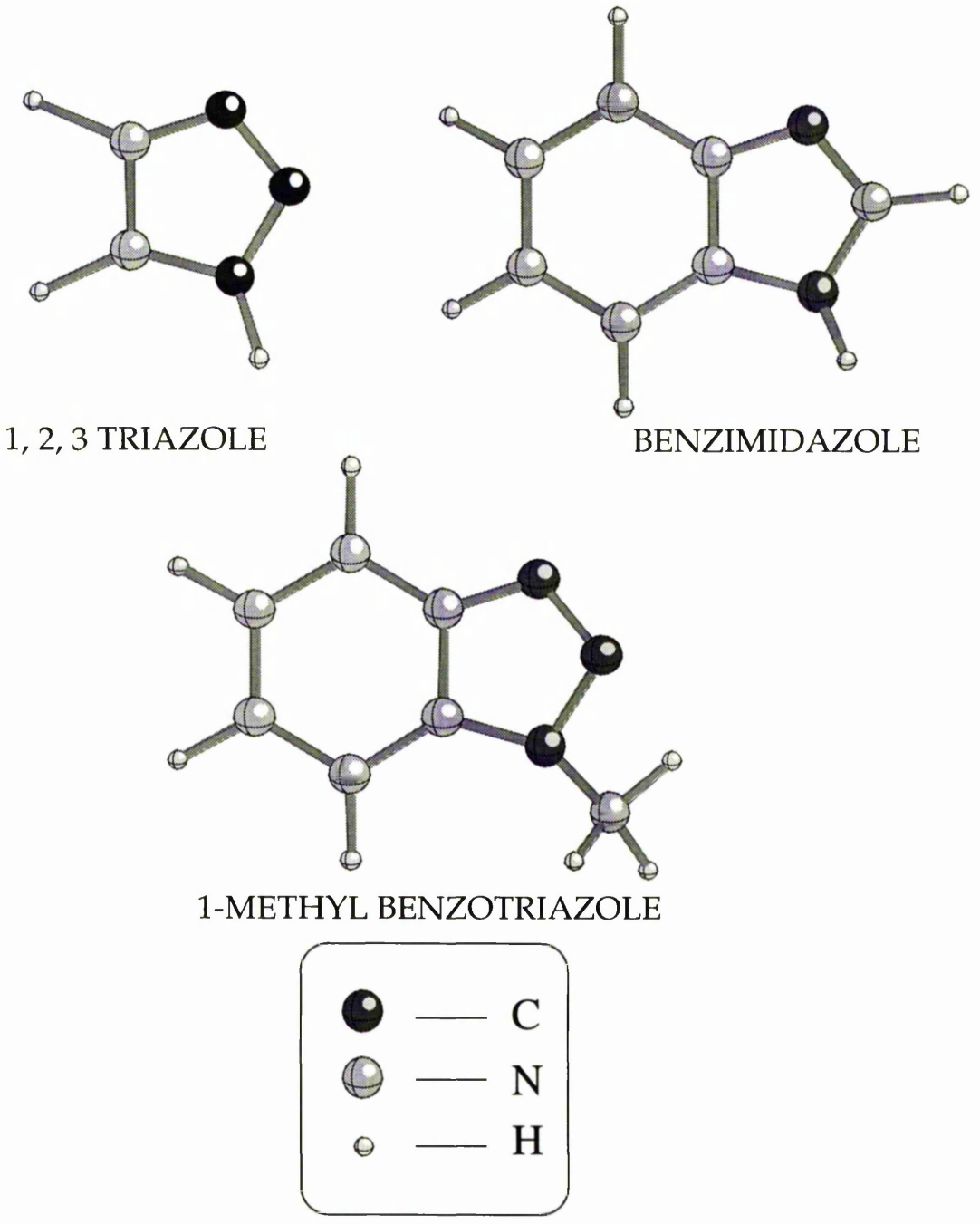

Figure 5.1. Three relatively poor corrosion inhibitors studied on Cu(100) by HREELS and RAIRS.

the Cu(100) surface and being reflected through a similar hemispherical analyser with a similar pass energy acquiring spectra with a resolution of 9 meV (FWHM). In the specular collection mode the angle of incidence of the electron beam was 60° to the surface normal and the reflected electron beam was collected at the same angle. For the off-specular collection mode the angle of collection was changed to 67° to the surface normal, recording spectra at 7° off-specular.

The infrared facility (see section 2.4) consisted of an infrared beam from the FT-IR spectrometer (Mattson Galaxy) focused through a differentially pumped KBr window onto the sample mounted in the UHV chamber. The system was aligned to give a single reflection off the surface at an angle of incidence of ~82°. The reflected light was collimated and focused onto a narrow band MCT detector which accessed the spectral range between 4000 and 700 cm^{-1} and spectra were aquired at a resolution of 4 cm^{-1}.

In both experiments the Cu(100) sample was cleaned via argon ion (1 keV) bombardment and annealing to a temperature of 900 K to produce a well ordered (1 x 1) LEED pattern. In the HREELS chamber, samples were dosed directionally at a pressure of 1×10^{-9} mbar for varying periods of time. In the RAIRS experiment samples were dosed from the background at a pressure of 1×10^{-9} mbar.

5.3 1, 2, 3 triazole

5.3.1 Group Theoretical Considerations

Similar to the other azoles 1, 2, 3 triazole is expected to lose a proton when adsorbed on the surface at room temperature . In the deprotonated form the triazolate anion would be of C_2V (see Fig. 5.2) symmetry. Group theory then

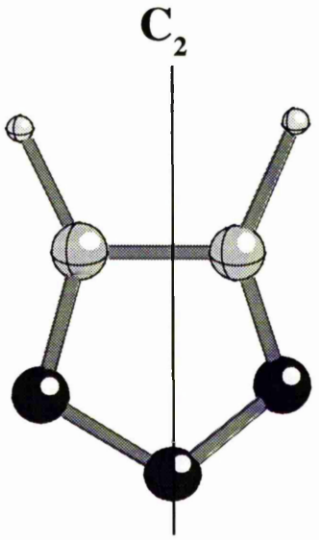

Figure 5.2. The deprotonated 1, 2, 3 triazole molecule (triazolate anion) with the C_2 axis indicated.

gives the anion a total of 15 vibrations, which can be represented:

$6\,A_1 + 2\,A_2 + 2\,B_1 + 5\,B_2$,

all of which are IR active apart from the A_2 modes.

5.3.2 Results and Discussion

RAIR spectra of Cu(100) after exposure to 1, 2, 3 triazole are shown in Fig 5.3. Initially, at low exposures, the spectra are dominated by a single band at 789 cm^{-1}, which increases to a maximum intensity on exposure of 3 L. After further exposure the 789 cm^{-1} band loses intensity and bands at 976, 1026, 1088, 1159, 1192, 1375, 1418, 1439 and 3128 cm^{-1} emerge. An exposure of 12 L marks the point where any further exposure fails to produce a change in the band intensities although saturation coverage may well have been reached earlier.

Both the experimental frequencies and the mode assignments are shown in Table 5.1 together with work from the literature for comparison in Table 5.2 [1].

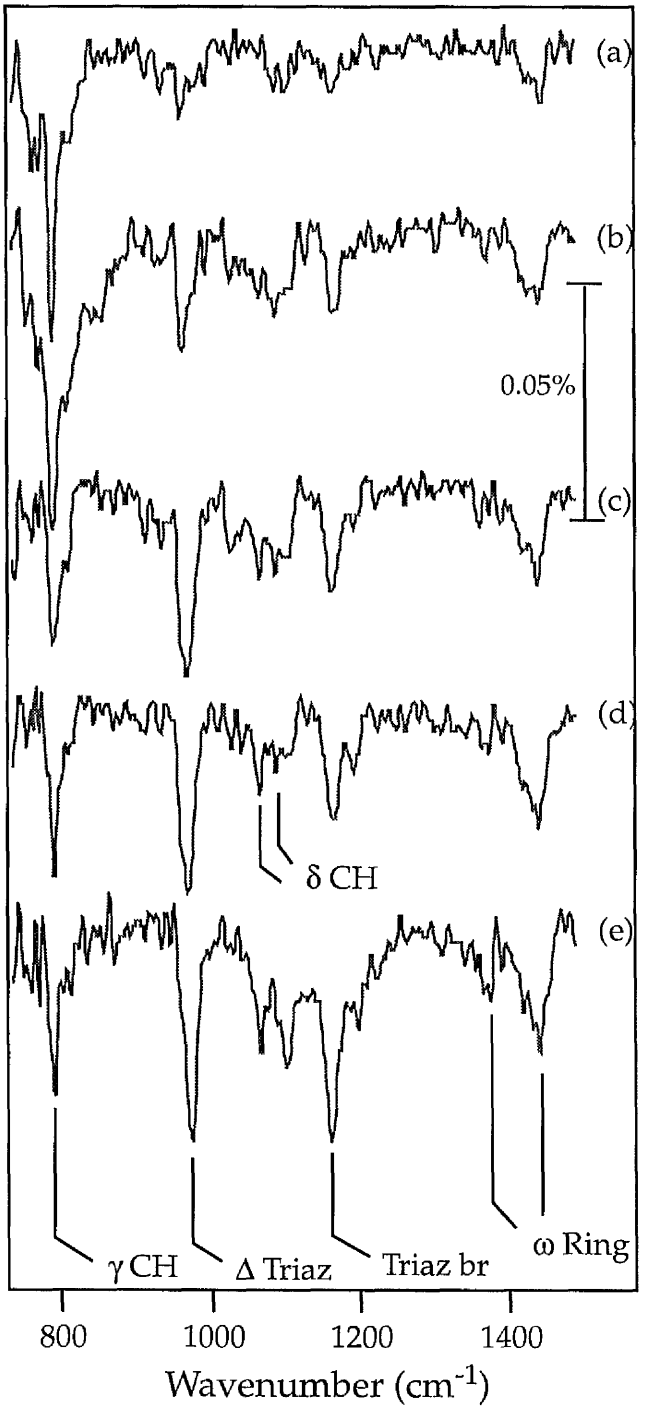

Figure 5.3 RAIRS spectra of 1, 2, 3 triazole adsorbed on Cu(100) at exposures of (a) 1.5 L, (b) 3 L (c) 4.5 L, (d) 6 L and (e) 12 L. (Triaz = triazole, br = breathing, Δ= ring in-plane bend, δ = in-plane bend, ω = stretching).

RAIRS frequencies of 1, 2, 3 Triazolate on Cu(100) at 298 K	
RAIRS (cm^{-1})	Assignment
789	γ CH
976	Δ Triaz
1065	δ CH
1101	δ CH
1159	Triaz br
1375	ω Ring
1439	ω Ring
3151	ω CH

Table 5.1. RAIRS frequencies and assignment of the triazolate anion adsorbed on Cu(100) at 298 K. (Triaz = triazole, br = breathing, Δ= ring in-plane bend, δ = in-plane bend, br = breathing, ω = stretching).

The band frequencies compare very well with those of the literature and are assigned accordingly. Some of the more important assignments are commented on further in this section.

The band at 789 cm^{-1} is assigned to the CH out-of-plane mode [1]. Since the data in Fig 5.3 display only this band at low exposure of 1, 2, 3 triazole to the surface, then it follows from the perpendicular dipole selection rule that it must be the only mode with an appreciable dipole moment normal to the surface. The latter observation is consistent with the molecule being in a parallel geometry. After further exposure the relative intensity increase of the in-plane modes located in the 800-3200 cm^{-1} region suggest an orientational phase transition takes place to a more upright geometry. Since neither the in-plane nor out-of-plane modes disappear at saturation coverage, the two extreme orientations,

1, 2, 3, Triazole

Vapour (cm^{-1})	Type	Liquid (cm^{-1})	Soln. (cm^{-1})	Assignment
482s 502s 524s	C	506vw		γ(NH)
630w	C	633w		Γ
688s 698s 706s 713s 728s	C	701m	702m*	Γ
765w	C	790br	783s*	γ(CH)
808vs 821vs 826vs 827vs 829vs 848vs	C	840br	826s*	γ(CH)
		880br	883br*	γ(NH) (Associate)
938s 952s 959s,m	A + B	955s	950s (956)	Δ
964s,m 975m	B + A	976s	976m	Δ
1037m 1045m 1051m 1062m	B + A	1075s	1076w (1082)	δ(CH)
1099s 1105s 1108s 1111s 1124s 1125s	A + B	1096s 1115m 1130	1108s (1116)	δ(NH)
1165vw		1164w		Breathing
1224m 1236m 1248m	A + B	1225s 1235sh	1237w	δ(CH)
1380sh		1383w	1380w	ω
1398m 1402m 1409m 1418m	B + A	1413m	1407w	ω
1430w		1440m	1420	ω
1512vw		1510sh		comb.
1520w 1535w 1546w	A + B	1533m	1535w	ω

Table 2. IR frequencies and assignment of 1, 2, 3 triazole taken from reference [1]. (bands in parentheses dissapear at low concentrations. *solvent $CHBr_3$; the other frequencies refer to solutions in CCl_4 .Triaz = triazole, Γ= ring torsion, br = breathing, Δ= ring in-plane bend, δ = in-plane bend, ω = stretching)

'flat' or 'standing up' can be discounted. Therefore, the molecule must be tilted with respect to the surface normal at saturation coverage. Thus, the orientation seems to be very similar to that of BTAH on Cu(100), which was discussed in chapter 3. This point is discussed further in section 5.3.3.

The 900-1100 cm^{-1} region: This region contains the 976 cm^{-1} band, which Borello et al.[1] assigned to the triazole in-plane bend. Bands in the 900-1020 cm^{-1} were assigned to these modes in the RAIR spectra of the benzene-ring-containing azoles. The bands seen here at 1065 and 1101 cm^{-1} are assigned to the CH in-plane bends which occur at a lower frequency than the corresponding CH in-plane bends of the benzene ring containing azoles studied [1, 2].

1100 - 1300 cm^{-1} region: Rubim et al [3] assigned a band at 1161 cm^{-1} to the triazole breathing mode involving the symmetric N=N=N stretch when assigning the Raman spectra of BTAH exposed to a Cu electrode. The vibrational data in chapter 3 of the BTA^- anion on Cu(100) contains a similar band at 1161 cm^{-1}, which is assigned here to this mode. The triazole spectra also contain a band at 1161 cm^{-1} assigned to the ring breathing mode involving the N=N=N stretch. This band does not appear in the low temperature spectra (100 K), when the molecule is in the protonated form. Instead an intense band appears at 1240 cm^{-1} which is ascribed to the breathing mode involving the N=N stretch. Again the latter observation is consistent with a band observed in the same region (1211 cm^{-1}) in the RAIRS spectra of BTAH on Cu(100) at low temperature (100 K). However, this assignment of the 1240 cm^{-1} band does disagree with the assignment of a weak band in the same region made by Borello et al. [1] in his liquid IR spectra of 1, 2, 3 triazole. He assigned this band to a CH in-plane bend.

Further evidence for deprotonation before subsequent bonding to the surface

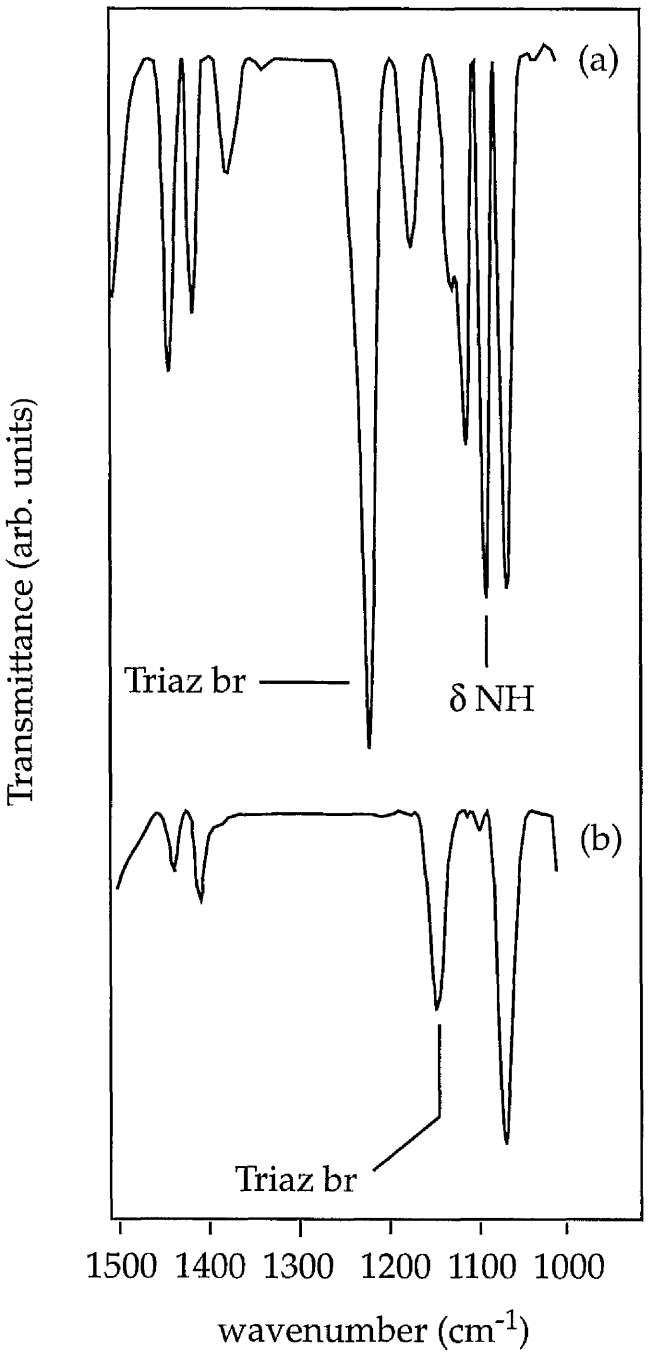

Figure 5.4. IR spectra of (a) 1, 2, 3 triazole taken in CaF_2 plates and (b) 1, 2, 3 triazole in a solution of NaOH at pH 10 taken in CaF_2 plates ; (Triaz = triazole, br = breathing, δ = in-plane bend)

is seen from the IR spectrum of 1, 2, 3 triazole taken at atmosphere under differing pH conditions. Importantly, the IR spectrum of 1, 2, 3 triazole taken at pH 10 on CaF_2 plates (Fig 5.4, spectrum (b)), does not contain a N-H in-plane bend

mode, usually seen at 1114 cm^{-1} [1]. The molecule is assumed to be deprotonated under these conditions similar to the adsorption of the molecule on Cu(100) at room temperature. A band at 1142 cm^{-1} is also seen in Fig. 5.4 (b), assigned to the ring breathing mode. It is assigned to a slightly higher frequency of 1161 cm^{-1} in the RAIR spectra of the triazolate anion on Cu(100). Fig. 5.4 (a) shows the liquid IR data of 1, 2, 3 triazole taken on CaF_2 plates. In contrast to spectrum Fig. 5.4(b), a large band is seen at 1114 cm^{-1} indicating the presence of a proton, but no intense band is seen in the 1100-1200 cm^{-1} region. Instead a new intense band is seen at 1223 cm^{-1} assigned to the triazole breathing mode involving the N=N stretch. This is probably analogous to the band seen at 1240 cm^{-1} in the RAIR spectra of 1, 2, 3 triazole on Cu(100) at low temperature, shown in section 5.3.4. Similar observations are evident in the corresponding BTAH experiments which are described in section 3.2.5.

1300 - 1500 cm^{-1} region: Triazole ring stretches are seen at 1375 and 1439 cm^{-1}. These are characteristic of the azoles and can be assigned with reference to the IR work of Borello et al [1].

High frequency region: Similar to the other azoles studied, the room temperature RAIR spectra does not contain any N-H features . This is in contrast to the low temperature spectra which show the intense N-H in-plane bend at 1113 cm^{-1} [1], commented on earlier, as well as several bands of high intensity in the 2800-3200 cm^{-1} region. These bands cannot be assigned with certainty but they are thought to be a mixture of combination and NH stretching bands and are discussed further in section 5.3.4.

5.3.3 Observations On Possible Bonding Modes

The bonding modes differ depending on the surface coverage. At low coverages

due to its flat geometry, the triazolate anion is assumed to bond to the surface via the π orbitals of the carbon and nitrogen atoms. However at saturation coverage the bonding mode must change accounting for the more 'upright' geometry, and bonding probably takes place through the σ orbitals of the nitrogen atoms on the triazole ring.

The vibrational analysis in chapter 3 suggested that the BTA^- anion is compatible with 3 possible bonding modes to Cu(100). These were shown in section 3.2.7. The triazolate anion can be treated in a similar manner and equivalent bonding modes are shown in Fig. 5.5. Model A requires the terminal nitrogen atom to be the only one involved in the bonding to a surface copper atom. Here, there is an obvious ability for the molecule to rotate about this single bond.

Model C is called the 'arrowhead' mode of bonding which also occurs in corresponding inorganic analogues of BTAH such as that seen in the penta-nuclear copper cluster [4] shown in Fig. 3.16. The analogous copper cluster has also been formed using 1, 2, 3 triazole [5]. In this structure the three nitrogen atoms bond to copper atoms in a similar manner. On the surface we can imagine the peripheral nitrogen atoms bonding to copper atoms in the first layer, while the nitrogen at the 'head of the arrow' is bound to a copper atom in the second layer.

The equivalent of Model B for the BTA^- anion requires 2 nitrogen atoms to be anchored to the surface to two separate copper atoms, leaving the remaining nitrogen atom to interact with a hydrogen atom on an adjacent molecule. This would most likely occur via the α hydrogen atom on the benzene ring, closest to the triazole ring. If we compare the analogous model for the triazolate anion on Cu(100), then the requirement of a hydrogen on the benzene ring in the

A B C

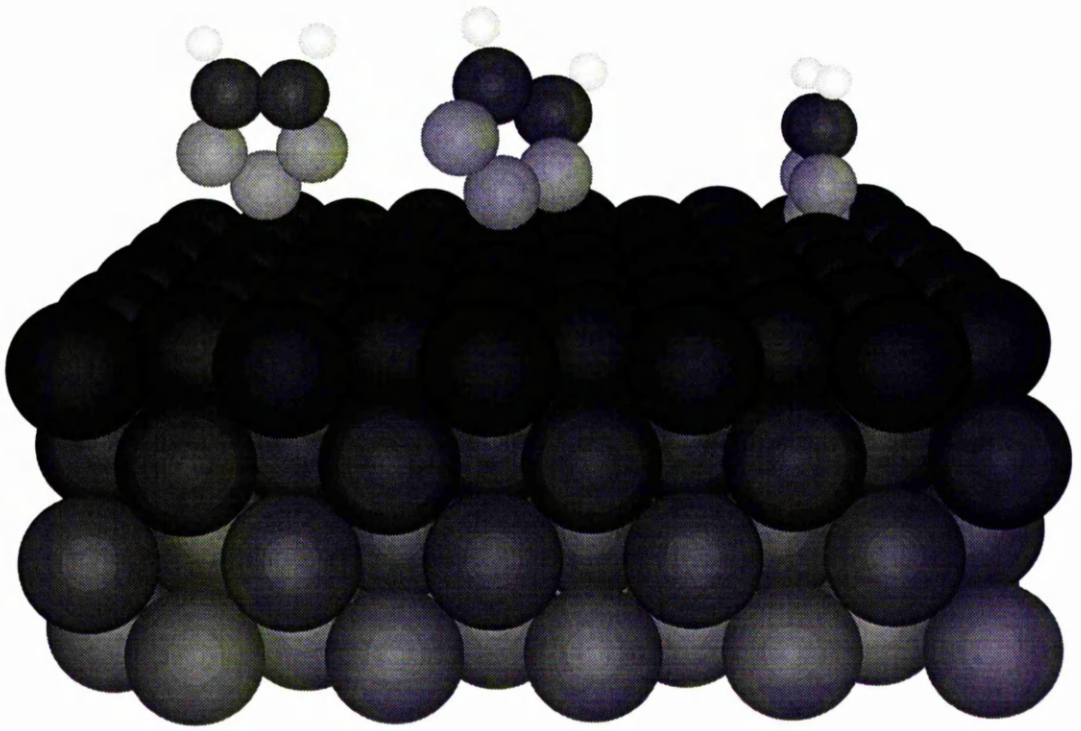

Figure 5.5 A side view of the proposed structural models for the adsorption sites of 1, 2, 3 triazole on Cu(100) : (A) bonded via the central nitrogen to one copper atom; (B) bonded via two adjacent nitrogens to two copper atoms; (C) bonded with each nitrogen atom bound to a copper atom, the central nitrogen being bound to a copper atom in the second layer, with adjacent nitrogen atoms each bound to a separate surface copper atom.

molecular structure is not satisfied, due to the obvious absence of a benzene ring. Thus molecular interaction through this mechanism cannot occur. Of course this type of molecular interaction between neighbouring molecules is not a necessary requirement. However, the previous points discussed do possibly suggest that Model C may be a better candidate. When we also consider the striking similarity between the molecular framework and the orientation of the triazolate anion and BTA^- anions on Cu(100), there is a distinct possibility that both have similar bonding modes, and may bond through model C.

The overall picture seems to suggest that the N atoms are important in the bonding process and therefore the corrosion inhibition properties. The latter point is further reinforced when it is shown that the position of the N atoms in the azole ring are also of some importance in determining orientation and therefore the bonding modes of the azole series on Cu(100). This is discussed in section 5.4, where the bonding of benzimidazole on Cu(100) is analysed.

5.3.4 RAIRS of 1, 2, 3 triazole at low temperature

The RAIRS spectra of 1, 2, 3 triazole at 100 K can be seen in Fig 5.6. The spectra are quite noisy and therefore only bands which can be seen clearly are referred to. The band frequencies and mode assignment are shown in Table 5.3 and compare closely with that of the literature [1] shown in Table 5.2. Some of the spectral regions are discussed further below.

700 - 1000 cm^{-1} region: There seems to be no appearance of the CH out-of-plane bend, seen at 790 cm^{-1} in the room temperature spectra, which suggests that as opposed to the other azoles at low temperature, 1, 2, 3 triazole does not orient in a parallel geometry. The spectra are very noisy however and the growth of the peak may have been lost in the noise level.

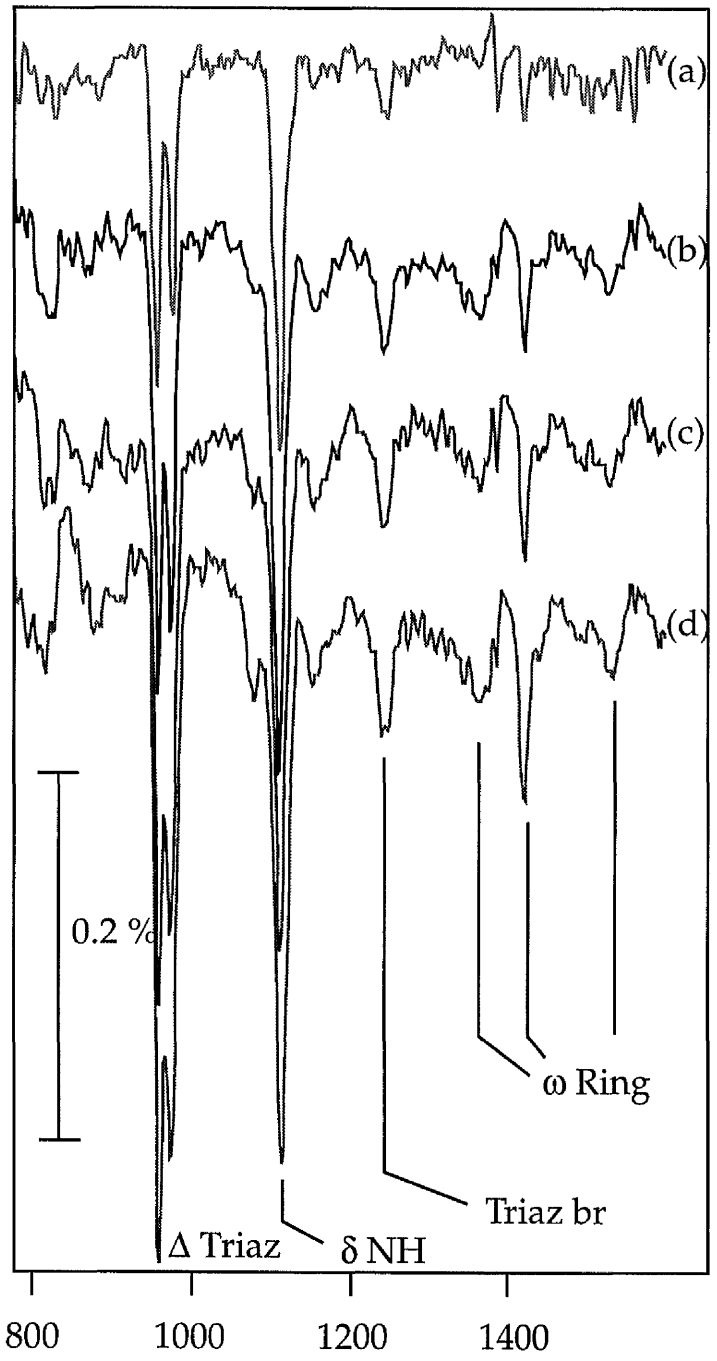

Figure 5.6 RAIRS spectra of 1, 2, 3 triazole adsorbed on Cu(100) at 100 K at exposures of (a) 0.9 L, (b) 1.2 L, (c) 1.8 L, and (d) 3 L.(Triaz = triazole, br = breathing, Δ= ring in-plane bend, δ = in-plane bend, br = breathing, ω = stretching)

RAIRS frequencies of 1, 2, 3 Triazole on Cu(100) at 100 K	
RAIRS (cm^{-1})	Assignment
958	ΔTriaz
976	ΔTriaz
1113	δNH
1078	δ CH
1240	Triaz br
1362	ωRing
1420	ωRing
1532	ωRing

Table 3. RAIRS frequencies and assignment of 1, 2, 3 triazole adsorbed on Cu(100) at 100 K. (Triaz = triazole, br = breathing, Δ= ring in-plane bend, δ = in-plane bend, br = breathing, ω = stretching).

The N-H features are very strong in the spectra. In particular there is an intense N-H in-plane bend mode at 1114 cm^{-1} and also the N-H stretch in the high frequency region of the spectra, which is commented on later in this section. The NH in-plane bend is also seen as a very intense peak in the liquid IR spectrum of the triazole molecule taken at atmospheric pressure, as shown by Fig 5.4 in the previous section, but is missing in the IR spectra taken at pH 10 indicating the deprotonation of the triazole ring, thus reinforcing this assignment.

1100 - 1600 cm^{-1} Borello et al [1] assigned a band at 1241 cm^{-1} to a CH in-plane-bend when assigning the IR spectrum of 1, 2, 3 triazole but it is assigned here to the breathing mode involving the N=N stretch due to the very similar changes in the vibrational spectra of the BTAH and 1, 2, 3 triazole when going from low

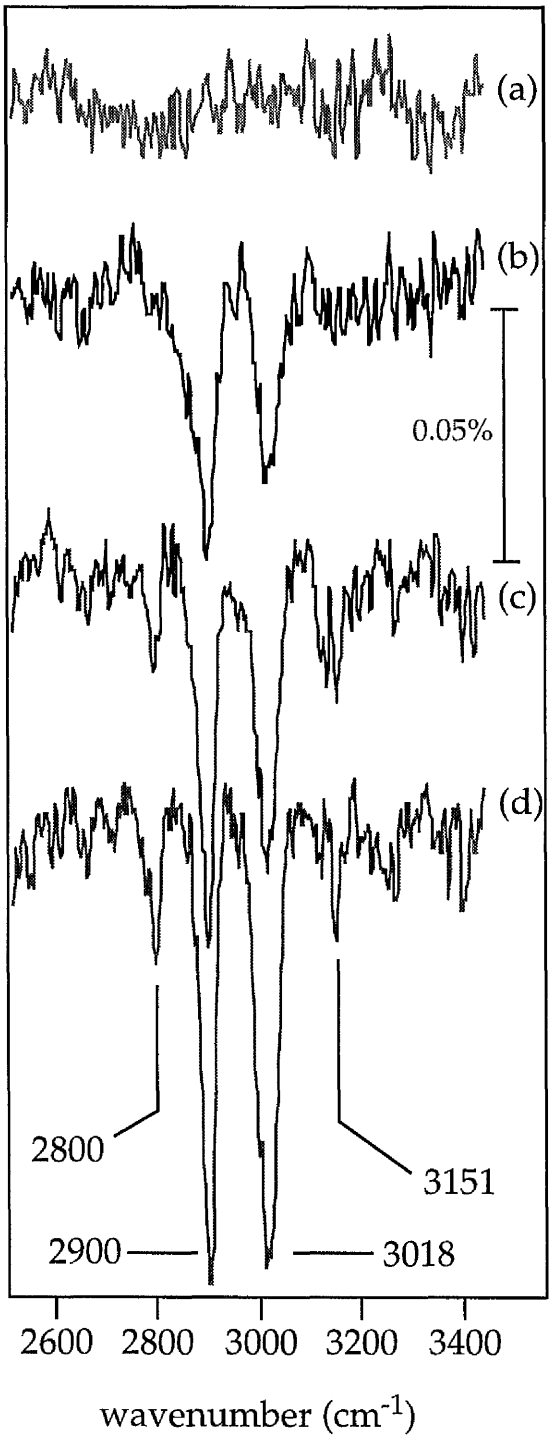

Figure 5.7 High frequency region of the RAIR spectra of 1, 2, 3 triazole adsorbed on Cu(100) at 100 K following a exposures of (a) 0.9 L, (b) 1.2 L, (c) 1.8 L and (d) 3 L.

RAIRS combination bands of 1, 2, 3 triazole on Cu(100) at 100 K	
RAIRS (cm^{-1})	Assignment/Possible combination
3151	ω C-H
3012	ω N-H
2900	1366 + 1528 = 2894
2798	1422 + 1366 = 2788

Table 5.4. RAIRS frequencies and possible combinations in the 2800-3200 cm^{-1} region of 1, 2, 3 triazole adsorbed on Cu(100) at 100 K.

to room temperature. This has been discussed in section 5.3.

The ring stretches are assigned in Table 5.1 according to the peaks seen at characteristic frequencies by a number of authors [1, 6], the 1362 cm^{-1} band being the only ring stretch to shift to a slightly lower frequency from 1380 or 1383 cm^{-1} seen by Bougard et al [6] and Borello et al [1] respectively.

High frequency region: The high frequency region of the spectra (see Fig. 5.7) show four bands at 2798, 2900, 3012, and 3151 cm^{-1}. The band at 3151 cm^{-1} can be assigned to the CH stretch with reference to the IR work done by Borello et al [1] on 1, 2, 3 triazole [1] and Bougard et al. on 1, 2, 4, triazole [6]. The N-H stretch usually occurs in the 3450-3550 cm^{-1} region, but similar to the N-H stretch in the low temperature spectra of indazole described in Chapter 5, is shifted to lower frequency. Bougard et al [6] assigned a band as low as 2700 cm^{-1} to the N-H stretch in the IR spectrum of crystalline 1, 2, 4 triazole. Pimental et al [7] found that both the width as well as the intensity of the down shifted N-H stretch increases when it takes part in hydrogen bonding in solutions and solids. Therefore the band at 3012 cm^{-1} which has a FWHM which is appreciably

larger than that of the other bands in Fig. 5.7 is tentatively assigned to the N-H stretch, although the increased width may well be due to the superposition of combination bands. The molecules probably bond to form dimers or trimers similar to that found in solutions of pyrazole [8, 9]. Therefore it cannot be discounted that several bands may account for the N-H stretches of the polymeric molecules. However, combination bands are also expected to be seen in this region, as was the case in the low temperature RAIRS spectra of indazole on Cu(100) described in chapter 4. The intensity of the combination bands are almost certainly increased as a result of Fermi resonance effects, explaining their unusually high intensity. The latter effects are documented extensively by several authors in the literature using several different azoles [8,9, 10] and basically show that Fermi resonances occur with one or more of the N-H stretching fundamentals and the combination bands resulting in a substantial increase in the intensity of the combination bands. The latter subject is briefly reviewed in section 4.3. Possible combinations for some of the bands are given in Table 5.4.

5.4 Benzimidazole

5.4.1 Group Theoretical Considerations

Again the benzimidazole deprotonated molecule is considered rather than the molecule by analogy with BTAH [11 - 15]. The benzimidazolate anion is of C_{2v} symmetry as shown in Fig. 5.8. It has a total of 36 vibrational modes which can be described;

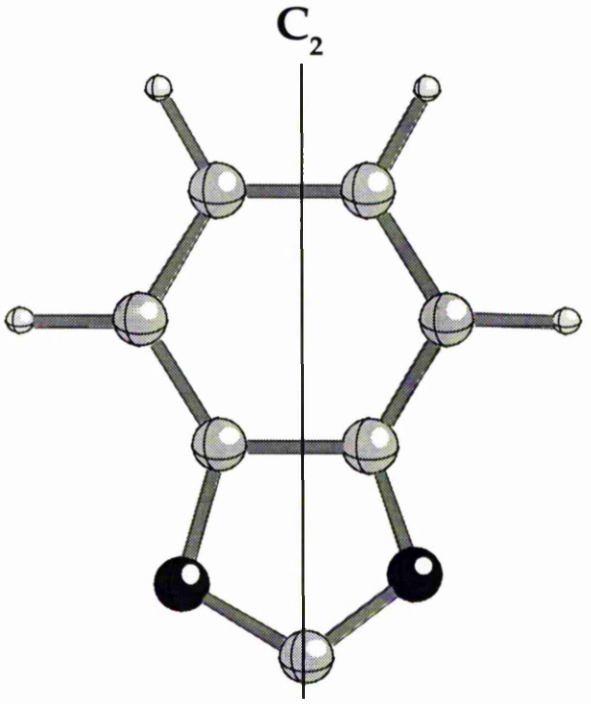

Figure 5.8 The deprotonated benzimidazole molecule (BIM^- anion, with the C_2 axis indicated).

$13A_1 + 5A_2 + 12B_1 + 6B_2$,

all of which are IR active apart from the $5A_2$ mode.

5.4.2 Results and Discussion

The specular HREEL spectra of benzimidazole can be seen in Fig. 5.9. The spectra show the growth of two isolated bands at 425 and 758 cm^{-1} at low exposures of benzimidazole (BIMH). On further exposure the 425 and 758 cm^{-1} bands reach a maximum intensity on exposure of 3 L whilst two small features at 1153 and 1274 cm^{-1} emerge, these being only just distinguishable at saturation coverage (3 L exposure).

The features at 425 and 758 cm^{-1} are more intense in the off-specular HREELS spectra shown in Fig 5.10. Also present are a several bands not seen in the specular spectra. As well as the loss features at 1153 and 1264 cm^{-1} which appear to have increased in intensity relative to the 425 and 758 cm^{-1} features when going from specular to off-specular, several new features in the 1400-1600 cm^{-1} region and at 3073 cm^{-1} are clearly distinguishable.

Benzimidazole has two intense out-of-plane modes assigned to the CH out-of-plane bend and the out-of-plane ring torsion at 425 cm^{-1} and 758 cm^{-1} [3]. The transition dipole moments associated with these modes must have a large contribution perpendicular to the surface hence their high intensity in the specular spectra. These observations are consistent with the molecule lying parallel to the surface where the out-of-plane modes would be enhanced, and the in-plane modes are screened by their image dipoles. The corresponding features were also seen intensely in HREEL spectra of BTAH on Cu(100), at low exposures of BTAH when the molecule was found to be lying 'flat'.

This interpretation is further reinforced by the off-specular data (fig 5.10) which contain several bands not seen in the specular spectra. Fig 5.11 shows a comparison of the specular and off-specular data recorded following a 3 L expo-

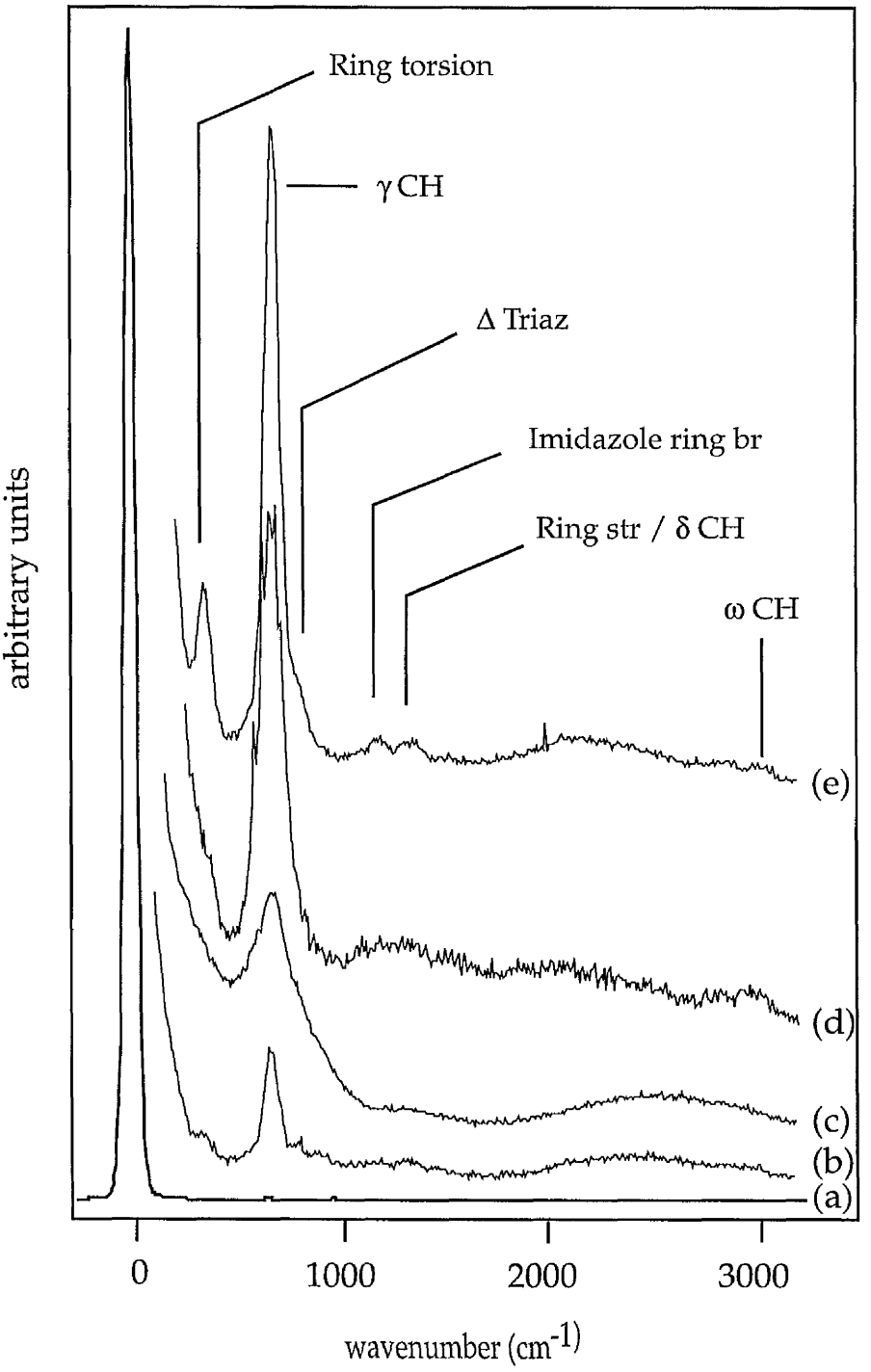

Figure 5.9 Specular HREELS spectra recorded following (a) 0 L, (b) 0.05 L, (c) 0.1 L, (d) 0.4 L and (e) 3 L doses of BIMH onto Cu(100) at room temperature. $\theta_i = \theta_r = 60°$, primary beam energy = 7 eV, FWHM (elastic peak) = 64 cm^{-1}. All spectra have been normalised to the elastic peak.

(γ = out of plane bend, Γ = torsion, δ = in-plane bend br = breathing, ω = stretching, Triaz = triazole)

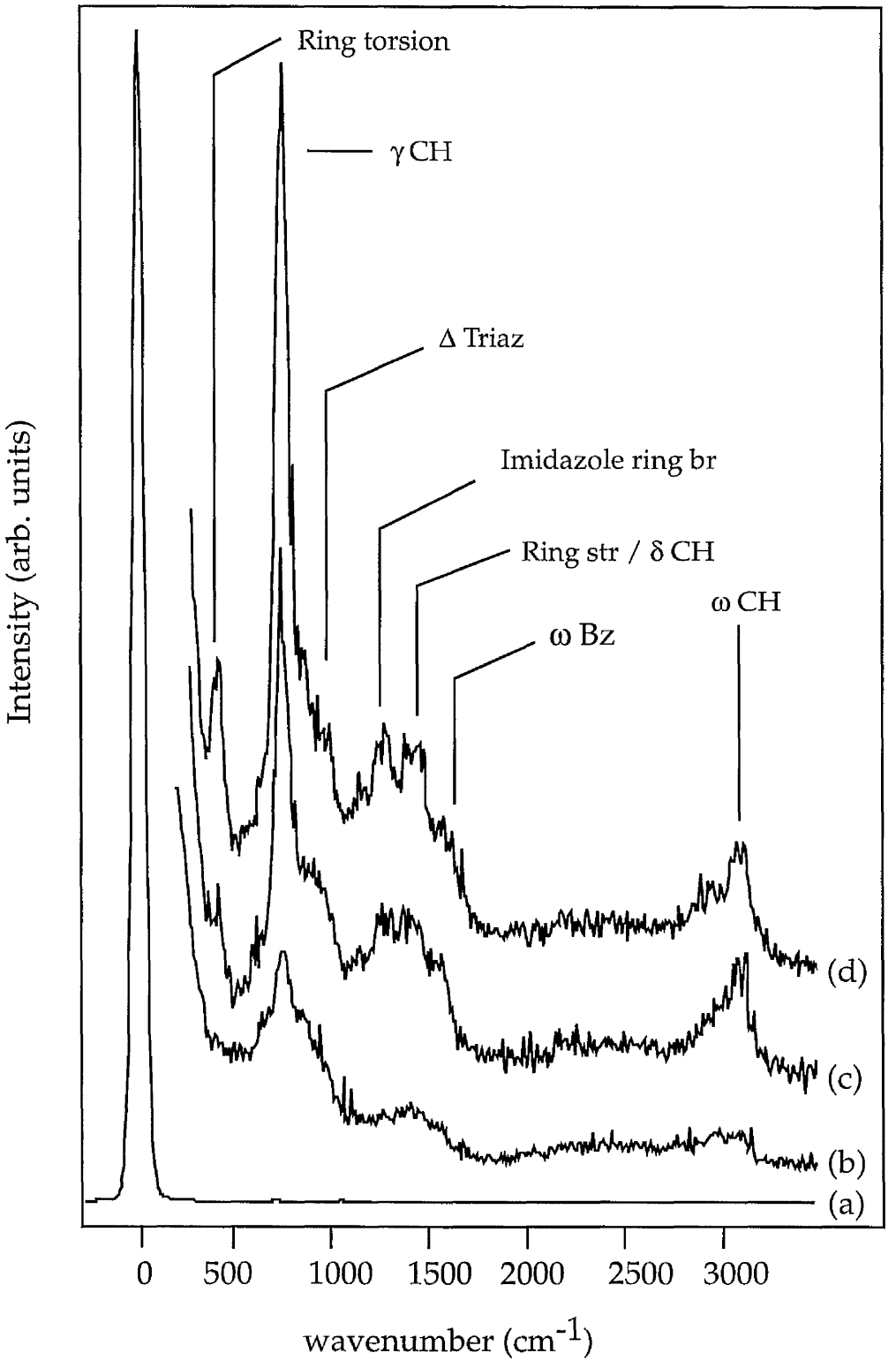

Figure 5.10 7° off specular HREELS spectra recorded following (a)0 L, (b) 0.05 L, (c) 0.2 L, (e) 3 L doses of BIMH onto Cu(100) at room temperature. θ_i = 60°, θ_r = 67°, primary beam energy = 7 eV, FWHM (elastic peak) = 70 cm^{-1}. All spectra have been normalised to the elastic peak.

(γ = out of plane bend, Γ = torsion, δ = in-plane bend, br = breathing, ω = stretching, Triaz = triazole, Δ = ring in-plane bend).

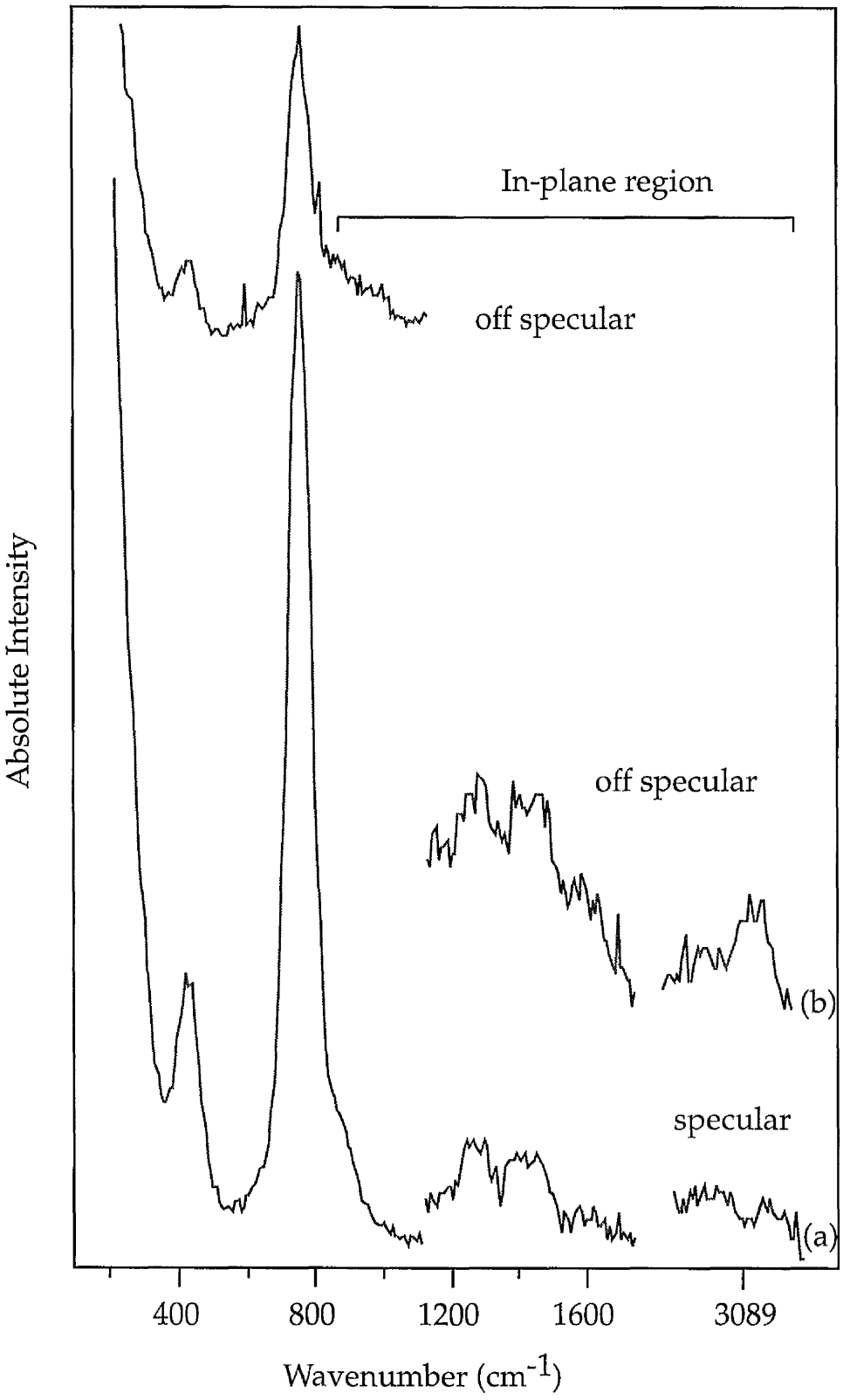

Figure 5.11 HREELS spectra recorded following a 3 L BIMH exposure to Cu(100) at room temperature. Spectra were recorded on specular and 7° off-specular. Specular, $\theta_i = \theta_r = 60°$; off-specular $\theta_i = 60°$, $\theta_r = 67°$, primary beam energy = 7 eV, FWHM (elastic peak) = 64 cm^{-1}. All spectra have been normalised to the elaetic peak.

HREELS frequencies of BIMH on Cu(100) at 298 K	
RAIRS (cm^{-1})	Assignment
436	Γ Ring
758	γ CH
1000	Δ Imidazole
1153	Imidazole br / δ CH
1265	δ CH
1440	ω Ring
1581	ω Bz
2912	combinations
3073	ω CH

Table 5.5 HREELS frequencies and assignment of the BIM^- anion adsorbed on Cu(100) at 298 K. (γ = out-of-plane bend, br = breathing, Δ= ring in-plane bend, δ = in-plane bend, br = breathing, ω = stretching).

sure (saturation coverage) of BIMH to Cu(100) at room temperature. A large drop in the intensity of the 435 cm^{-1} and 758 cm^{-1} loss features is evident in the off-specular spectrum (Fig. 5.11 (b)) when compared with the analogous bands in the specular spectrum (Fig 5.11(a)). This coincides with an increase in intensity of the in-plane modes (1000 - 3080 cm^{-1}). These observations are indicative of the flat geometry of the molecule where perpendicular dipoles are seen intensely in the specular spectrum (dipole scattered) but are seen less intensely, relative to parallel modes (impact scattered), in the off-specular spectrum. Apart from the two dipolar scattered features, it is difficult to distinguish individual vibrational modes as the intensity and resolution of the loss features are relatively low but features can be seen at approximately 435, 758, 1000, 1153, 1264, 1581 and 3073 cm^{-1}. Speculative assignments of the broad features have been

Species	Frequency No. υ	Observed FTIR (cm^{-1})	RAMAN (cm^{-1})	Assignment/PED %
a'	1	3460 m		(N-H) stretching (98)
a'	2	3124 w		(C-H) stretching (94)
a'	3	3104 w		(C-H) stretching (93)
a'	4	3068 m		(C-H) stretching (97)
a'	5	3044 m		(C-H) stretching (97)
a'	6	3016 vm		(C-H) stretching (99)
		2985 m		(1698 + 1302)
		2952 m		(1588 + 1365)
		2900 vw		(1621 + 1273)
		2852 m		(1478 + 1365)
		2811 w		(2 x 1410)
		1930 w		(3044 - 1114)
		1895 w		(1410 + 478)
		1772		(1545 + 228)
a'	7	1689 m		(C=N) stretching (85), υ_{11} (11)
a'	8	1621 m		(C=C) stretching (91)
a'	9	1588 m		(C=C) stretching (80), υ15 (16)
a'	10	1545 vw	1567 m	(N-H) in-plane bending (72), υ20 (18)
		1496 vw		(2 x 749)
a'	11	1478 s	1486 w	(C=C) stretching (89)
a'	12	1459 s		(C=C) stretching (85), υ19 (12)
a'	13	1410 vs	1408 w	(C=C) stretching (91)
a'	14	1365 m		(C-N) stretching (80)
a'	15	1348 w		(C-N) stretching (90)
a'	16	1302 s	1305 m	(C-N) stretching (92)
a'	17	1273 s	1270 s	(C-H) in-plane bending (84)
a'	18	1247 vs	1256 m	(C-C) stetching (88), υ21 (10)
a'	19	1202 m		(C-H) in-plane bending (81)
a'	20	1157 w		(C-H) in-plane bending (75)
a'	21	1135 m		(C-H) in-plane bending (87)
a'	22	1114 vw		(C-H) in-plane bending (69), υ34 (21)
a'	23	1004 m	1007 s	(C-C-C) trigonal bending (77), υ26 (11)
a"	28	958 s		(C-H) out-of-plane bending (78)
a"	29	933 w		(C-H) out-of-plane bending (69), υ36 (22)
a"	30	885 m	890 m	(C-H) out-of-plane bending (84)
a'	24	835 vw		(C-C) ring breathing mode (69), υ25 (28)
a"	31	769 s	770 s	(C-H) out-of-plane bending (85)
a"	32	749 vs		(C-H) out-of-plane bending (71), υ34 (16)
a"	33	676 vw		(C-C-C) out-of-plane bending (70), υ37 (21)
a'	25	631 m		(C-C-C) in-plane bending (81), υ15
a"	34	628 w	626 w	(N-H) out of plane bending (80), υ30 (12)
a"	35	577 w		(C-C-C) out-of-plane bending (82)
a'	26	545 vw		(C-C-C) in-plane bending (65) υ21 (23)
a"	36	478 w		(C-C-C) out-of-plane bending (75)
a'	27	421 s	417 m	(C-C-C) in-plane bending (71), υ22 (19)
a"	37		272 w	(C-C-C) out-of-plane bending (70), υ22 (19)
a"	38		244 m	(C-C-C) out-of-plane bending (65), υ29 (15)
a"	39		228 w	(C-C-C) out-of-plane bending (61), υ37 (30)

Table 5.6 IR and RAMAN frequencies and assignments of BIMH taken from reference [10]. (solvent $CHBr_3$; the other frequencies refer to solutions in CCl_4). PED = Potential Energy Distribution

made in Table 5.5. A full mode assignment has been made by Mohan et al. [16] which is shown in table 5.6.

5.4.3 Observations on Possible Bonding modes

With virtually no change in orientation with coverage, the bonding mode of the BIM^- anion to the Cu(100) surface can be commented on with some certainty. Similar to BTA^- and the triazolate anions at low coverages the BIM^- ion is thought to bond to the surface in a flat geometry via the π cloud of the two rings. This disagrees with the conclusions made by Walsh et al [17], who found the molecule to be unoriented at monolayer coverage on the basis of NEXAFS results.

The bonding modes of the other azoles have been commented on extensively in Chapters 3, 4 and 5 and it is believed that bonding takes place in these molecules via the N atoms in the azole ring in an upright geometry at saturation coverage. However the fact that BIM^- is thought to bond in a parallel geometry via the π cloud lends credence to the opinion that the orientation and therefore bonding modes of the azoles are sensitive to the C and N atomic positions in the framework of the molecules. Azoles discussed in previous sections such as indazole, BTAH and triazole have an N atom at the head of the azole ring with at least one adjacent N atom enabling bonding via the N atoms and therefore probably allowing an upright geometry. In contrast, BIMH has its 2 N atoms at the peripheral positions in the azole ring with a C atom separating them at the head of the ring, and therefore the lack of an adjacent N atom probably restricts the transition to an upright geometry. The poor corrosion inhibition properties of BIMH probably has its origins in the latter fact. Further research is possibly required into the difference in bond strength between several σ bonded N atoms (indazole and BTAH) and the π cloud of the BIMH molecule on Cu(100).

5.5 - Methyl benzotriazole

5.5.1 Group Theoretical Considerations

The 1 - Methyl benzotriazole (1 - Me-BTAH) molecule (see Fig. 5.12), in contrast to the other azoles studied, does not have an acidic proton therefore must bond in the molecular form. Thus, it has C_s symmetry when adsorbed on the

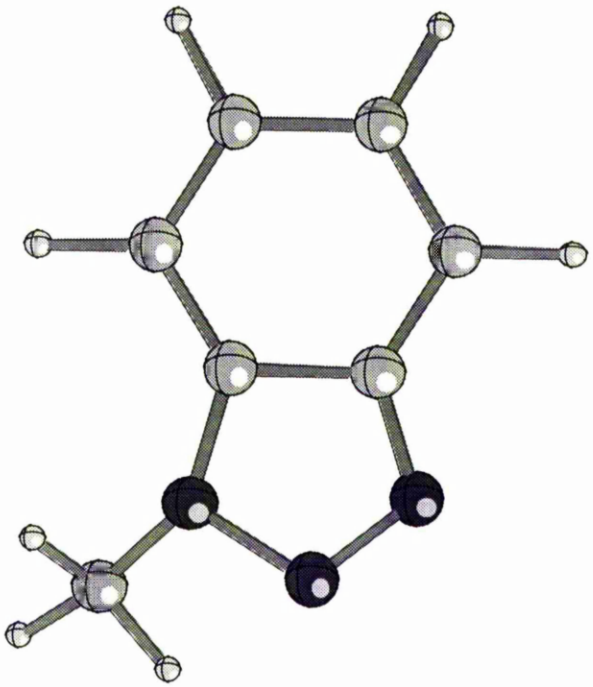

Figure 5.12 The 1-Me BTAH molecule.

surface. Group theory then gives the molecule a total of 45 vibrations which can be represented:

31A" + 14 A',

all of which are IR active.

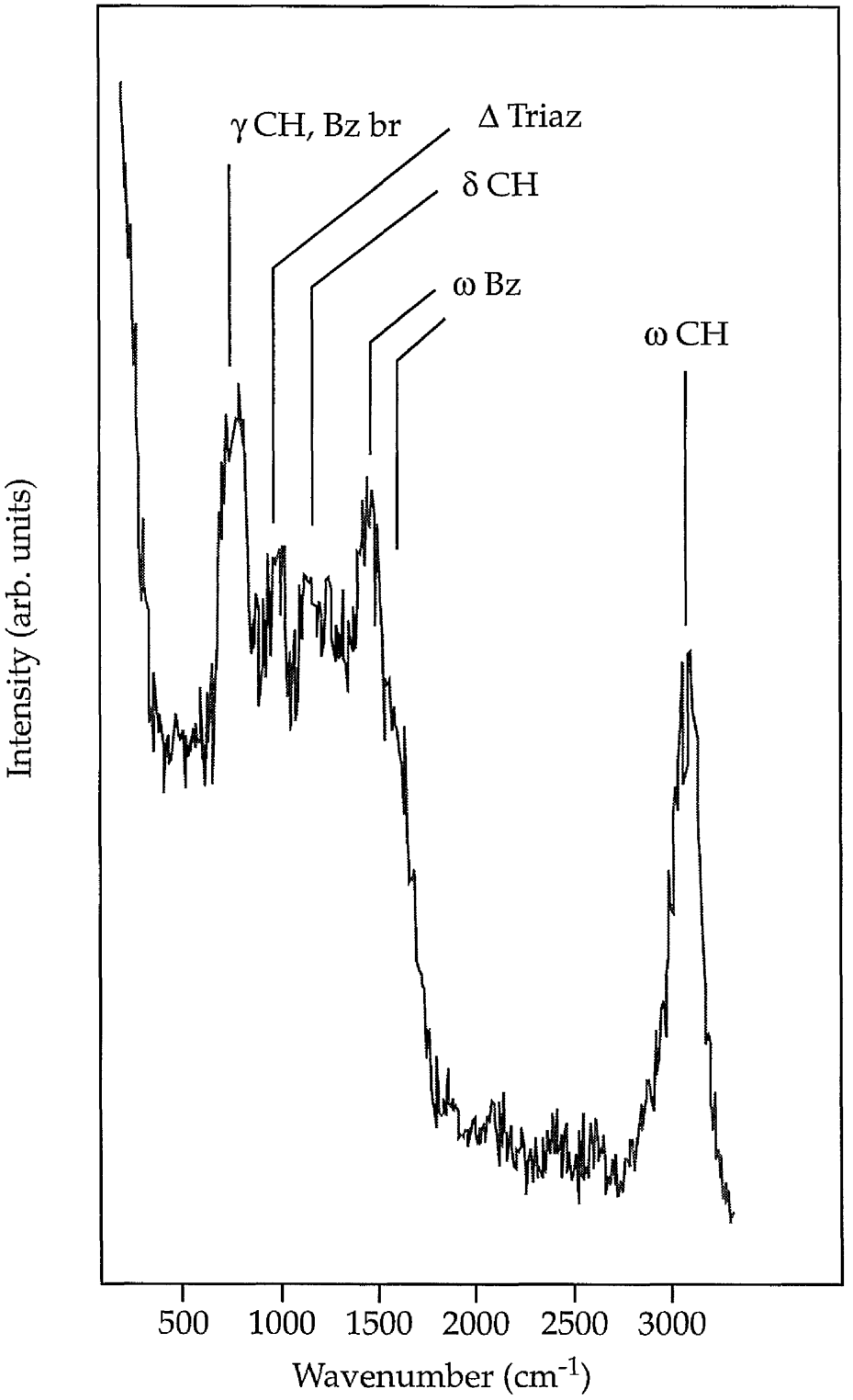

Figure 5.13. Specular HREELS spectra recorded following a dose 30 L of 1-Me BTAH onto Cu(100) taken at room temperature. ($\theta_i = \theta_r = 60°$, primary beam energy = 7 eV, FWHM (elastic peak) = 104 cm^{-1}. All spectra have been normalised to the elaetic peak).(γ = out of plane bend, δ = in-plane bend. br = breathing, ω = stretching).

5.5.2 Results and Discussion

The 1-MeBTAH molecule was the only azole studiedwhich failed to stick to the surface at room temperature. However the molecule did bond at 100 K. Fig 5.13 shows the spectrum obtained after an exposure of 30 L of 1-MeBTAH to Cu(100).

The spectrum is quite noisy and of relatively poor resolution, however the main characteristic features can still be seen. These are labelled on Fig 5.13. The reader is referred to Chapter 3 for the assignment of the lower intensity modes.

The interesting point concerning the 1-MeBTAH molecule is its inability to bond to the surface at room temperature. It shows the importance of the N atoms in the azole ring in the role of bonding to the surface. Presumably the steric hindrance of the methyl group will not allow the N atoms in the azole ring to bond to the surface.

5.6 - Summary

In summary, the RAIRS spectra have shown 1, 2, 3 triazole to deprotonate on adsorption and orient in a flat geometry at low exposures to Cu(100) before undergoing an orientational phase transition such that it orients in a more 'tilted' configuration at higher exposures. Striking similarities in the molecular framework and the respective data of 1,2 3, triazolate and BTA^- adsorbed on Cu(100) have been commented upon, suggesting that both molecules adsorb in a similar fashion to the surface, possibly bonding via 2 or 3 of the nitrogens in the triazole ring. At multilayer coverage the 1, 2, 3 triazole is found not to deprotonate and is thought to orient in a upright geometry.

The benzimidazolate anion is found to bond in a flat geometry at all exposures to Cu(100) at 298 K suggesting that the position N atoms in the azole ring have a large influence in the orientation of the species on the surface and therefore possibly its corrosion inhibition properties.

Further evidence for the importance of the molecular framework and N atoms in the azole ring is 1-Methyl benzotriazole fails to bond to Cu(100) at 298 K providing further evidence for the importance of the molecular framework and N atoms in the azole ring.

References

[1] E. Borello, J. Chem. Soc. B, (1969), 307.

[2] G. Socrates, Infrared Characteristic Group Frequencies, 2nd. Ed., (1994),*publ. Wiley.*

[3] J. Rubim, I. G. R. Gutz, O. Sala and W.J. Orville-Thomas, J. Mol. Struct. 100 (1985) 571.

[4] P.A. Escande and J.L. Galigné, Acta. Cryst. B30, 1647, (1974).

[5] M. Murray, Private communication.

Fang et al.

[6] D. Bougard, J. Chem Phys, Vol 64, 5152, 1976.

[7] G. C. Pimentel and A. L. McClellan, The Hydrogen Bond, p94, (1960), Freeman, San Francisco.

[8] H. Wolff and H. Muller, Spetrochim. Acta, 1976, 32A, 561.

[9] H. Wolff and H. Muller, J. Chem. Phys., 1974, 60, 2938. 1961, Part I, 140.

[10] D. M. W. Anderson, J. L. Duncan and F. J. C. Rossotti, J. Chem. Soc.,

[11] C. Thornkvist, D. Thierry, J. Bergman, B. Liedberg and C. Leygraf, J, Electrochem Soc. 136 (1989) 58.

[12] J. Rubim, I. G. R. Gutz, O. Sala and W.J. Orville-Thomas, J. Mol. Struct. 100 (1985) 571.

[13] J. O. Nillson, C. Tornkvist, B. Liedberg, Applied Surf. Sci. 37 (1989) 306-326H.L. J. Bellamy, The Infrared Spectra of Complex Molecules, volume 2, second edition.

[14] D. Thierry, C. Leygraf, J. Electrochem. Soc., Vol. 132. No. 5, 1009, 1985.

[15] J. Handley, D. Collison, C.D. Garner, M. Helliwell, R. Docherty, J.R. Lawson and P.A. Tasker, Angew. Chem. Int. Ed. Engl. **32**, 1036, (1983).

[16] S. Mohan and N. Sundaraganesan, Spectrochimic. Acta., Vol. 47A, No. 8, 1111-1115, 1991.

[17] J. Walsh, PhD thesis, Manchester University, (1994).

Appendix : Summary of vibrational data.

HREELS and RAIRS frequencies of Azoles on Cu(100) (cm^{-1})

BTA^-	BTAH	indazolate anion	indazole	triazolate anion	1, 2, 3 triazole	BIM^-	1-Me-BTAH	Assignment
			3188, 3217		3012			ω NH
3059	3089	3056	3056	3151	3151	3073	3073	ω CH
		1651						ω CN
	1624	1615	1624				1560-1621	ω Bz
1570			1584			1581		ω Bz
					1532			ω Azole
1481		1497	1501					ω Bz
1439		1449				1440	1443	ω Bz
				1439	1420			ω Azole
1387	1387	1377	1368	1375	1362			ω Azole
			1354					δ CNH
		1308						
1275	1267	1285	1244-1080			1265	1265	δ CH / skeletal
1217								δ CH
	1211				1240			Azole br/δ CH
				1159				Azole br
1171								
1140	1140			1101		1153	1153	δ CH
1122	1126	1123		1065	1078			δ CH
					1113			δ NH
992	1013	997	1001	976	976	1000	992	Δ Azole
	905	901	953		958			Δ Azole
			854					γ CH or γ NH
			833					γ CH or γ NH
787	785	774	769					Bz br
			752					γ CH
738	740		742	789		758	758	γ CH
		637						Δ Bz
580		556						Δ Bz
435		435				435	451	Γ Ring / δ Bz
250		233-250						Cu-N